TiAM
kwartalnik naukowo-techniczny

TECHNOLOGIA I AUTOMATYZACJA MONTAŻU
ZESPOŁÓW • MASZYN • URZĄDZEŃ

Wydawca: Łukasiewicz – IMBIGS • Oficyna Wydawnicza Politechniki Rzeszowskiej • Patronat SIMP • Istnieje od 1993 r.
Open Access: www.tiam.prz.edu.pl • Zeszyt nr 4/2022 (118)

RZESZOW UNIVERSITY OF TECHNOLOGY

Łukasiewicz IMBiGS

TiAM kwartalnik naukowo-techniczny
TECHNOLOGIA I AUTOMATYZACJA MONTAŻU
ZESPOŁÓW • MASZYN • URZĄDZEŃ

ASSEMBLY TECHNIQUES AND TECHNOLOGIES

e-ISSN-2450-8217

ADRES REDAKCJI
Kwartalnik „Technologia i Automatyzacja Montażu" Al. Powstańców Warszawy 8, 35-959 Rzeszów, Poland, tel: +48 17 865 1452,
fax.: +48 17 854 1184, e-mail: tiam@prz.edu.pl, www.tiam.prz.edu.pl

REKLAMA
Redakcja: tel:+48 17 865 1452, fax.: +48 17 865 1184,
e-mail: tiam@prz.edu.pl

SKŁAD I ŁAMANIE
Oficyna Wydawnicza Politechniki Rzeszowskiej

WYDAWCA

Łukasiewicz IMBiGS

Sieć Badawcza Łukasiewicz
Instytut Mechanizacji Budownictwa i Górnictwa Skalnego
ul. Racjonalizacji 6/8, 02-673 Warszawa

RZESZOW UNIVERSITY OF TECHNOLOGY

Politechnika Rzeszowska,
al. Powstańców Warszawy 12, 35-959 Rzeszów

PATRONAT
Stowarzyszenie Inżynierów Mechaników i Techników Polskich
Za treść ogłoszeń i artykułów promocyjnych redakcja nie odpowiada
Wersja pierwotna: elektroniczna

WSKAZÓWKI DOTYCZĄCE PRZYGOTOWANIA ARTYKUŁÓW

- Artykuły przeznaczone do opublikowania w kwartalniku „Technologia i Automatyzacja Montażu" powinny mieć oryginalny i naukowo-techniczny charakter i być zgodne z problematyką czasopisma. Redakcja przyjmuje artykuły w jęz. polskim, jęz. angielskim i jęz. rosyjskim.
- Artykuł o maksymalnej objętości 5 stron A4 wraz z ilustracjami powinien być napisany czcionką Times Roman lub Arial 11 pkt, z interlinią 12 pkt. Formatowany tekst nie powinien mieć podziału na kolumny.
- Tytuł artykułu należy podać w jęz. polskim i jęz. angielskim. Tytuł nieprzekraczający 10 słów powinien odzwierciedlać istotne elementy treści artykułu.
- Struktura artykułów naukowo-technicznych prezentujących prace autora(ów) powinna być następująca: wstęp (wprowadzenie); metodyka (badań, analiz, pracy z podaniem ewentualnie materiałów, założeń itp.); wyniki (badań, analiz); omówienie wyników; wnioski; spis literatury.
- Podpisy pod ilustracjami oraz tytuły tablic należy podać w jęz. artykułu i jęz. angielskim.
- Ilustracje należy dołączyć również jako osobne pliki w formacie: .jpg, .tiff, z rozdzielczością co najmniej 300 dpi. Wszystkie zamieszczane ilustracje powinny być własnością autora(ów) lub należy podać źródło pochodzenia rysunków.
- Wzory matematyczne pisane w edytorze równań Microsoft Equation i powinny być oznaczane kolejnym numerem w nawiasie okrągłym. Wszystkie symbole powinny być objaśnione. Należy stosować jednostki układu SI.
- Spis literatury należy podać w kolejności cytowania w tekście, a odnośniki w tekście powinny być ponumerowane cyframi arabskimi i umieszczone w nawiasach kwadratowych. W przypadku korzystania z Internetu należy podać adres strony i datę odczytu. Liczbę autocytowań należy ograniczyć do niezbędnych.
- Do artykułu należy dołączyć streszczenie w jęz. artykułu i jęz. angielskim, zawierające minimum 200-250 słów.
- Pod streszczeniem należy podać 3-6 słów kluczowych w jęz. artykułu i jęz. angielskim, zwracając uwagę, by nie były one powtórzeniem tytułu pracy.
- Po spisie literatury zaleca się podanie źródła finansowania pracy.
- Na końcu artykułu należy podać: imiona i nazwiska autorów, tytuły naukowe lub zawodowe, telefon, faks, e-mail, miejsce zatrudnienia wraz z adresem do korespondencji.

PROCEDURA RECENZOWANIA

Procedura recenzowania artykułów w czasopiśmie jest zgodna z zaleceniami Ministerstwa Naukii Szkolnictwa Wyższego zawartymi w opracowaniu „Dobre praktyki w procedurach recenzyjnych w nauce", Warszawa 2011.

Wszystkie artykuły naukowo-techniczne publikowane w kwartalniku „Technologia i Automatyzacja Montażu" są recenzowane.

Nadesłane artykuły są poddawane redakcyjnej ocenie formalnej i otrzymują numer redakcyjny, identyfikujący je na dalszych etapach procesu wydawniczego, a redakcja wysyła do autorów informację o przyjęciu artykułu i wysłaniu go do recenzentów. Do oceny każdej publikacji powołuje się co najmniej dwóch niezależnych recenzentów. Redakcja dobiera recenzentów rzetelnych i kompetentnych w danej dziedzinie. Nadesłane artykuły nie są nigdy wysyłane do recenzentów z tej samej placówki, z której pochodzi autor. Prace recenzentów są poufne i anonimowe. Recenzja musi mieć formę pisemną i kończyć się jednoznacznym wnioskiem o dopuszczeniu artykułu do publikacji w czasopiśmie lub jego odrzuceniu. W przypadku pracy w języku obcym, co najmniej jeden z recenzentów jest afiliowany w instytucji zagranicznej innej niż narodowość autora pracy. Autorzy są informowani o wynikach recenzji oraz otrzymują je do wglądu. W sytuacjach spornych redakcja powołuje dodatkowych recenzentów.

Lista recenzentów publikowana jest w ostatnim zeszycie każdego rocznika.

Kwartalnik „Technologia i Automatyzacja Montażu" ukazuje się w formie elektronicznej w otwartym dostępie (Open Access) i jest dostępny na www.tiam.prz.edu.pl

CONTENTS / W NUMERZE

TiAM kwartalnik naukowo-techniczny
TECHNOLOGIA I AUTOMATYZACJA MONTAŻU
ZESPOŁÓW • MASZYN • URZĄDZEŃ

Elżbieta Doluk[1], Anna Rudawska[2]
Izabela Miturska-Barańska[3], Jacek Ogrodniczek[4]

DOI: 10.7862/tiam.2022.4.1

EFFECT OF OVERLAP LENGTH ON THE STRENGTH OF ADHESIVE JOINTS OF STEEL SHEETS

WPŁYW DŁUGOŚCI ZAKŁADKI NA WYTRZYMAŁOŚĆ POŁĄCZEŃ KLEJOWYCH BLACH STALOWYCH

Abstract

The study evaluates the shear strength of the single-lap adhesive joints made of C45 carbon steel. The influence of the overlap length on the shear strength of the adhesive joint was tested. The elongation of the samples was also tested. Before the bonding process, the samples were treated with P180 abrasive paper and degreased. The adhesive joints were made using the Epidian 53/Z1/100:10 adhesive composition. The strength tests were carried out on a Zwick/Roell Z150 testing machine. The maximum value of the shear strength was obtained for the lap L_{z1} = 13 mm and the minimum for L_{z4} = 19 mm.

Keywords: adhesive joint, shear strength, elongation, overlap length

Streszczenie

W pracy dokonano oceny wpływu długości zakładki na wytrzymałość na ścinanie jednozakładkowych połączeń klejonych wykonanych ze stali węglowej C45. Podczas eksperymentu zbadano także wydłużenie próbek. Przed rozpoczęciem procesu klejenia próbki zostały obrobione papierem ściernym P180 i odtłuszczone. Połączenia klejowe wykonano przy użyciu kompozycji klejowej Epidian 53/Z1/100:10. Badania wytrzymałościowe przeprowadzono na maszynie wytrzymałościowej Zwick/Roell Z150. Maksymalną wartość wytrzymałości na ścinanie uzyskano dla długości zakładki L_{z1} = 13 mm, a minimalną dla L_{z4} = 19 mm.

Słowa kluczowe: połączenie klejowe, wytrzymałość na ścianie, wydłużenie, długość zakładki

1. Introduction

The continuous development of the bonding process is associated with the use of adhesive joints in many fields of industries, including the aviation, shipbuilding, transport, medicine and construction [1-3].

The bonding is a complex process because it covers many issues related to the phenomenon of adhesion, but also the problem of choosing adhesive and material, technology of making joints and their strength [4-6].

The strength properties of adhesive joints depend on the adhesive technology, including surface treatment, adhesive preparation and application and the curing conditions [7,8]. The strength of adhesive joints is defined as the joint's resistance to the damaging effects of mechanical and thermo-mechanical factors. It is also referred to as load capacity. The condition for proper design of the adhesive joints is achieving a specific static strength of the adhesive joint. The strength of the adhesive joints can be adjusted by changing the dimensions of the adhesive joint. The maximum strength of compression joints and even peeling occurs for the thinnest joints. The

[1] Elżbieta Doluk (corresponding author), Lublin University of Technology, Faculty of Mechanical Engineering, Nadbystrzycka 36, 20-618 Lublin, Poland, e-mail: e.doluk@pollub.pl, ORCID: 0000-0003-2605-1394.
[2] Anna Rudawska, Lublin University of Technology, Faculty of Mechanical Engineering, Nadbystrzycka 36, 20-618 Lublin, Poland, e-mail: a.rudawska@pollub.pl, ORCID: 0000-0003-3592-8047.
[3] Izabela Miturska-Barańska, Lublin University of Technology, Faculty of Mechanical Engineering, Nadbystrzycka 36, 20-618 Lublin, Poland, e-mail: i.miturska@pollub.pl, ORCID: 0000-0003-4140-4768.
[4] Jacek Ogrodniczek, University of Life Sciences in Lublin, Faculty of Production Engineering, Głęboka 28, 20-612 Lublin, Poland, e-mail: jacek.ogrodniczek@up.lublin.pl, ORCID: 0000-0002-6484-2245.

joint thickness is controlled by applying appropriate pressure during the bonding process [9-14].

Volkersen determined the shear stress distribution of lap adhesive joints, assuming the following:

- adhesive joints and elements behave like linear elastic bodies,
- adherends in all sections are evenly stretched,
- eccentricity of load action, causing bending of joined elements does not affect the distribution of shear stress in the adhesive joint [15, 16].

The shear strength is one of the most commonly used methods to control the adhesive joints. It makes it possible to reconstruct and measure the strength of a structural element in standard operating conditions. The shear strength is directly proportional to the width of the sample [16-18].

Factors affecting the strength of adhesive joints can be divided into structural, material and technological groups. Achieving the adhesive joints with appropriate properties and strength requires consideration of all the above-mentioned aspects. The single-lap adhesive joints are, next to double-lap adhesive joints, the most frequently used adhesive joints in practice. They are usually used to joint materials of relatively small thicknesses. Due to the simple geometry and easy assembly they are treated as easy to make adhesive joints. The main structural factors include the overlap length, thickness of adherends, thickness of adhesive joints, stiffness of the elements, stiffness of the adhesive, size of the spew fillet, bevelling of the end of the lap, method of constituting the joints [15, 19, 20]. Operating conditions also have a significant influence on the strength of the adhesive joint. One of the main operational factors affecting the reduction of adhesive and cohesive strength is temperature [21].

This study investigates the effect of the overlap length on the strength of steel sheet adhesive joints.

2. Materials and methods

The single-lap adhesive joint specimens made of C45 carbon steel were tested. The shape and dimensions of the samples are shown in Fig. 1.

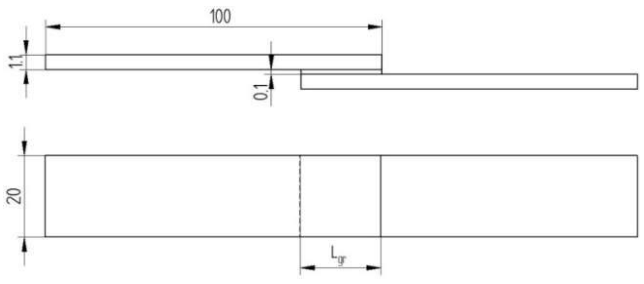

Fig. 1. Tested adhesive joints

The border length of the lap L_{gr} was calculated on the basis of formula (1) assuming the same thickness of the joined sheets [15, 16].

$$L_{gr} \geq 5\sqrt{\frac{E\delta\delta_k}{2G_k}} \tag{1}$$

The dimensions of joints assembled in the study were:

$E = 2.1 \times 10^5$ MPa – Young's modulus of the adherends,

$\delta = 1.1$ mm – thickness of the adherends,

$\delta_k = 0.1$ mm – thickness of the adhesive layer,

$G_k = 1000$ MPa – shear modulus of adhesive.

Based on the L_{gr}, there were selected 5 overlap lengths: two lower and two higher than the border length (Table 1).

Table 1. Overlap lengths

Mark	Overlap length
L_{z1}	13 mm
L_{z2}	15 mm
$L_{z3} = L_{gr}$	17 mm
L_{z4}	19 mm
L_{z5}	21 mm

The sheets were prepared with P180 abrasive paper and degreasing using acetone (3 repetitions) [9]. The sheets were joined using Epidian 53 epoxy resin and triethylenetetramine curing agent (Z-1, trade name), mixed in a ratio of 100:10 (Epidian 53/Z1/100:10), applied on the one of the surface. The temperature during the joining process was 25°C±1°C and humidity 32%±2%. The samples were cured for 7 days under a load of 0.09 MPa. After this period, the samples were subjected to the strength tests on a Zwick/Roell Z150 testing machine in accordance with the recommendations of PN-EN:1465:2009 standard. The test speed was 5 mm/min.

3. Results

The results of strength tests of the single-lap adhesive joints are presented in Fig. 2. The error bars shown in Fig. 2 and Fig. 3 represent the standard deviation.

The highest value of the shear strength (4.37 MPa) was obtained for the overlap length $L_{z1} = 13$ mm and the lowest (3.40 MPa) for the length $L_{z4} = 19$ mm. The strength of the adhesive joint with a border length ($L_{z3} = 17$ mm) was 3.71 MPa. The difference between the extremes of the obtained strength resulted was about 22%. The disproportion between the maximum strength value and the value obtained for the border

length was 15% and between the minimum and L_{gr} was nearly 8.4%.

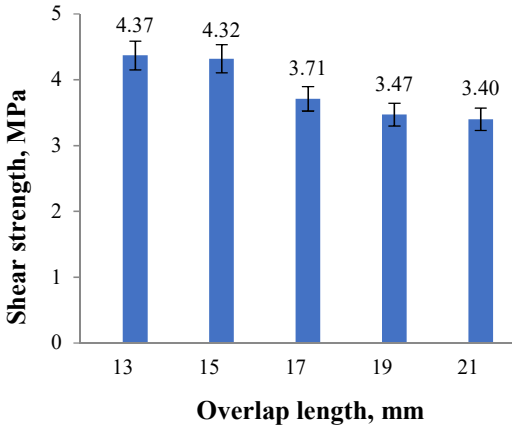

Fig. 2. Shear strength results

The effect of the overlap length on the shear strength was analysed using one-factor ANOVA (Table 2). The statistical analysis were performed using Statistica program at the confidence interval $\alpha = 0.05$. It can be seen that the tested factor does not significantly affected the strength result.

The Pearson linear correlation coefficient r was used to investigate the correlation between the tested factors. It was noticed that the r-Value was about -0.49, which proves a moderate linear correlation between the shear strength and the overlap length. Based on the coefficient of determination (r^2) it can be stated that 25% shear strength is explained by the variability of the overlap length (Table 3).

Table 2. One-factor ANOVA for shear strength

Source	Sum of Squares	df	Mean Square	F-Ratio	p-Value
Overlap length	4.17	4	1.04	2.00	0.13
Total error	10.42	20	0.52		
Total (corrected)	14.59	24			

Table 3. Correlations of shear strength and overlap length

Correlation	Mean	Standard deviation	r	r^2	t	p-Value
shear strength vs overlap length	3.85	0.78	-0.49	0.24	-2.72	0.01

Fig. 3 shows the results of the elongation of the adhesive joints. The highest average value of elongation (0.38 mm) was obtained for the lap $L_{z2} = 15$ mm, and the lowest (0.28 mm) for the adhesive joint with the overlap length $L_{z1} = 13$ mm. The difference between the extremes was almost 26%. The elongation value obtained for the border length. L_{gr} was more than 5% lower than the maximum elongation value.

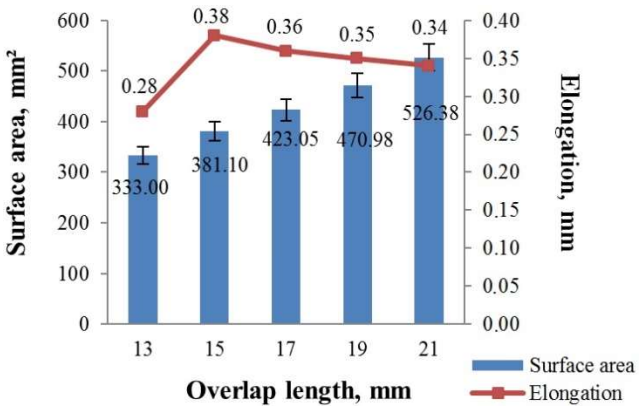

Fig. 3. Elongation results

4. Summary

The purpose of the work was to determine the overlap length on the strength of the single-lap adhesive joints. Analyzing the above results, it can be seen that the overlap length affects the strength of the adhesive joint. This result is in agreement with the literature [10, 23]. The maximum value of the shear strength was obtained for the shortest lap ($L_{z1} = 13$ mm), hence it can be concluded that a shorter lap increases the strength of the adhesive joint.

The statistical analysis showed the change of the tested factor did not statistically significantly affect the strength of the adhesive joints ($p > 0.05$). On the other hand, there was a moderate correlation between the studied variables. It can be concluded that strength of adhesive joint cannot be clearly predicted, therefore experimental testing is required.

It was also noticed that with the increase in the overlap length (starting from the border lap L_{gr}), there was a decrease in the elongation of the samples.

References

1. Kim Seung-Gwang, Suzuki Asuka, Takata Naoki, Kobash Makoto. 2019. “Joining of metals and polymers using powder metallurgy with laser irradiation”. Journal of Materials Processing Technology 270: 1–7.
2. Shang Xinlong, Marques Eduardo, Machado, Jose, Carbas Ricardo, Jiang, Dazhi, Da Silva, Lucas F.M.. 2019. “Review on techniques to improve the strength of adhesive joints with composite adherends”. Composite Part B: Engineering 177: 107363.
3. Stein Nicolas, Felger Julian, Becker Wilfreid. 2017. “Analytical models for functionally graded adhesive single lap joints: a comparative study”. International Journal of Adhesion and Adhesives 76: 70–82.
4. Anes Vitor, Pedro R., Henriques Elsa, Freitas, Manuel, Reis, Luis. 2016. “Bonded joints of dissimilar adherends at very low temperatures-an adhesive selection approach”. Theoretical and Applied Fracture Mechanics 85: 99–112.
5. Li Jianfeng, Yan Ying, Zhang Taotao, Liang Zudian. 2015. “Experimental study of adhesively bonded CFRP joints subjected to tensile loads”. International Journal of Adhesion and Adhesives 57: 95–104.
6. Heidarpour Farhad, Farahani Mohammadreza, Ghabezi Pouyan. 2018. “Experimental investigation of the effects of adhesive defects on the single lap joint strength”. International Journal of Adhesion and Adhesives 80: 128–132.
7. Rudawska Anna, Niedziałkowski Paweł, Miturska, Izabela, Szabelski Jakub, Grzesiczak Dominik. 2018. Selected strength aspects of adhesive lap joints and butt welded joints of various structural materials. Advances in Science and Technology Research Journal 12: 135–141.
8. Borsellino Chiara, Di Bella Guido, Ruisi Vincenzo Fortunato. 2009. “Adhesive joining of aluminium AA6082: The effects of resin and surface treatment”. International Journal of Adhesion and Adhesives 29: 36–44.
9. Weißgraeber Philipp, Felger Julian, Talmon l’Armée Andreas, Becker Wilfried. 2015. “Crack initiation in single lap joints: effects of geometrical and material properties”. International Journal of Fracture 192: 155–66.
10. Da Silva, Lucas F.M., Carbas Ricardo, Critchlow Gary, Figueiredo Miguel, Brown, K., 2009. “Effect of material, geometry, surface treatment and environment on the shear strength of single lap joints”. International Journal of Adhesion and Adhesives 29: 621–632.
11. Samaei Mojtaba, Zehsaz Mohammad, Chakherlou Tajbakhsh Navid. 2016. “Experimental and numerical study of fatigue crack growth of aluminum alloy 2024-T3 single lap simple bolted and hybrid (adhesive/bolted) joints”. Engineering Failure Analisys 59: 253–268.
12. Ramalho Luis, Campilho Raul, Belinha Jorge, Da Silva Lucas. 2020. “Static strength prediction of adhesive joints: A review”. International Journal of Adhesion and Adhesives 96: 102451.
13. De Freitas, Sofia, Sinke Jos. 2015. “Failure analysis of adhesively-bonded skin-to-stiffener joints: metal–metal vs. composite–metal”. Engineering Failure Analisys 56: 2–13.
14. Bamberg Pedro, Reisgen Uwe, Schiebahn, Alexander, Barbosa, J.D.V., Marx Bernd, Coelho Rodrigo. 2018. “Digital image correlation analysis of the effects of the overlap length, adhesive thickness and adherends yield strength over similar”. International Journal of Adhesion and Adhesives 83: 69–75.
15. Rudawska Anna. 2014. “Selected aspects of the effect of mechanical treatment on surface roughness and adhesive joint strength of steel sheets”. International Journal of Adhesion and Adhesives 50: 235–243.
16. Kubit Andrzej, Ciecińska Barbara, Drozd Kamil. 2015. “The influence of lap size on shear strength of adhesive joints”. Advances in Science and Tecchnology Research Journal *9: 104–108.*
17. Boutar Yasmina, Naïmi Sami, Mezlini Salah, Sik Ali Moez Ben. 2016. “Effect of surface treatment on the shear strength of aluminium adhesive single-lap joints for automotive applications”. International Journal of Adhesion and Adhesives 67: 38-43.
18. Correia Sergio, Anes Vitor, Reis Luis. 2018. “Effect of surface treatment on adhesively bonded aluminium-aluminium joints regarding aeronautical structures”. Engineering Failure Analysis 84: 34–45.
19. Akhavan-Safar Alireza, Ayatollahi Majid, Da Silva Lucas. 2017. “Strength prediction of adhesively bonded single lap joints with different bondline thicknesses: a critical longitudinal strain approach”. International Journal of Solids Structures 109: 189–98.
20. De Sousa Christopher, Campilho Raul, Marques Eduard, Costa Marcelo, Da Silva Lucas. 2017. “Overview of different strength prediction techniques for single-lap bonded joints”. Proceedings of the Institution of Mechanical Engineers Part L Journal of Materials Design and Applications 231(1-2): 210–223.
21. Jouan Alexandre, Constantinescu Andrei. 2018. “A critical comparison of shear tests for adhesive joints”. International Journal of Adhesion and Adhesives 84: 63–79.
22. Rangaswamy Hanumantharaya, Sogalad Irappa, Basavarajappa, S., Acharya Santhosh, Patel Manjunath. “Experimental analysis and prediction of strength of adhesive-bonded single-lap composite joints: Taguchi and artificial neural network approaches”. SN Applied Sciences 2: 1055.

TiAM kwartalnik naukowo-techniczny
TECHNOLOGIA I AUTOMATYZACJA MONTAŻU
ZESPOŁÓW • MASZYN • URZĄDZEŃ

Paula Kolbusz[1]

DOI: 10.7862/tiam.2022.4.2

THE USE OF THE SIX SIGMA METHODOLOGY IN A PROJECT IMPROVING THE MANUFACTURING PROCESS

WYKORZYSTANIE METODOLOGII SIX SIGMA W PROJEKCIE USPRAWNIAJĄCYM PROCES PRODUKCYJNY

Abstract

In the current, full of technological novelties, companies that want to maintain their position on the market are obliged to implement continuous improvement of their operations. A frequent and recently popular phenomenon is the creation of workplaces in organizations for specialists in the field of continuous improvement. Improvement is a laborious and long-lasting process. The activities of the company that create added value for the customer should be improved, in other words they increase the competitive advantage on the market, then they will be effective for the company. The article presents the possibility of using the Six Sigma methodology to improve the efficiency of the production process of a rubber product on one of the production lines. To achieve the intended goal, qualitative and quantitative research methods were used to analyze the results obtained as part of the company's case study. In addition, the statistical analysis of the obtained results allowed to identify factors in the areas affecting the efficiency of the manufacturing process and to determine the action plan identifying the actions that should be implemented to improve the production process.

Keywords: improvement of the production process, DMAIC, Six Sigma

Streszczenie

W obecnych, pełnych nowinek technologicznych firmach, które chcą utrzymać swoją pozycję na rynku, zobligowane jest do ciągłego doskonalenia swojej działalności. Częstym i ostatnio popularnym zjawiskiem jest tworzenie w organizacjach miejsc pracy dla specjalistów z zakresu ciągłego doskonalenia. Doskonalenie jest pracochłonnym i długotrwałym procesem. Działania firmy, które tworzą wartość dodaną dla klienta powinny być doskonalone, czyli zwiększają przewagę konkurencyjną na rynku, wtedy będą efektywne dla firmy. W artykule przedstawiono możliwości wykorzystania metodyki Six Sigma do poprawy efektywności procesu produkcji wyrobu gumowego na jednej z linii produkcyjnych. Aby osiągnąć zamierzony cel, zastosowano jakościowe i ilościowe metody badawcze do analizy wyników uzyskanych w ramach studium przypadku firmy. Ponadto analiza statystyczna uzyskanych wyników pozwoliła zidentyfikować czynniki w obszarach wpływających na efektywność procesu produkcyjnego oraz ustalić plan działania określający działania, które należy wdrożyć, aby usprawnić proces produkcyjny.

Słowa kluczowe: doskonalenie procesu produkcyjnego, DMAIC, Six Sigma

1. Introduction

In the automotive industry, an often heard term is "striving for the highest quality". The 70s of the twentieth century were abundant in ideologies and strategies for improving the level of quality and productivity in enterprises. The topics of the concepts in question were focused on the foundations of competitiveness, including: quality indicators, production costs of the final product and timeliness of deliveries. The growing pace of technology development, increasing customer requirements not only as to the quality of the product offered by the company, but also the time of production and delivery, are aspects that the management of enterprises is currently struggling with. Many institutions have been obliged to work at a high level of quality (Bogdanienko, 2011).

In the last century, mass production was developed, which is associated with a greater possibility of production errors, which resulted in an increase in demand for quality control of products. The very term of the word perfection derives from the Latin word "perfectio", which literally means "to do something, to do to the end", that is, it defines "accomplishment,

[1] Paula Kolbusz, Politechnika Rzeszowska, Szkoła Doktorska Nauk Inżynieryjno-Technicznych, Al. Powstańców Warszawy 12, 35-959 Rzeszów, ORCID: 0000-0002-6058-041X.

finishing". This idea was extended by Tatarkiewicz and defined perfection as "that which fulfills all its proper functions and that which has achieved its goal, something that is simple, uniform, non-complex". The term improvement is replaced by "improving, modernizing, changing.

Six Sigma was implemented in the mid-80s by Bill Smith and Bob Galvin at Motorola, for which the American Quality Award was received, the methodology was used as a production training program in organizations (Watson and DeYong, 2010). This approach was initially based on areas in the electronics industry, only later reached many other sectors (Arnheiter and Maleyeff, 2005). Six Sigma spent years developing until it evolved into a comprehensive quality management system, called TQM (Green, 2006). Over the past twenty years, the methodology has become more common as its principles have also been implemented in service industries in the context of the supply chain (Wei et al., 2010), as well as hospitals, local governments and the public sector (Arnheiter and Maleyeff, 2005).

As a project-based approach to management, the scope of Six Sigma implementation now also includes continuous cost reduction in the company by reducing losses resulting from insufficient quality. In order to determine this method, customer expectations were examined in order to determine critical values for and goals for individual levels of company management were defined (Kwak and Anbari, 2006).

The aim of this study is to analyze the use of the Six Sigma methodology to improve the efficiency of the production process in a selected enterprise. The structure of the article is as follows: Chapter 2 presents the research methodology, Chapter 3 presents the Six Sigma tools used for a specific case study. However, the conclusions are set out in Chapter 4.

2. Purpose and methodology of research

2.1. Six Sigma in practice

The foundation of both ideologies and productivity improvements in the company is the practice of activities according to the management philosophy, which is focused on the quality of the product or service (Total Quality Management), while others focus on the entire restructuring of processes in the enterprise (Business Process Reengineering, Just In Time). The activities of another group of concepts were focused on reducing and finally completely eliminating waste (Lean Management) or on increasing the stateof seriousness in processes focused on the critical characteristics of the finished product (Six Sigma). The last two methodologies were combined into one in this way, obtaining Lean Six Sigma (LSS).

In a recent review of the literature, it will distinguish the spread of LSS in four important sectors of the economy: manufacturing, healthcare, finance and education. It will also presentthe critical barriers and benefits of implementing this methodology. A companies using Lean Six Sigma must be awareof the challenges and success factors when implementing LSS in various sectors of the company, such as production, finance, human resourcese. The effects of the use of LSS are, among other things: reduction of waste, defects and improvement of the process, which in turn ensures high-quality products at minimal cost, and this leads to customer satisfaction, which ultimately raises the standard of social life.

The economy have been forced to retaliate by becoming more aware of sustainability and the requirements for environmentally friendly products to reflect on their business operations. In most countries, traditional methods of producing and using fossil fuels have been adopted in industries. Manufacturing industries in developed countries release four times less dioxideto coal compared to emerging countries. Therefore, for the sake of society and environmental protection, the industrial sector is obliged to take into account green technologies and in its activities. Over the past tenyears, many ideas and approaches have developed, such as Lean, Green, Six Sigma to produce the highest quality products.

The composition of GLS consists of three unique approaches, i.e. Green, Lean and Six Sigma, through which the dynamics of profitability are increased by reducing emissions, waste and reprocessing. Combined Green Lean Six Sigma is able to produce a product that is not only of high quality and cheap, but also friendly to environment. GLS combines Lean and Green waste in the defining phase of the DMAIC Six Sigma methodology. Ubecomes and investigates the causes of process-related waste and emissions. Then, possible solutions are sought for improvements in different dimensions of organizational sustainability. The next stage is to wdrożenie the best solution to it, and the performance is used for further development.

In the history and industrial revolutions of the last three centuries, it highlights the transition from power sources through automation, information technology and automated manufacturing, to connectivity. Industry 4.0 has been defined by the World Economic Forum as the latest industrial revolution that revolves around the so-called cyber-physical era, with this revolution occurring with the integration of the physical and digital worlds through the proliferation of sensors and devices forming a connected ecosystem. Froma customer-centric product cycle approach to a customer-centric experience cycle, it has been implemented as a result of the fourth revolution. This

means that the customeris involved in the product life cycle from concept to post-purchase feedback, and customer experience has been included as the key to the success of companies, in every sector. In the literature, the term Industry 4.0 means a profound change in many sectors: from production to use. Industry 4.0 is able to create value throughout the life cycle of a product, process or service. For the reasons described above, the effect of this revolution can be an object, but also a service designed for the end user, the development of which is driven by innovation in several areas: IT, mechanical engineering, embedded systems, manufacturing, automation technology and all these combined to provide the more complex systems that are known today. The automotive industry is experimenting with new challenges and frontiers with so-called autonomous and connected vehicles, which are "smart" and completely connected to the rest of the world thanks to internet technologies.

2.2. Description of the company covered by the case study

The research was carried out in a company that has been active in the Automotive industry for years. The main goal of the group is to create products that are comfortable, safe and at attractive prices for the user. The expertise of the corporation includes such industries as:

- Sealing of the structure,
- Precision tightness,
- Fluid flow monitoring,
- Materials and structures,
- Anti-vibration systems,
- Transmission systems.

The selected company specializes in the tightness of structures and in the automotive industry. It is a market full of stringent requirements and specific requirements. The advantages of these products include: comfort of use, energy result and protection. The products met are: reduction of pollutant emissions and the level of energy consumption, acoustic result, proper management of thermal consequences, optimization of mechanical force, weight reduction and reduction of dimensions without compromising the quality of manufactured products. The activity of the company in which the case study was examined dates back to the second half of 2017 and the manufactured products are thermoplastic seals and rubber seals. The production area of rubber processing, which is the production line, was selected for the analysis. Which includes: extruders, metal accumulators, furnaces, mastic machine, rubber profile transporters, cutting machine, welding machines. The analyzed area is the finishing operation performed after extruding the rubber profile, which consists in stiffening the area of the trunk gasket.

2.3. Research problem

The main problem of the process under study is the increased percentage of non-compliant parts. This is due to the fact that insufficiently strong connection of the gasket was observed or incorrectly glued together at the site of the incision, which is used to stiffen it. The consequence is the disposal of poorly prepared final product, increased working cycle time and greater - than expected - consumption of production components. This contributes to the overall increase in the cost of production of the finished product. The increase in production costs causes the weakening of the company's role on the market, in addition, it may happen that an inadequately prepared final product will not be stopped at the final inspection, it is tantamount to a complaint from the customer and his dissatisfaction, and thus in the future may have an impact on reducing the company's market share.

Therefore, the following research problem was defined: identification of factors affecting the high and unstable percentage of recoil of the part – during the final inspection after the stiffening process for the trunk gasket. Part of the analysis of the problem was also to definition actions that should be identified and then validated in order to improve the described process.

2.4. Description of the manufacturing process of the case study

The production process of rubber processing products is a complex process. The production of products is a large number of stages during which the presence of specialists is necessary: from designers, CAD specialists through technologists, process engineers, people responsible for material, employees responsible for machines, to the quality department and production line operators. The beginnings of production are already in CAD programs, where a drawing with functional characteristics and dimensional tolerances was created. On the basis of the customer's drawing, was designed with the appropriate extrusion mold, thanks to which he will give the gasket the desired shape that meets the drawing requirements with an accuracy of 1 mm. When all machines and tools were prepared along the production line, this was initiated proces of manufacturing under the supervision of a team of specialists.

The metal was stretched using a roller system, which is the skeleton of the gasket cross-section. At the same time, rubber compounds were taken from the containers for extruders under the set pressure and temperature. The rubber is transported through the

moulds and the seal is given the right shape. The next step is an alternating vulcanization process in furnaces and cooling in cooling baths. Thanks to such operation, the correct properties of the product were obtained. After verification that the vulcanization process was successful, the product is subjected to laser firing of vent holes and in the laser printerit burns the appropriate identification print. Then, using the special cut machine with programm the product was cut into pieces of appropriate length. The final stages are thermal bonding of the product, final inspection and packaging.

One of the profiles belonging to the design of products from the Z group requires an additional operation, which is the stiffening process, called the process X. This product is called with the Y profile and it is a gasket for trunk doors. Due to its purpose, it has a longer dimension than other profiles, which is why it requires strengthening. For this purpose, in a defined place, a special tool is made about the incision. Previously prepared with a stiffening element, for this purpose cut by it into drawing lengths and glue it at one end, which allows it to be placed inside the product. In addition, it is a solution that facilitates the process X. The process X itself requires manual skills and precision. The stiffening element islocated through the cut hole, then with the appropriate material it is dried at the incision site and glued together with quick-drying glue. The final stage is visual inspection and packaging of the gasket into serial packaging according to the defined packaging instructions of the finished product.

2.5. Research methodology

The start in Six Sigma began with a start with measurements and collecting the results of analyzes obtained from them. First of all, it is necessary to determine: parameters, places and methodology of measurements. These are the decisive points for the quality, process and cost of the organization. Methodology is a meticulous representation of the actual state. Collecting the results from the measurements is the basis for the analysis of the process in the verified research project. The conclusions drawn on the basis of the assessment are a factor for the implementation of corrective actions and then a plan for continuous improvement. The continuous duration of this process is due to the repetitive circus of the stairs (Fig. 1).

To analyze the research problem, the Six Sigma methodology based on the phases of the DMAIC cycle, i.e. Define, Measure, Analyse, Improve and Control, was used.

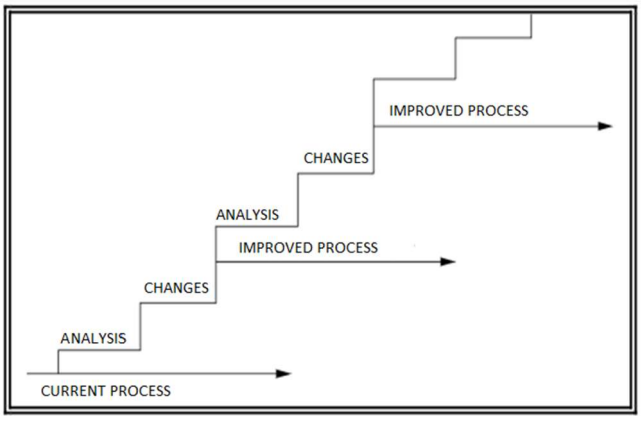

Figure 1. Map of the way of improvement.

In the first of these phases:

- a project card has been prepared to define the problem,
- the process under investigation has been identified on the basis of the SIPIOC method,
- milestones and project costs have been established.

In the next phase:

- a data collection plan has been defined,
- a preliminary analysis of the collected data was carried out,
- it has been checked whether the current measurement system is functioning correctly.

The Analysis phase of the Six Sigma project concerned:

- from defining the current process capacity,
- identification of the root cause when using various Six Sigma tools.

In the fourth phase of the SS project under discussion:

- initial improvements to the process in question have been made,
- a plan of corrective actions has been developed,
- FMEA analysis of potential improvements was performed.

During the Control phase:

- an audit plan has been drawn up,
- re-collected from the process,
- the implemented improvements were assessed on the basis of the current capacity of the process.

3. Implementation of the Six Sigma methodology for process analysis – case study

3.1. The Six Sigma Project – faza definition

The first activity of the project team was to define the problem to be faced – the preparation of a Project charter. Project charter, otherwise known as the

Project Charter, is a description of the problem in a way that everyone can understand, facilitates communication between team members as well as other interested parties who may have their share in the project. The project charter should be as precise as possible. It consists of the following elements (Fig. 2):

- define a problem,
- define a specific goal,
- setting the expected goals,
- define constant process with which the problem is associated,
- selection of appropriate team members,
- define project milestone amine.

During the first phase of the DMAIC cycle was also defined SIPOC, in which individual letters are an abbreviation of English words, successively: suppliers, inputs, process, outputs, customers. This tool illustrates the process that has been analysed and will enable team members to unanimously define the results and aspects that can have an impact in the search for strengths and weaknesses in the research project (Figure 3).

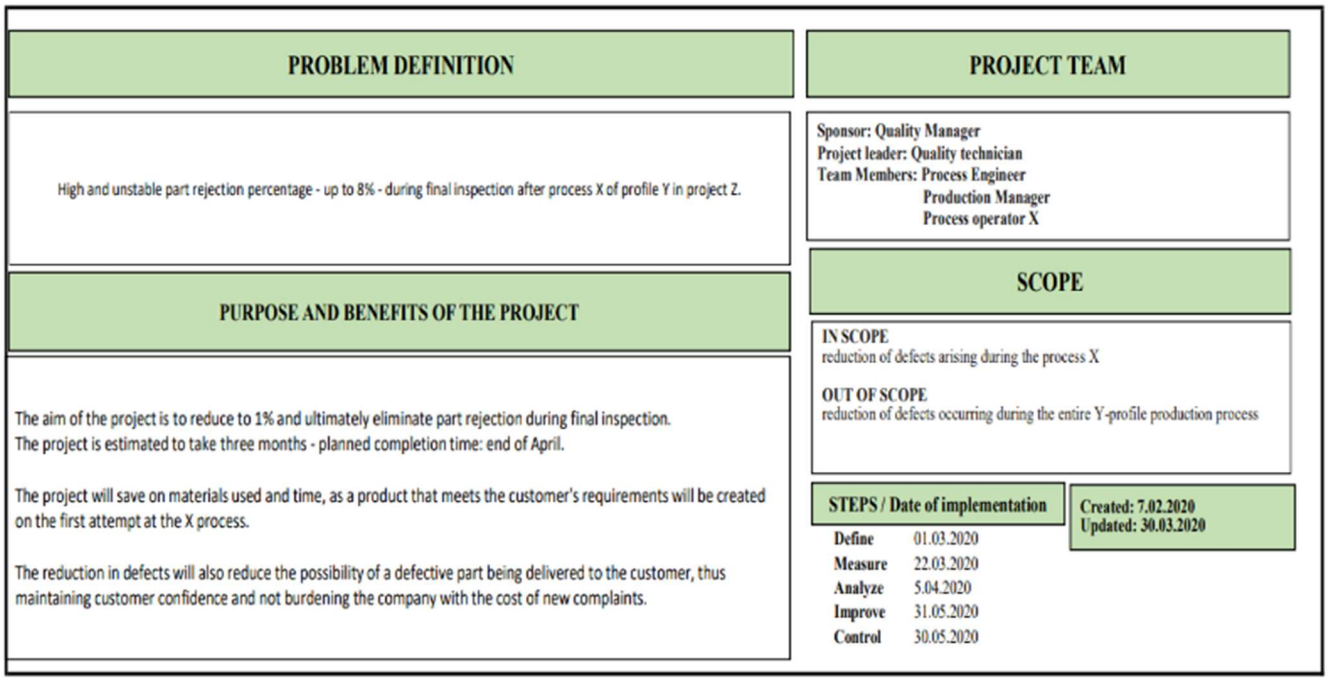

Figure 2. Project card for the issue under consideration

Suppliers	Inputs	Process	Output	Customers
EPDM extrusion	Extruded seal	Cut the gasket in the right place	Product meeting customer requirements	External customer
Glue supplier	Glue		Customer satisfaction	Sorting company
Supplier of structural reinforcement element - spline	Stiffening element	Location of the stiffening element - spline	Rejection - non-compliant product	Facility Director
Supplier of incision tools for the insertion of a reinforcing element	Notching tool		Product to be repaired	Quality manager
Supplier of line gauges	Material for drying the incision site	Sealing the incision site	Report with the results of the final audit	EPDM extrusion area manager
Supplier of tools for dispensing glue into the notch area	Solution for positioning the stiffening element	Final control of the plugging process		
	Linear gauge			

Figure 3. SIPOC of this Six Sigma project

In the first phase of the streamlining projects, a tool called the voice of the customer was also used. Taking into account that these are opinions of a general nature, it is important to specify the customer's requirements to which these opinions relate on the basis of the collected data. The precise, measurable requirements in question are called CTQ (Critical to Quality), in other words, product properties or process parameters that are critical to the customer – having a significant impact on his approval (Table 1).

Table 1. Defined CTQ in a Six Sigma project

CTQ	
percentage of non-compliant products	Feature of the process
percentage value of products that do not comply with customer requirements	Measure
max 1% of non-compliant products	Target
99% probability that 1% of non-compliant products will appear	Required result

CTQ is also presented using another form – elements in the form of a tree (Fig. 4).

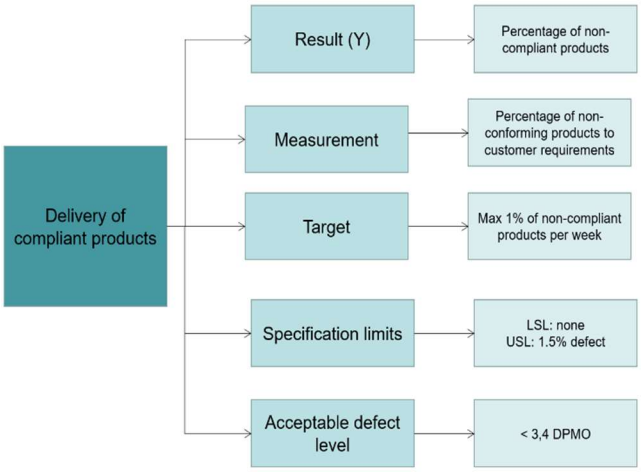

Figure 4. CTQ tree of the improvement project in question

3.2. Six Sigma project – measurement phase

In order to achieve the expected values of the number of non-compliant parts during the final inspection after the X process, data was collected, which was collected from the 39th week of 2020 to the end of this year. On the basis of this information, such defects as: incorrect seal joining, visible metal part, displacement of the edge of the gasket at the place of joining, incorrect gluing of the incision site, impurities, lumps, foreign bodies, gasket deformation, bad identification labels, visible metal part at the place of joining and others were distinguished.

Table 2. Collected data on defects in 2020

% of recoil	71 456	Controled parts	Results
3,18%	2 269	NOK parts	
30,41%	690	Incorrect gasket connection	Defect names
0,00%	0	Visible metal part	
2,51%	57	Offset on gasket connection	
51,17%	1161	Incorrect gluing of the incision	
11,90%	270	Pollution	
0,40%	9	Papules	
0,75%	17	Foreign body	
1,28%	29	Deformed gasket	
0,22%	5	Wrong label	
0,48%	11	Visible metal part	
0,84%	19	Other	

With the help of Pareto-Lorenz diagram, they show that the greatest deficiencies can be observed during the stage of gluing the incision site, necessary to carry out the X process. Thanks to the use of this diagram, the defect that generated the largest number of rejected parts was selected and further design steps were focused on its improvement.

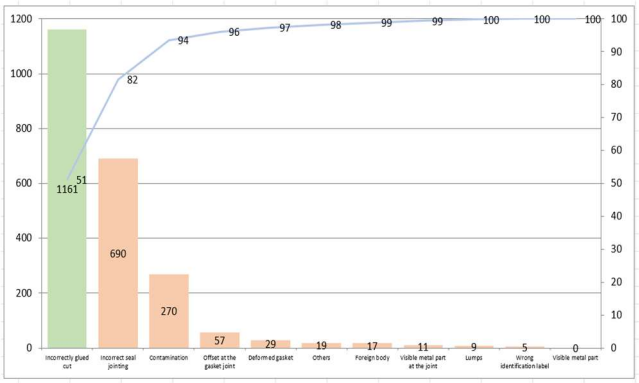

Chart 1. Pareto diagram – Lorenz defects during process X for results from the second half of last year

In order to go through this stage of analysis and then process improvement, it was necessary to verify whether the current measurement system, which is the pattern control of defects, works correctly. For this purpose, a system analysis was carried out using the Kappa method of MSA testing for attribute data. The studywas attended by 3 operators and an expert. Each member of the study had the task of verifying 50 finished products on a NOK/OK basis by visual inspection, assuming that half were OK and the other half were NOK. The products were given three times for inspection in random order. Then, the results of the operators were compared with an expert (Table 3).

Table 3. Results of MSA analysis by Kappa method

Ustalenie danych z badania oceną alternatywną

Część	A-1	A-2	A-3	B-1	B-2	B-3	C-1	C-2	C-3	Ekspert
1	1	1	1	1	1	1	1	1	1	1
2	1	1	1	1	1	1	1	1	1	1
3	1	1	1	1	1	1	1	1	1	1
4	1	1	1	1	1	1	1	1	1	1
5	0	0	0	0	0	0	0	0	0	0
6	0	0	0	0	0	0	0	0	0	0
7	0	0	0	0	0	0	0	0	0	0
8	0	0	0	0	0	0	0	0	0	0
9	1	1	1	1	1	1	1	1	1	1
10	1	1	1	1	1	0	1	1	1	1
11	1	1	1	1	1	1	1	1	1	1
12	0	0	0	0	0	0	0	0	0	0
13	0	0	0	0	0	0	0	0	0	0
14	0	0	0	0	0	0	0	0	0	0
15	1	1	1	1	1	1	1	1	1	1
16	1	1	1	1	1	1	1	1	1	1
17	1	1	1	1	1	1	1	1	1	1
18	0	0	0	0	0	0	0	0	0	0
19	0	0	0	0	0	0	0	0	0	0
20	0	0	0	0	0	0	0	0	0	0
21	1	1	1	1	1	1	1	1	1	1
22	1	1	1	1	1	1	1	1	1	1
23	1	1	1	1	1	1	1	1	1	1
24	1	1	1	1	1	1	1	1	0	1
25	0	0	0	0	0	0	0	0	0	0
26	0	0	0	0	0	0	0	0	0	0
27	0	0	0	0	0	0	0	0	0	0
28	0	0	0	0	0	0	0	0	0	0
29	1	1	1	1	1	1	1	1	1	1
30	1	1	1	1	1	1	1	1	1	1
31	1	1	1	1	1	1	1	1	1	1
32	0	0	0	0	0	0	0	0	0	0
33	0	0	0	0	0	0	0	0	0	0
34	0	0	0	0	0	0	0	0	0	0
35	0	0	0	0	0	0	0	0	0	0
36	1	1	1	1	1	1	1	1	1	1
37	1	1	1	1	1	1	1	1	1	1
38	1	1	1	1	1	1	1	1	1	1
39	1	1	1	1	1	1	1	1	1	1
40	0	0	0	0	0	0	0	0	0	0
41	0	0	0	0	0	0	0	0	0	0
42	0	0	0	0	0	0	0	0	0	0
43	0	0	0	0	0	0	0	0	0	0
44	1	1	0	1	1	1	1	1	1	1
45	1	1	1	1	1	1	1	1	1	1
46	1	1	1	1	1	1	1	1	1	1
47	1	1	1	1	1	1	1	1	1	1
48	0	0	0	0	0	0	0	0	0	0
49	0	0	0	0	0	0	0	0	0	0
50	0	0	0	0	0	0	0	0	0	0

Wyniki badania:

		A	B	C	E
k (Kappa)	A	-	97%	96%	99%
	B	-	-	96%	99%
	C	-	-	-	97%
skuteczność		98%	98%	98%	-
fałszywy alarm		1%	1%	3%	-
niewychwycenie		0%	0%	0%	-

Kryteria		
>=90%	>=80%	< 80%
<=5%	<=10%	>10%
=0%	<=5%	> 5%

Decyzja	System zgodny

The success of a streamlining project depends mainly on the definition of the method of conducting the research, its appropriatebymeasures and procedures. All attributes used must be adequate to the assumed improvement of the critical feature. To this end, it will draw up the so-called Data Collection Plan taking into account the elements in question (Table 4).

Table 4. Data collection plan for the implemented improvement project

CTQ	Adequate % of non-compliant products during process X
Variable	% of product waste
Measure type	N/A
Data type	Quantities of NOK pieces, attribute data
Operational definition	Daily data at the process station X collected every day, on each shift, the number of PIECES OF SAI for each container with 88 pieces is stored
Measurement procedure	Visual assessment of the ART OF NOK/OK Measurement is made by each change – measurement is made after operation X – measurement is made by the person responsible for the final control – the measurement is recorded on the data collection sheet
Measuring system	The measurement is made by visual method by the final inspection operator at the X operation station
Measurement unit	Pieces OK./NOK
Sampling time	Period of 6 months – from week 39
Sample size	Any process X
X	The operator who evaluates the attribute data. The change on which the attribute data is collected. The date on which the data was retrieved.

Having confirmed the effectiveness of the measurement system, it was determined that the data will be collected after the improvements for the next 8 weeks according to a team-defined data collection sheet.

3.3. Six Sigma Project – Analysis Phase

The following are the results of the % recoil of non-compliant parts in the weeks in which the production process of the Y-profile took place (chart 2).

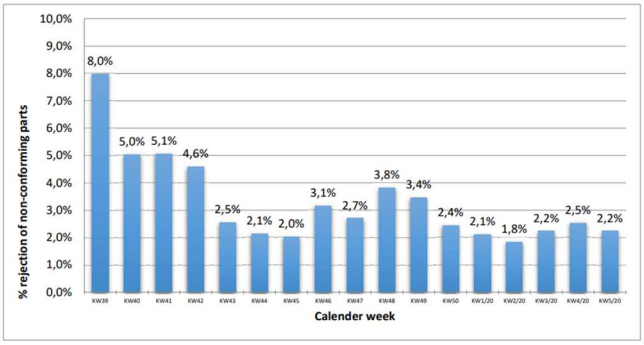

Chart 2. Weekly final inspection results during process X for results from the second half of last year

During the eight-week inspection, decrease in the level of recoil was observed compared to week 39, but it is still not a target value, as it fluctuates between 1.8% – 3.8%. Taking into account the results so far, the current capacity of the process was calculated. To calculate it with the attribute CTQ, use:

- Sample size: 71456, i.e. 812 containers of 88 pieces in each,
- Measures of process capability:
  - ✓ % defects = 3.18%,
  - ✓ Number of critical characteristics per unit = = 11,
  - ✓ DPU = 8,8,
  - ✓ DPMO = 31754,
  - ✓ Process Sigma Level = 3.4.

In this step a project team was organized in order to brainstorm the root causes of the problem.

The Ishikawa cause and effect diagram, otherwise known as "fish bone", is a popular quality management tool that allows you to learn about the inconsistencies occurring at the workplace in question and specify the root cause of the problem. Project teams often use them because it standardizes thoughts – the schematic fish bone graphically presents the relationships between the causes and their hierarchy, which results in a chronological and logical ordering of the factors causing the problem. This diagram should be handled using the following steps:

1. Defining the problem.
2. Determination of the category of causes.
3. Brainstorming the factors in each category.

Actions should begin with the collection of data on the occurrence of a defect or deviation in the process. This is a necessary operation to identify the root cause of the problem. An inherent element of this tool is the selection of a working group that will jointly analyze this problem, including operators who deal with the manufacturing process on a daily basis – this will facilitate accurate and clear determination of the sub-incompatibility.

In this improvement project based on an earlier analysis using the Pareto-Lorenz diagram , it is known that the largest percentage of rejected parts during the final inspection has a disadvantage: incorrect gluing of the incision site. It is understood as: a cracking incision place, or an unsightly gluing of this place – an excess of glue. Ishikawa's diagram (Fig. 5) showed that this problem is influenced by many different aspects. By giving the reason a weight according to the scale: 8, 6, 4, 2 and 1, with the assumption that each digit can be used once, the project team assigned them to the reasons, as follows:

8 – do not dry the gasket at the incision site
6 – glue stored in inappropriate conditions
4 – failure to act according to the standard of work
2 – inappropriate method of gasket incision
1 – lack of employee control during operation X

Thanks to this classification, the project team was able to focus improvement activities on those root causes that have the most significant impact.

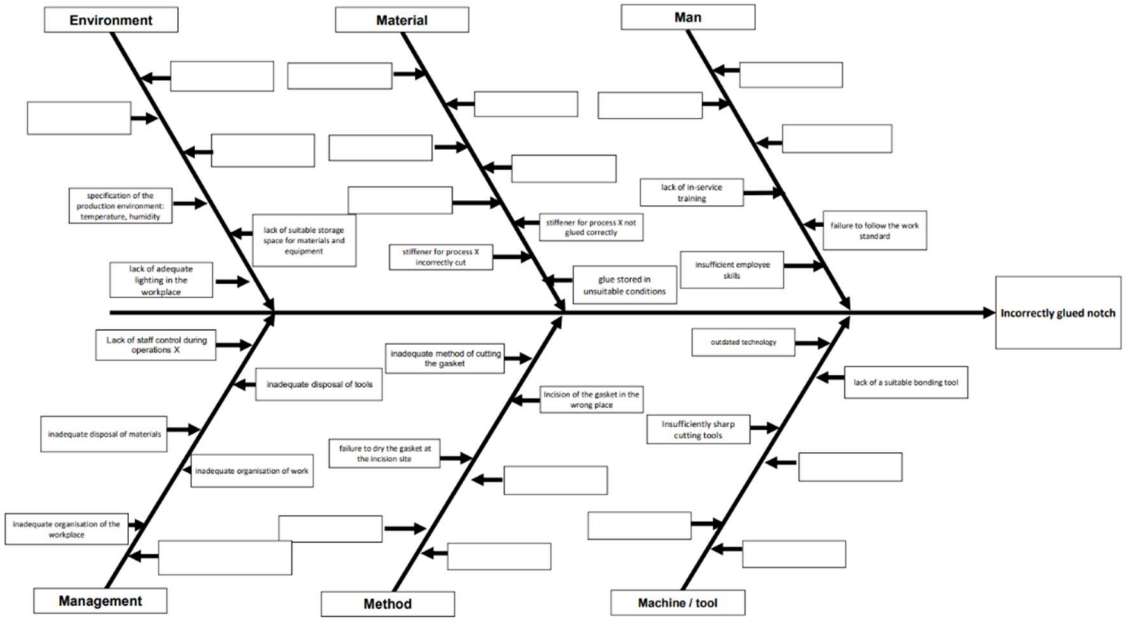

Figure 5. Ishikawa cause-and-effect diagram

After the Ishikawa cause-and-effect diagram was completed, an analysis was performed using a technique called 5WHY. The statement should be based on two grounds, i.e. the cause of the occurrence and the reason for not detecting the error. The firstfactor defines the reason why the defective product was manufactured, so the technological approach was used in this case. The second factor concerns the method of control, the group examining the case wonders why, despite the supervision of the process, the error was not detected in the standard procedure.

A similar scheme of action was used in the discussed research problem, which is why the nextyear was to use the 5WHY technique to understand why the defect, which is the incorrect gluing of the incision, arose. This problem was considered in two planes, i.e. in the aspect of the occurrence of errors and then in the sphere of not finding this error during visual inspection (Fig. 6). During the use of the 5WHY technique, it was shown that source deficiencies were found already in the work manual and the standard of work performed by the final control operator.

Presentation	1WHY	2WHY	3WHY	4WHY	5WHY
Incorrectly glued notch	The glue has dried, the bonding area has cracked	Lack of suitable adhesive properties	At the time of gluing, the incision site was dry, but a solution remained in the gasket channel to accommodate the stiffening element	The operator did not wait sufficient time after placing the stiffener and before bonding	The waiting time is not clearly defined in the work instructions
Non-detection	**1WHY**	**2WHY**	**3WHY**	**4WHY**	**5WHY**
Incorrectly glued notch	The operator performing process X did not notice the bonding error	At the time of gluing, the defect is not visible	The defect becomes apparent after a period of time when the solution for placing the stiffener flows from the gasket channel to the incision site	Operator did not wait adequate time after bonding to verify it	Failure to maintain standard of work during final inspection

Figure 6. The use of the 5WHY technique for the problem under consideration

3.4. Six Sigma Project – Improvement Phase

On the basis of the analysis, the following reasons were selected in the improvement process:

- not drying the gasket at the place of incision,
- glue stored in inappropriate conditions,
- lack of compliance with the standard of work,
- inadequate method of incision of the gasket,
- lack of employee control during operation X.

Meetings of the working group allowed forthe organizationof the Planat corrective actions (tab. 5).

Table 5. Corrective action plan for improving process X

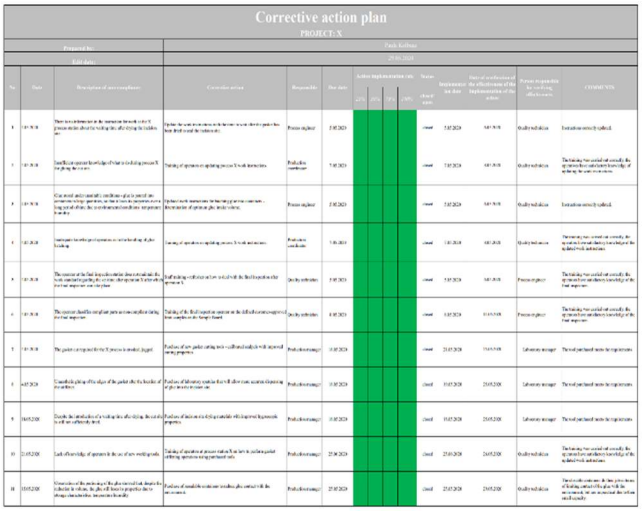

Corrective action plan

PROJECT-X

The Corrective Action Plan defines 11 corrective actions to improve process X. The main process activities are the replacement of tools intended for operation X, and then training operators in the standard of work at the workplace using these instruments. In addition, final inspection operators were reminded of the rules and boundary samples categorizing finished products as compliant and non-compliant.

In addition, the FMEA was updated during this phase of the Six Sigma project. This tool allows you to prevent the occurrence of non-compliance in the production process. In addition to identifying errors, it allows you to determine the risk they are burdened with. Errors include both the finished product and the manufacturing process. Knowing the cause that caused the problem, you can limit its occurrence or completely eliminate it. This method can also be used to understand and analyze risks already at the product and process planning stage. Below are the possibilities of using this method:

- development of new projects,
- process optimization,
- start of production in the series,
- elimination of process variability.

The purposeof the FMEA is to constantly look for errors that can occur for both the product and the manufacturing. Knowing the potential threat, preventive actions are taken that will minimize or completely eliminate the cause of the probable error. This results in the continuous improvement of the company's activities in the areas that are covered by the above activities. The essence of using FMEA is to isolate and understand the factors affecting the problematic fulfillment of specificationand technical requirements or the stability of the manufacturing process.

When using FMEA, a group of several people usually from 4 to 8 uses a scheme of action (Fig. 7).

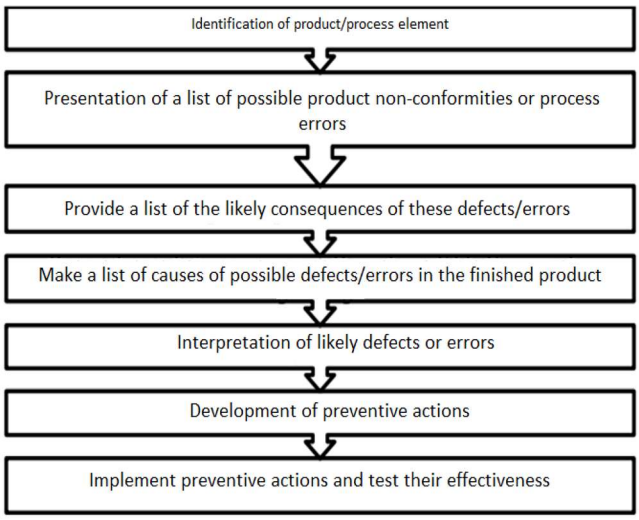

Figure 7. FMEA operation diagram

Knowing the area of occurrence of the error, actions were taken to identify other possible defects and their effects. The existing security system was classified in terms of preventing and detecting these potential errors. The FMEA method was used for this purpose. The disadvantages with the highest number of LPR are the crack at the gluing site and the final inspection not in accordance with the standard of work (tab. 6).

Table 6. FMEA for process X

Proces	Potential defect	Potential effect	L P W	Potential cause	The current process of prevention	L P Z	The current detection process	L P O	LPR	Actions	Person responsible	Due date	L P W	L P Z	L P O	LPR
X	Crack in the notch of the Y-profile.	Possibility of leakage, change of location of stiffening element / functional defect.	8	Employee - failure to comply with dedicated work instructions.	Work instructions dedicated to process X.	7	Final inspection operator at process station X. Visual method.	5	280	Update of work instructions on process X. Staff training on updates.	Process Engineer, Production Manager	7.05.2020	3	5	3	45
			8	Use of inappropriate tools at the workplace.	Work instructions dedicated to process X.	7	Final inspection operator at process station X. Visual method.	5	280	Purchase of new tools at process station X.	Production Manager, Laboratory Manager	22.05.2020	3	5	3	45
	Incorrect position of brace element.	Functional defect - gasket stiffened in a different location than per drawing recommendations.	3	Incorrect use of the instrument for measuring the position of the brace element.	Work instructions dedicated to process X.	6	Final inspection operator at process station X. Visual method.	5	90	Introducing a standard for measuring with a gauge, Training of operators.	Quality technician, production manager	31.05.2020	2	4	3	24
	Glue contamination around the incision site.	Aesthetic flaw, surface not visible.	6	Lack of a precise tool to dispense adhesive into the notch, not meeting the requirements of the adhesive properties.	Work instructions dedicated to process X.	1	Final inspection operator at process station X. Visual method.	3	18	Replacement of the glue dispensing tool in place of the notched, defined maximum glue intake volume.	Quality technician, Laboratory manager, Production manager	28.05.2020	4	1	3	12
	Gasket cut in a different location - scratch on Y profile.	Visual defect - visible as well as invisible side.	2	Inattention of the operator, lack of concentration on doing the job.	A work instruction dedicated to process X, which defines how to use the tools.	7	Final inspection operator at process station X. Visual method.	3	42	Re-training of operators in the use of equipment on the job site.	Quality technician, process engineer	31.05.2020	1	7	3	21
	Lighting damage at the final inspection station.	Possibility of non-compliance not being detected during final inspection.	2	Worn-out light bulb.	Maintenance activities - checking the lighting at the workstation once a month.	6	Final inspection operator at process station X. Visual method.	6	72	Increase workplace lighting inspections to twice a month.	Maintenance staff	30.06.2020	2	6	3	36
	Inspection not in accordance with the final inspection instructions and the Table Samples.	Non-compliant part qualified as compliant or reversed.	5	Inadequate staff knowledge of the final inspection standard.	Supervision of the final control operator's work by the shift leader.	5	Final inspection operator at the X operation station. Visual method. Table of Boundary Samples.	7	175	Training of employees in the execution of final inspection and Boundary Samples and internal audits by the quality technician once a week.	Quality technician	31.05.2020	3	5	5	75

3.5. Six Sigma Project – Control Phase

After the introduction of improvement activities, a process control was carried out according to the Control Plan (Table 7).

Table 7. Control plan for process X

Process control plan X

Process name	**Process X**	**Prepared by:**	**Quality technician**	**Page:**	**1 of 1**
Customer	**XXX**	**Checked:**	**Quality leader**	**Document number:**	**1**
Location	**YYY**	**Approved:**	**Quality manager**	**Date of revision:**	**31.05.2020**
Supplier	**Company XYZ**				

Process	Process step	CTQ		Specification	Specification limits	Measurement method	Sample size	Frequency	Person responsible	Recording of the result	Decision rule / Corrective action	Audit plan
		Process	Product		USL LSL							
X	Preparation of the stiffener		x	Length	Length range within tolerances: 900 +/- 10 mm	Linear gauge up to 1000 mm at process station X	1	100%	Process operator X responsible for the preparation of stiffeners	Process Characteristics Register X - R.01	If non-compliance occurs, follow procedure P.01 Dealing with non-compliance	Audit each day by a leader on each shift and a quality technician once a week
	Notch of the gasket at the location of the stiffener		x	Notch width	Width range within a tolerance of 10 +/- 2 mm	Linear gauge up to 20 mm at process station X	1	Raz na godzinę	Process operator X responsible for the preparation of stiffeners			
	Positioning of the stiffener in the gasket		x	Correct position	Position of the stiffener from the notch: 10 mm +/- 5 mm	Linear gauge up to 20 mm at process station X	1	100%	Process operator X responsible for placing element X in the seal			
	Drying the incision site		x	Moisture content of the incision site	No wet spots	Visual	1	100%	Process operator X responsible for drying the incision site			
	Bonding the incision site		x	Aesthetics	No glue stains	Visual	1	100%	Process operator X responsible for bonding			
	Final control		x	Product compliance	The characteristic limits are specified in the final control instruction KK.01	Visual	1	100%	Person performing the final control			

Control of action for 4 weeks. The results were recorded in the Final Control Sheet. After week 4, the results were collected and the percentage of recoil of non-compliant parts was calculated. Again, withthe help of the Pareto-Lorenz diagram, the dominant defect that has the greatest impact on the % of recoil during the final control is shown (chart 3).

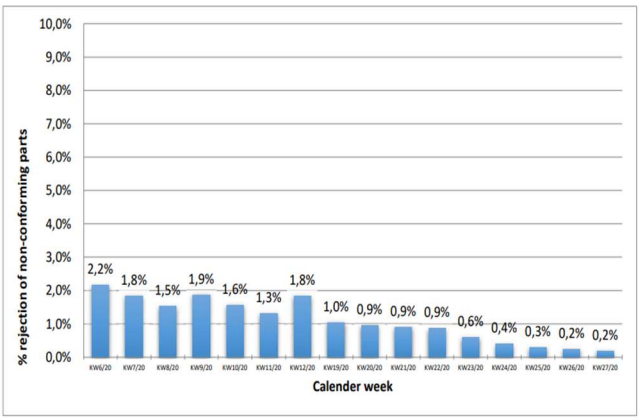

Chart 3. Results of the final inspection in weeks 6–27 of 2021

The results from the final control from the 6th week of 2021 were summarized (Table 8) and the Pareto-Lorenz diagram (chart 4) was made on their basis. It shows that this time the dominant defect is the incorrect gluing of the incision.

Table 8. Results of the final inspection for process X in weeks 6–27 of 2021

% of recoil	45 245	**Controled parts**	**Results**
1,03%	465	**NOK parts**	
30,32%	141	**Incorrect gasket connection**	**Defect names**
0,00%	0	**Visible metal part**	
10,54%	49	**Offset on gasket connection**	
38,92%	181	**Incorrect gluing of the incision**	
3,87%	18	**Pollution**	
0,00%	0	**Papules**	
0,00%	0	**Foreign body**	
0,43%	2	**Deformed gasket**	
0,00%	0	**Wrong label**	
0,22%	1	**Visible metal part**	
1,94%	9	**Other**	

Taking into account the results so far, the current capacity of the process was calculated. To determine it with the attribute CTQ, use:

- Sample size: 45245, i.e. 514 containers of 88 pieces in each
- Measures of process capability:
  - ✓ % defects = 1.03%,
  - ✓ Number of critical characteristics per unit = = 11,
  - ✓ DPU = 12,6,
  - ✓ DPMO = 9548,
  - ✓ Process Sigma Level = 3.8,

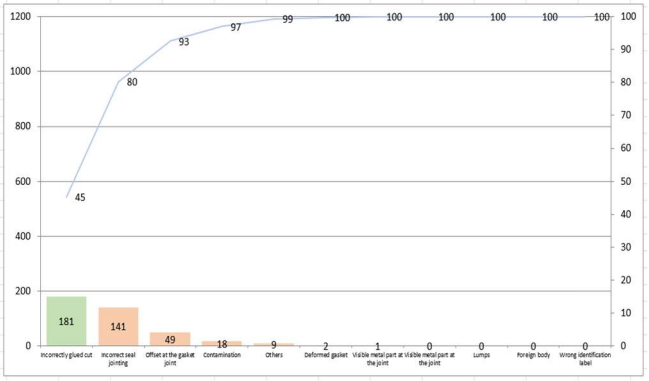

Chart 4. Pareto– Lorenz diagram of defects during process X for results in weeks 6–27 of 2021

4. Conclusions

The purpose of this study on the use of the Six Sigma methodology in process improvement in one of the selected companies was to present the possibilities of improving the manufacturing process in enterprises using the Six Sigma methodology. The implementation of this goal required analytical research to implement a project improving the process of manufacturing a rubber product. The selected problem concerned one of the stages of production, namely it was the stage of strengthening the product structure in the X process.

According to the described Six Sigma methodology and the assumptions of the DMAIC cycle, the project consisted of the following steps:

- DEFINE,
- MEASURMENT,
- ANALYZE,
- IMPROVE,
- CONTROL.

In each of the steps of the DMAIC cycle, many methods and tools characteristic of this methodology were used. The aim of the project was to reduce the percentage of recoil of non-compliant parts during the final inspection, which verifies the stiffening process, called the X process.

Comparing the final result that was obtained from the period of the 39th week of 2020 to the 6th week in 2021 with the result from the period after the implementation of corrective actions, it can be concluded that the project carried out brought the expected results. The percentage of recoil fell from 3.18% to 1.03%. The sum of non-compliant parts from the second half of 2020 is 2269, with as many as 1161 falling into the category of defect, which was incorrect gluing of the incision site and accounted for more than

half of all rejected parts, i.e. 51.17%, and the sigma level was 3.4. In weeks 6 to 27 in 2021, a lower percentage recoil of non-compliant parts can be observed during the final inspection. During this period, the sum of rejected non-compliant pieces was 465, where for the defect incorrect glued notch the result was 181, the percentage share of this category of defects to the total gives a result of 38.92%, which means that it shows a downward trend and decreased by 12%, the sigma level for this result is 3.8.

The improvement measures carried out were appropriate and allowed to reduce the weekly recoil of non-compliant parts by 8% to 0.2%. Activities related to updating documents, training andequipping the organization with equipment were carried out efficiently. The purchase of lockable containers with a smaller capacity used to store a sufficiently small volume of glue in them, which was intended to ensure a longer usefulness of the glue, was not a good solution. The containers are too small and thus make it difficult for operators to work, as the need to take glue from the chemical warehouse increases several times. In addition, a common case is the loss of caps and the glue containers themselves due to their small size. Therefore, it was decided to leave the existing containers taking into account the collection of smaller volumes of glue.

The charts of weekly discards tend to decrease, in my opinion, carrying out the inspection for the next 4 weeks would bring even better results than before.

References

1. Arnheiter E.D. and Maleyeff J. 2005), “The integration of lean management and Six Sigma”, The TQM Magazine, vol. 17, no. 1, pp. 5-18.
2. Bogacz P., Pulp M., Application of Lean Six Sigma in the improvement of production processes in the mining industry, Mineral Engineering, "Journal of the Polish Mineral Engineering Society", Kraków 2016.
3. Bogdanienko J., Knowledge and innovation in the company, National Defense Academy, Warsaw 2011.
4. Czyż-Gwiazda W., The Concept of Lean Management in Organization Management, Scientific Notebooks of the University of Economics in Katowice, No. 233, 2015.
5. Gupta S.K., Gunasekaran A., Antony J., Gupta S., Bag S., Roubaud D., Systematic literature review of project failures: Current trends and scope for future research, Computers & Industrial Engineering, Volume 127, Pages 274-285, 2019.
6. Huber Z., WHY Method 5, Issue 1, 2006.
7. Jagusiak-Kocik J., PDCA cycle as a part of continuous improvement in the production company – a case study, Production Engineering Archives, 14, 2017, 19-22.
8. Jednoróg A., Olejnik M., Torczewski K., The use of quality management methods and techniques in Polish enterprises, [in]: Six Sigma International Conference, Wrocław Technology Transfer Center, Wrocław 2004.
9. Kaswan M.S., Rathi R., Analysis and modeling the enablers of Green Lean Six Sigma implementation using Interpretive Structural Modeling, Journal of Cleaner Production, Volume 231, Pages 1182-1191, 2019.
10. Knop K., Mielczarek K., Aspects of improving the production process, Quality Scientific Notebooks. Production. Improvement, No. 1, Częstochowa 2015.
11. Carmelita K, Greber T., Determinants of the effectiveness of FMEA analysis, FMEA Center, [available at:] https://fmea.com.pl/determinanty-skutecznosci-analizy-fmea/, 22.05.2020.
12. Kwak Y.H. and Anbari F.T. (2006), "Benefits, Obstacles and future of Six Sigma approach", Technovation, vol. 26, no. 5-6, pp. 708-71.
13. Magnusson K., Six Sigma – a Quantity Improvement in Operating Performence, ABB BATPT, 1996.
14. Mazur A., Gołaś H., Principles, methods and techniques used in quality management, Poznan University of Technology, Poznan 2010.
15. Mikel H., The Vision of Six Sigma – A Roadmap for Breakthrough. Sigma Publishing Company, Pheonix, Arizona, USA 1994.
16. Magnusson K., Six Sigma – a Quantity Improvement in Operating Performence, ABB BATPT, 1996.
17. Mazur A., Gołaś H., Principles, methods and techniques used in quality management, Poznan University of Technology, Poznan 2010.
18. Mikel H., The Vision of Six Sigma – A Roadmap for Breakthrough. Sigma Publishing Company, Pheonix, Arizona, USA 1994.
19. Molenda M., Szewczyk P., Improvement of quality management systems in selected industrial enterprises in Poland, Silesian University of Technology, Gliwice
20. Pieroni A., Scarpato N., Brilli M., Industry 4.0 Revolution in Autonomous and Connected Vehicle A non-conventional approach to manage Big Data. Journal of Theoretical and Applied Information Technology January 2018 Vol. 96 No.1, 2018.
21. Pieroni A., Scarpato N., Brilli M., Performance Study in Autonomous and Connected Vehicles, an Industry 4.0 Issue. Journal of Theoretical and Applied Information Technology January 2018 Vol. 96 No.2, 2018.
22. Poloczek Ł., Kiełbus A., Dybowski B., Application of Ishikawa's cause-and-effect diagram in the diagnosis of casting defects, [available at:] http://www.ptzp.org.pl/files/konferencje/kzz/artyk_pdf_2017/T2/t2_370.pdf, 12.06.2020.
23. Popławski W., Six Sigma philosophy as a way to improve the efficiency of the company, Electronic document [available at:] https://docplayer.pl/2813671-Filozofia-six-sigma-jako-sposob-na-poprawe-efektywnosci-przedsiebiorstwa.html of 21.03.2020.
24. Rusecki A., Practical application of the FMEA method on the example of pulley production in a selected enterprise, [in:] Quality Production Improvement, No. 1, 2018.
25. Singh M. and Rathi R., "A structured review of Lean Six Sigma in various industrial sectors", International Journal of Lean Six Sigma, Vol. 10 No. 2, pp. 622-664, 2019.
26. Skotnicka-Zasada B., Improvement of the production process in an industrial enterprise using quality design

methods, [ed]. Nosal R., "Innovations in management and production engineering", Oficyna Wydaw. Polish Society of Production Management, Opole 2013.
27. Schwab K., Davis N., Shaping the Fourth Industrial Revolution, Studio EMKA, 2018.
28. Ulewicz R., Novy F., Ensuring the quality and properties of selected construction materials., "Monograph.", Publishing House of the Faculty of Management of the Częstochowa University of Technology. Częstochowa 2016, pp. 55-56.
29. Verrier B., Rose B., Cailaud E., Remita H., Combining organizational performance with sustainable development issues: the Lean and Green project benchmarking repository, Journal of Cleaner Production, Volume 85, Pages 83-93, 2014.
30. Watson G.H. and DeYong C.F. (2010), "Design for Six Sigma: caveat emptor", International Journal of Lean Six Sigma, vol. 1, No. 1, pp. 66-84.
31. Wei C., Sheen G., Tai C. and Lee K. (2010), "Using Six Sigma to improve replenishment process in a direct selling company, Supply Chain Management, vol. 15, issue 1, pp. 3-9.
32. Wiśniewska M., Grudowski P., Quality management and innovation in the light of the experience of the pomerania organization., InnoBaltica Sp. z o.o., Gdańsk 2014.
33. Wolniak R., Lean Production methods and tools and their role in shaping innovation in industry, [in]: "Innovations in management and production engineering," [ed.] Knosala R. Oficyna Wydawnicza Polskiego Towarzystwa Zarządzania Produkcji. Opole, 2013.
34. Wrona A., Wrona M., Application of selected Six Sigma tools in technological processes, http://www.ptzp.org.pl/files/konferencje/kzz/artyk_pdf_2009/126_Wrona_Wrona.pdf, 22.03.2020.
35. https://cgrowth.pl/metoda-5s/, accessed on: 17.04.2020.
36. https://media.statsoft.pl/_old_dnn/downloads/czym_sie_rozni_szesc_sigma_od_trzy_sigma.pdf, accessed 15.06.2020.

TiAM kwartalnik naukowo-techniczny
TECHNOLOGIA I AUTOMATYZACJA MONTAŻU
ZESPOŁÓW • MASZYN • URZĄDZEŃ

Jacek Janiszewski[1], Paweł Przybyłek[2], Rafał Bieńczak[3], Łukasz Komorek[4], Miłosz Sobieski zu Schwarzenberg[5]

DOI: 10.7862/tiam.2022.4.3

THE INFLUENCE OF THE MANUFACTURING METHOD ON THE MECHANICAL PROPERTIES OF THE HONEYCOMB CORE SANDWICH COMPOSITE

WPŁYW METODY WYTWARZANIA NA WŁAŚCIWOŚCI MECHANICZNE KOMPOZYTU PRZEKŁADKOWEGO Z WYPEŁNIACZEM ULOWYM

Abstract

Reducing weight and fuel consumption is one of the main goals of modern aeronautical engineering. The most common materials to achieve this goal are composite layered materials, including the sandwich ones. High strength, stiffness and low density have made sandwich composites one of the fundamental materials of the aerospace industry. Sandwich-structured composites can be manufactured with a variety of methods, differing primarily in the manufacturing time, which translates into an overall cost of making a composite component. The research focused on three methods of manufacturing sandwich composite materials with a honeycomb core, differing in the number of operations, during which it was possible to obtain a finished composite panel (single-phase, two-phase and three-phase methods). The authors manufactured and examined composites with a honeycomb cover and two composite glass fibre-reinforced covers. The composites were made by means of the vacuum bag method. As a result of the conducted study, it was found that composites manufactured with the single-phase method have the shortest manufacture time as well as the lowest material consumption, however their strength properties are the lowest. The two-phase method requires a longer manufacture time and more material consumption, however it makes it possible to obtain a composite with higher strength compared with the single-phase method. The three-phase method has the longest composite manufacture time and the highest material consumption.

Keywords: sandwich composites, composite manufacturing processes, vacuum bagging technique, impact strength, shear strength

Streszczenie

Zmniejszenie masy i zużycia paliwa jest jednym z głównych celów współczesnej inżynierii lotniczej. Najpopularniejsze materiały, które pozwalają osiągnąć ten cel, to materiały kompozytowe warstwowe w tym przekładkowe. Wysoka wytrzymałość, sztywność i niska gęstość, sprawiły, że kompozyty przekładkowe stały się jednym z podstawowych materiałów przemysłu lotniczego. Kompozyty przekładkowe z wypełniaczem strukturalnym mogą być wytwarzane różnymi metodami, różniącymi się przede wszystkim czasem wytwarzania, co przekłada się na ogólny koszt wykonania elementu kompozytowego. W badaniach przeanalizowano trzy metody wytwarzania materiałów kompozytowych przekładkowych w wypełniaczem ulowym różniące się liczbą operacji podczas których uzyskano gotową płytę kompozytową (metoda jednofazowa, dwufazowa i trójfazowa). Wytworzono i badano kompozyty zbudowane z rdzenia ulowego oraz dwóch kompozytowych okładek wzmacnianych włóknami szklanymi. Kompozyty wykonano metodą worka próżniowego. W efekcie przeprowadzonych badań stwierdzono, że kompozyty wytworzone metodą jednofazową cechują się najkrótszym czasem produkcji jak i najmniejszym zużyciem materiałów, ale ich właściwości wytrzymałościowe są najniższe. Dwufazowa metoda wymaga dłuższego czasu produkcji i większego zużycia materiałów, natomiast pozwala uzyskać kompozyt o większej wytrzymałości w porównaniu do metody jednofazowej. Trójfazowa metoda cechuje się najdłuższym czasem wykonania kompozytu i największym zużyciem materiałów.

Słowa kluczowe: kompozyty przekładkowe, metoda wytwarzania kompozytu, technika worka próżniowego, udarność, wytrzymałość na ścinanie

[1] MSc. Eng. Jacek Janiszewski, Polish Air Force University, ul. Dywizjonu 303, no 35, 08-530 Dęblin, Poland, e- mail: j.janiszewski@law.mil.pl
[2] Phd. Eng. Paweł Przybyłek, Polish Air Force University, ul. Dywizjonu 303, 35, 08-530 Dęblin, Poland, e-mail: p.przybylek@law.mil.pl, ORCID: 0000-0002-7544-3813.
[3] Eng. Rafał Bieńczak, Polish Air Force University, ul. Dywizjonu 303 No. 35, 08-530 Dęblin, Poland, e-mail: r.bienczak@law.mil.pl
[4] Eng. Łukasz Komorek (corresponding author), Polish Air Force University, ul. Dywizjonu 303 No. 35, 08-530 Dęblin, Poland, e-mail: l.komorek5374@wsosp.edu.pl
[5] Eng. Miłosz Sobieski zu Schwarzenberg, Polish Air Force University, ul. Dywizjonu 303 No. 35, 08-530 Dęblin, Poland, e-mail: m.sobieskizuschwarzenberg4817@wsosp.edu.pl

1. Introduction

At present composites play an increasingly important role in aviation industry as well as in other areas of manufacturing [1, 2]. The most widely used type of such materials in aviation is sandwich structure composites, characterised by high mechanical strength at low density [3, 4]. Honeycomb core sandwich composites are used in different aerospace applications and are becoming the go-to material for critical substructures in rockets, aircraft, jet engines, and propellers, as well as similar non-aerospace structures, such as wind turbine blades [5]. In less sensitive applications, sandwich composites are also used in aircraft heating, ventilation, and air conditioning systems. This type of composites also includes materials with a sandwich structure, which consists of a rigid, low-density core with claddings on the outside. Such a structure ensures extremely high rigidity and a lightweight construction [5, 6].

Multi-layered composite materials can be manufactured by multiple methods. One of the most popular methods for the manufacture of such composites is a technique using the so-called vacuum bagging [7, 8]. Other commonly used techniques are the infusion technique [9], press method [10] and the autoclave technique [11], which however has been losing popularity in recent years due to high production costs and the possibility of replacing it with other production methods [12].

The aim of the presented research is to analyse various techniques for the manufacture of sandwich-structured composites. The composites are manufactured by three methods: single-phase, two-phase and three-phase, taking into account such criteria as: time and labour consumption of manufacturing the composite, the amount of material used and the mechanical strength of the obtained composite.

2. Manufacturing of composite panels

2.1. Two-phase method

2.1.1. Making the first phase of the composite

The authors decided to produce a composite, consisting of a honeycomb core and two-layer covers with a glass fabric reinforcement as the test material. The vacuum bag method was used to make the composites.

The composite used a 100 g/m^2 twill glass fabric and a 5 mm thick honeycomb paper core at a density of 29 kg/m^3. The dimensions of the composite panels which were later used for cutting the samples with the water jet method equalled 400 x 800 mm.

The components were manually saturated with L285 resin mixed with H285 hardener. The resin/hardener composition was prepared in a 100:40 weight ratio. It was intended to both connect the core and the covers, and to provide a matrix for the composites which make up the covers.

The manufacture of a composite using the two-phase method generally consists of the following phases [13]:

1. The manufacture of a semi-finished product (core with one cover) by making a composite cover in one phase and bonding it to the honeycomb core with a resin/hardener composition.
2. Making a second cover and combining it with a semi-finished product (covers and a honeycomb core produced in the first phase) into a finished composite panel using the vacuum bag method (Fig. 1).

Fig. 1. Curing the composite in phase I

The honeycomb core was applied to fibreglass fabrics, saturated with the resin composition, and then subjected to a light pressure over the entire surface, using a pressure plate to facilitate the bonding of the covers to the core in the vacuum bag.

Preparing the first phase of the composite using this method makes it possible to achieve a high-quality bond between the cover and the honeycomb filler. The PET foil, over which there is a glass fibre fabric, when spreading the resin makes all the resin seep through the two layers of glass fibre, ensuring solid adhesive bonding with the core. The delamination and the drainage mat located on the honeycomb filler during compression of the composite in the vacuum bag drains an excess resin and air that could degrade the quality of the composite.

A photograph taken with a Tagarno Magnus microscope (Fig. 2) shows an absence of resin in the cells of the honeycomb filler, whereas Fig. 3 shows full seepage of resin through the cover.

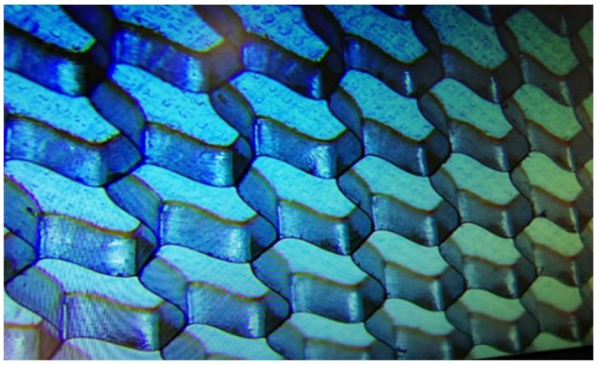

Fig. 2. Microscopic photograph which shows bonding of honeycomb core and cover (x20)

Fig. 3. Hardened composite cover visible from the outside

In the second phase of the composite manufacture, a key factor was to ensure the best possible bonding between the cover and the honeycomb core prepared in the first phase; the cover was prepared in the second phase. A problem in the second phase of the composite manufacture was a limited possibility to drain the excess of resin and air due to the cover enclosing the composite from the top. In order to produce a high-quality composite, a second phase of composite manufacture was proposed, using three different methods, in which a potential solution to this problem was experimentally tested.

2.1.2. The first method to carry out phase II of the composite manufacture

During phase II of the composite manufacture (Fig. 4) with the first method, the main idea was to remove the excess air and resin through a typical perforated separating foil with holes of approximately 0.5 mm in diameter when pressing the soaked layers of glass fabric onto the semi-finished product made in phase I. The method uses the following arrangement of materials:

- 2 layers of glass fabric,
- separation foil with 0.5 mm holes,
- delamination,
- drainage mat.

Fig. 4. Preparation process for phase II of the composite

The foil was to drain excess resin and air from the lower layers, while the delamination was to prevent the drainage mat from sticking to the rest of the materials.

Unfortunately, this attempt proved unsuccessful, as most of the resin, despite the 0.5 mm diameter holes, seeped into the lower layers of the materials, preventing the individual components of the composite from bonding together. Consequently, an insufficient amount of resin resulted in the cover not bonding properly with the honeycomb filler. Numerous discolourations from the seeped resin are visible throughout the delamination surface (Fig. 5).

Fig. 5. Cover peeling off from the semi-product manufactured in phase I

2.1.3. The second method of carrying out phase II of the composite manufacture

When conducting phase II of the composite using the second method, the main assumption was to compare the quality of the composite produced with and without the possibility of removing excess air. For this purpose, a PET foil was prepared (Fig. 6). It was split into two parts: the first one with a mesh consisting of 1,600 holes, each 2 mm in diameter, hand-made, using the drilling technology, and the second one with a uniform net. Consequently, when the first part of the composite (made in the first phase) was pressed against the second part (non-hardened cover), the air that had accumulated between the first part of the composite (made in the first phase) and the second part (non-hardened cover) could be removed through the holes made in the PET film.

Fig. 6. PET film with a mesh consisting of 1,600 holes

Half of the cover that was laid on the PET film with holes did not stick to the semi-product made in phase I. This was due to the resin seeping into the lower layers of the materials through the previously prepared holes. Half of the cover that was on the uniform part of the PET film had seeped through and bonded properly to the rest of the composite (Fig. 7).

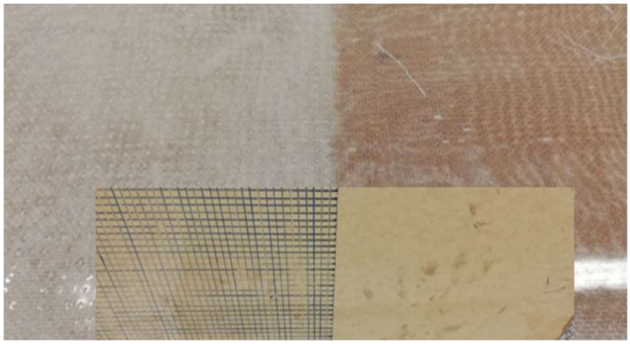

Fig. 7. Left part of composite cured on PET film with holes; right part on uniform film, without holes

2.1.4. Method 3 in conducting phase II in the composite manufacture

Basing on the previous trial, the third method that was used during the process of bonding the composite parts made in the first phase to the cover made in this phase was the application of a uniform PET film over the entire surface of the glass fabric when saturating and curing the cover in the vacuum bag. This allowed the resin to properly soak through all layers of the cover and properly bond the two parts of the composite. The disadvantage was the fact that excess air remained in the composite. However, this method proved to be the best one qualitatively (visual assessment) when producing the two-phase composite (Fig. 8).

Fig. 8. Cover produced in phase II

2.2. Analysis of the mechanical properties of the two-phase composite produced in accordance with the methodology described in section 2.1.4

In order to qualitatively assess the composite, it was decided to carry out static bending, tensile and adhesion tests, as well as dynamic impact and piercing resistance tests. Conducting a bending test of the composite allowed the authors to determine the Young's modulus and bending strength of the manufactured two-phase composite. Five samples, sized 60 x 80 mm, resting freely on supports and positioned 60 mm apart, underwent testing (Fig. 9).

Fig. 9. Sample during a bending test – Zwick/Roell 5kN machine

The test was conducted in accordance with the bending scheme of method A (three-point bending) described in EN ISO 14125 [14].

The obtained results are shown in the graphs (Fig. 10-11).

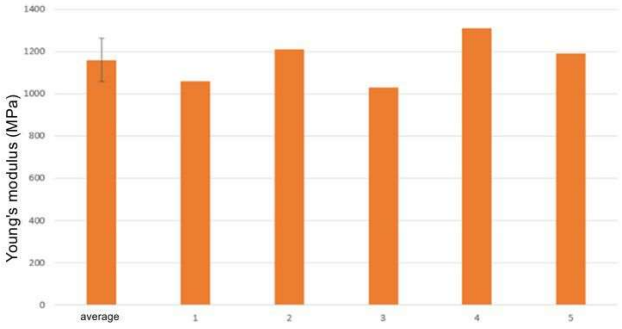

Fig. 10. Young's modulus of two-phase composite samples

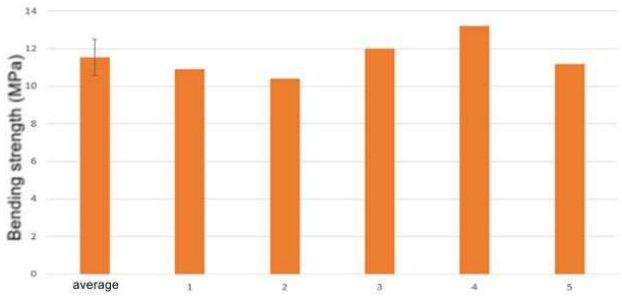

Fig. 11. Bending strength of the two-phase composite

Next, the 60 x 80 mm samples were subjected to a test which examined resistance to penetration. The tests which employed an INSTRON CEAST 9340 drop hammer, had the samples loaded with the following energies: 0.5; 1; 2; 3 and 5 J.

The 0.5 J energy did not damage the composite cover or the honeycomb filler (Fig. 12).

Fig. 12. View of sample loaded with 0.5 J

A load of 1 J caused a slight deformation and cracking of the cover in one part of the sample (Fig. 13).

An energy of 2 J caused the cover to deform and break in three directions propagating from the point of load application (Fig. 14).

Fig. 13. View of sample loaded surface with 1 J

Fig. 14. View of sample loaded surface with 2 J

Loading with an energy of 3 J resulted in a significant indentation and a crack in the composite structure on the side of the load application, propagating in four perpendicular directions (Fig. 15).

Fig. 15. View of sample loaded surface with 3 J

At a load of 5 J, it is possible to observe very deep indentations in the composite and cracking of the cover in four directions (perpendicular), propagating

from the point of load application. It is also noticeable, unlike other loading energies, that the cover peels away from the core at the edges of the sample (Fig. 16). It is worth noting that no damage is visible on the bottom cover.

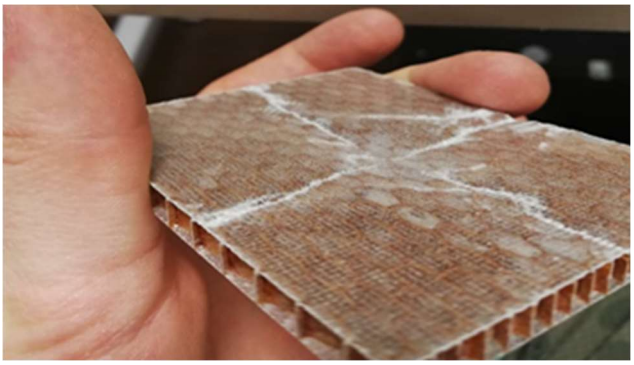

Fig. 16. View of sample loaded surface with 5 J

After the impact tests, the samples were subjected to bending in order to determine the residual bending strength. The obtained results are shown in Fig. 17.

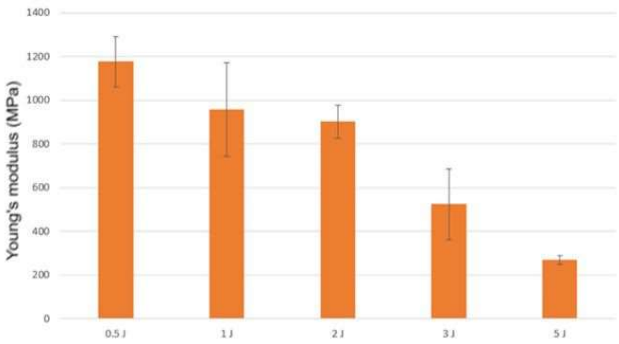

Fig. 17. Average residual bending strength of samples after an impact load

A loading energy of 0.5 J did not reduce the bending strength of the two-phase composite. At energies of 1 J and 2 J, a decrease in bending strength of approximately 200 MPa is apparent. An energy load of 3 J results in a twofold decrease in bending strength. Loading with an energy of 5 J results in a drastic decrease in bending strength in relation to other energies, due to damage to the composite structure and detachment of the cover from the honeycomb core.

Another examination was a tensile test, which involved axial sample stretching. The average value of the Young's modulus of the tested composite was 807 MPa, while the average tensile strength was 18.3 MPa.

The next test was an impact test using a pendulum hammer, with both plane (Fig. 18a) and edge (Fig. 18b) loading of the sample. The obtained results have been presented in Table 1.

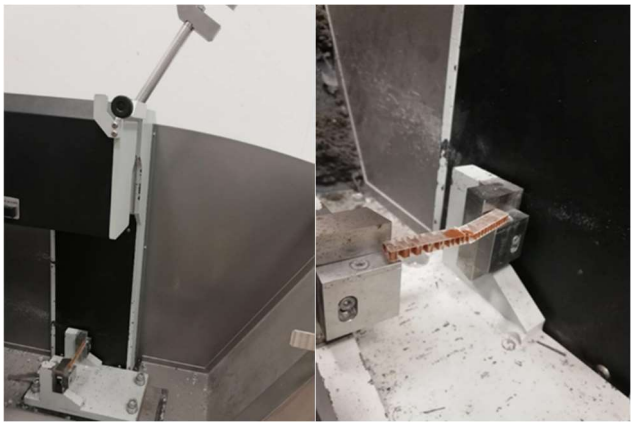

Fig. 18. Impact test under: a) plane loading, b) edge loading

Table 1. Impact strength

Impact strength (plane loading) (kJ/m^2)		Impact strength (edge loading) (kJ/m^2)	
3.97		7.21	
4.39		6.87	
4.07		6.97	
3.91		6.78	
4.12		6.22	
4.52		5.99	
4.31		5.61	
3.92		6.17	
Average	4.24	Average	6.32

A significantly higher impact strength of the edge-loaded composite can be observed, which is probably related to a higher impact strength of the edge-loaded covers. The final test of the composite was to examine adhesion between the cover and the core of the two--phase composite. The test was an attempt to determine the shear strength between the covers and the core. In order to investigate these properties, strength tests were performed on samples prepared from the composite with a shape similar to overlap samples, in which two flat elements glued together by a core were stretched in the core plane (Fig. 19). The test results are shown in Table 2.

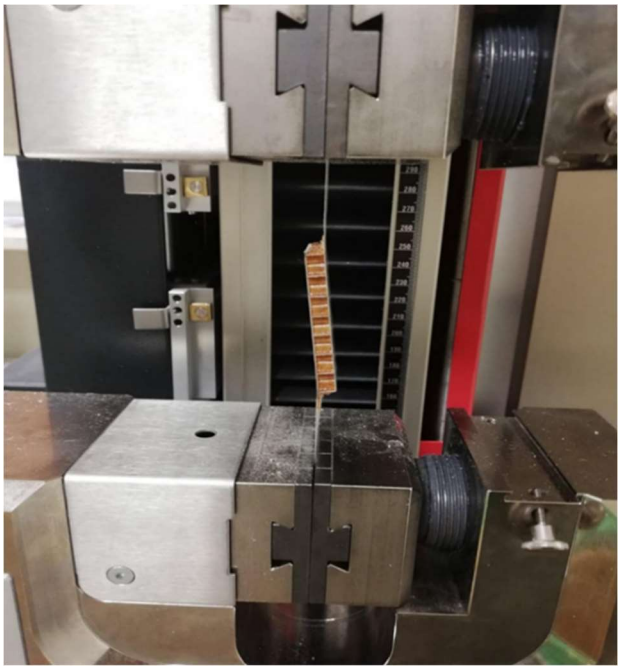

Fig. 19. Scheme of the adhesion test between cover and core

Table 2. Adhesion test findings of a two-phase composite

Sample	Shear strength (MPa)	Load capacity (N)
1	0.350	438
2	0.353	441
3	0.316	395
4	0.453	566
5	0.286	367

3. Analysis of the manufacture of sandwich composite materials, using a single-phase method

3.1. Single-phase composite manufacturing

In the single-phase method, analogous to the two-phase method, the vacuum bag method was used. The single-phase manufactured composite is characterised by the bonding of the core with the covers also made at this stage. Practically, this means that one curing process of the composite in the vacuum bag leads to a finished composite.

The same materials were used to produce the composite in one phase and in the two-phase method.

The manufacture of the composite using the single-phase method began by saturating two layers of glass fibre fabric with resin. Next, the saturated fabric layers had a honeycomb filler applied. The next step was to encapsulate the composite with two layers of fibreglass fabric saturated in resin. The uncured composite, prepared in such a way, was placed in a vacuum bag (Fig. 20-21).

Fig. 20. Composite arrangement

The order of materials when curing in the vacuum bag was as follows:

- fibreboard,
- drainage mat,
- PET film,
- 2 layers of glass fabric,
- honeycomb core
- 2 layers of glass fabric,
- PET film,
- drainage mat,
- fibreboard.

Fig. 21. Sealing off the vacuum bag

The composite produced by means of the single--phase method was characterised by the correct bonding of the covers and the honeycomb filler, as well as uniform curing of the composite covers over the entire surface. The covers were characterised by satisfactory stiffness and high quality. Nevertheless, due to a small possibility of removing excess air, air bubbles remained in some areas. Slight discolouration

was caused by residual air and the loss of some of the resin from the saturated glass fibre in the curing process inside the vacuum bag. The resin-soaked fibreglass fabrics of the upper cover leaked some of the resin to the lower cover under the influence of gravity. However, these were small amounts of resin, because the composite was still bonded properly and the cover had appropriate stiffness and hardness during the surface inspection (Fig. 22).

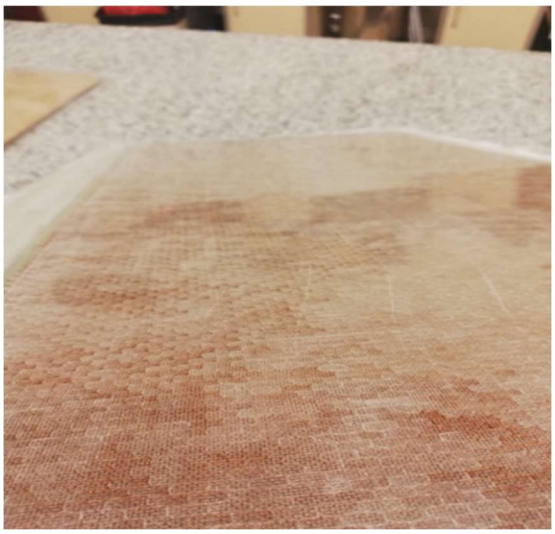

Fig. 22. Composite manufactured with a single-phase method

3.2. Analysis of mechanical properties of the single-phase composite

The bending test of the composite was carried out in a three-point bending test by means of a Zwick/Roell 5 kN universal testing machine. The test was conducted in accordance with the bending scheme of method A described in PN-EN ISO 14125. The obtained results have been shown in Table 3.

Table 3. Results of a single-phase composite bending strength test

Sample	Young's modulus (MPa)	Bending strength (MPa)
1	814	8.14
2	770	9.46
3	1020	10.30
4	805	10.40
5	974	10.10
Average	877	9.68

The samples were then subjected to an impact test. Similarly to the samples made by means of the two-phase method, the test was performed with following energy: 0.5; 1; 2; 3; 5 J, using the INSTRON CEAST 9340 system.

An energy of 0.5 J caused minor deformation in the cover and minimal indentation (Fig. 23).

Fig. 23. View of a single-phase sample loaded with 0.5 J

The 1 J energy caused damage to the cover in two places and indentation of the honeycomb core (Fig. 24).

Fig. 24. Image of a single-phase sample loaded with 1 J

An energy of 2 J caused three branching cracks in the cover, propagating from the point of load application, as well as a large indentation of the honeycomb filler (Fig. 25).

Fig. 25. View of a single-phase sample loaded with 2 J

An energy of 3 J caused three branching cracks in the cover, propagating from the point of load application, as well as a large indentation of the honeycomb filler (Fig. 25). The massive indentations of the honeycomb filler caused its fracture (Fig. 26).

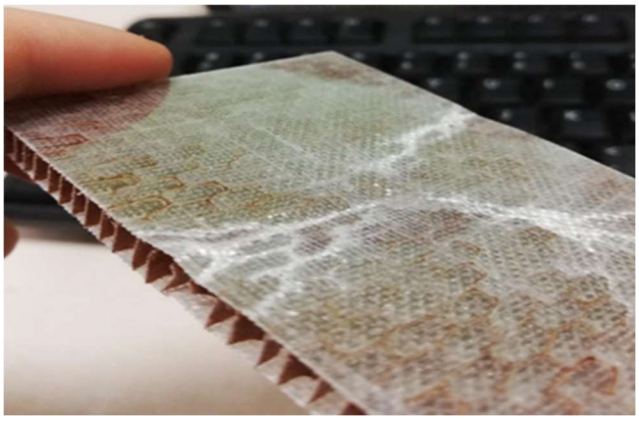

Fig. 26. Damage to a single-phase sample loaded with 3 J

An energy of 5 J caused extensive damage to the cover over the entire surface and detachment of the cover from its filler over 70 per cent of the surface (Fig. 27).

Fig. 27. Damage to a single-phase sample loaded with 5 J

After the load tests, the samples were subjected to bending in order to determine the residual bending strength. The obtained results have been presented in Table 4.

The bending strength of the single-phase composite did not deteriorate after the impact load of 0.5 J. The load of 1 J resulted in a decrease in bending strength of 200 MPa. However, at an impact energy of 2 J, the bending strength value dropped by approximately five times. The loading energies of 3 J and 5 J caused complete damage to the composite structure (detachment of the covers from the honeycomb core, fracture of the honeycomb core), therefore the strength characteristics after these tests were so low. The results obtained have been presented in the graph (Fig. 28).

Another examination was a tensile test, whose results have been shown in Fig. 29-30.

Table 4. Results of bending test after impact loading

Sample	Energy of load (J)	Bending strength (MPa)
1	0.5	10.30
2		10.40
3		10.10
4	1	8.16
5		9.87
6		7.72
7	2	3.12
8		2.60
9		0.77
10	3	0.81
11		3.11
12		1.11
13	5	0.36
14		1.51
15		1.36

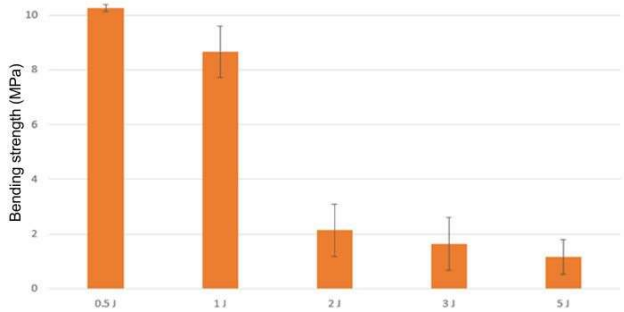

Fig. 28. Average residual bending strength of samples after examining the impact strength.

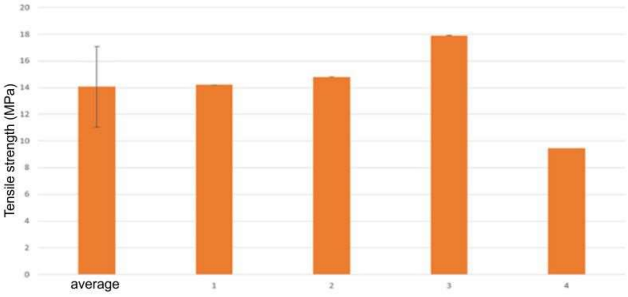

Fig. 29. Tensile strength of a single-phase composite

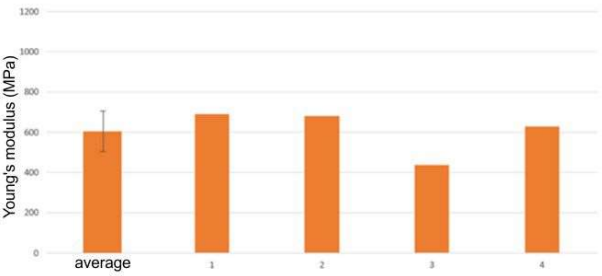

Fig. 30. Longitudinal modulus of elasticity of a single-phase composite

Next, the composites were subjected to an impact test using a pendulum hammer, with both plane and edge loading of the sample. The obtained results have been presented in Table 5.

Table 5. Research findings

Impact strength of planes (kJ/m^2)		Impact strength of edges (kJ/m^2)	
3.14		4.79	
3.52		4.83	
3.21		4.45	
2.97		3.92	
3.17		4.82	
2.91		3.84	
2.83		4.63	
3.76		4.31	
3.29		4.12	
2.77		4.86	
Average	3.16	Average	4.46

When analysing the results, it is noticeable that the impact strength of the edge-impacted composite is significantly higher compared to plane-impacted samples.

The final test of the composite was to examine adhesion between the cover and the core of the two-phase composite (Fig. 31) The test was carried out analogously to the two-phase composite. The test results are shown in Table 6.

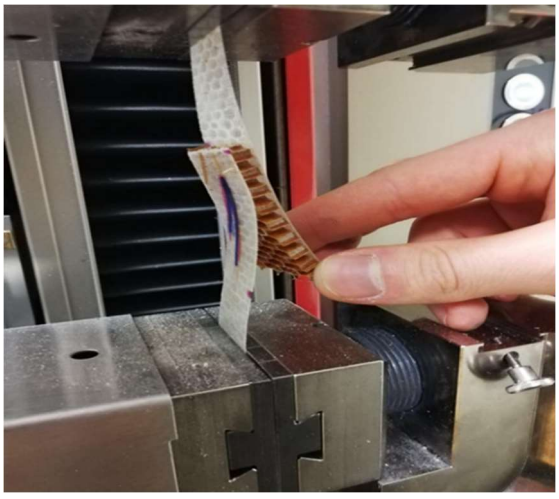

Fig. 31. Adhesion test between cover and core – Zwick/Roell 5 kN machine

Table 6. Adhesion test results of a two-phase composite

Number of sample	Shear strength (MPa)	Load capacity (N)
1	0.390	487
2	0.158	197
3	0.328	410
4	0.254	318
5	0.283	354

4. Analysis of the manufacture of sandwich composite materials using a three-phase method

4.1. The first method to run phase III in manufacturing a composite

The composite produced with the three-phase method has the longest manufacture time compared to the one- and two-phase methods. The process consists of the manufacture of glass fabric composite covers in Phases I and II. The third phase involves bonding the cured covers to the honeycomb core. The manufacture of the composite in each phase of this method requires the use of a drainage mat, PET film and delamination, making it the most costly of all the methods researched. The unquestionable advantage of this method is the fact that the covers are manufactured independently of each other, preventing excess air in the composite and ensuring good saturation of the covers. An additional advantage is also the fact that in one- or two-phase manufacture, at least two persons are required to produce such a composite. On the other hand, in the three-phase method, one person is able to handle every stage of the composite production.

Fig. 32. Preparation of composite covers

The manufacture of a composite using the two-phase method consists of the following phases:

1. Manufacture of the first cover from two resin-saturated fibreglass layers, using the vacuum bag method (Fig. 32).
2. Manufacture of a second cover from two layers of resin-saturated fibreglass, using the vacuum bag method.
3. Gluing the honeycomb filler covers together with a resin composition, using the vacuum bag technique.

In the process of making Phase I and Phase II covers by means of the vacuum bag method, the key element is to ensure the best possible saturation of the fabrics and removal of excess air. In order to achieve such effects, the following sequence of materials was

used in the manufacturing process of the composite cover: drainage mat, delamination, two layers of glass fibre, PET film, drainage mat, fibreboard. (Fig. 33).

Fig. 33. Materials put together to make the cover (1st and 2nd phase)

The two covers, produced in such a way, owing to good saturation of the fabrics and the removal of excess air, were characterised by good stiffness and high quality (Fig. 34).

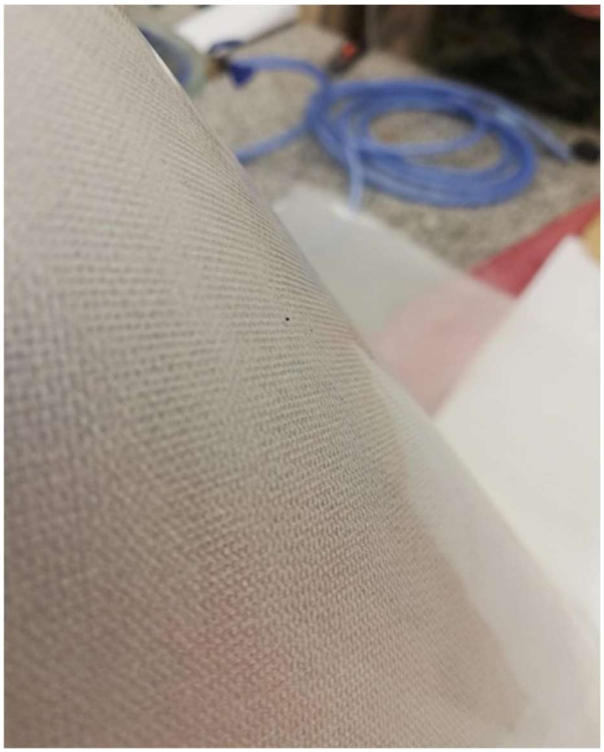

Fig. 34. Cover manufactured in phase I of composite preparation, using the three-phase method

Once the composite covers had been manufactured, the next step was to glue them to the honeycomb core. It was assumed that the composites cured in Phases I and II, i.e. the covers made in such a manner, had a homogeneous structure; after soaking them in resin in Phase III there would be no risk of the resin seeping into the lower layers of the materials, therefore only a drainage mat and a fibreboard were used under the composite covers. Unfortunately, the assumption of homogeneity of the covers turned out to be wrong and resulted in the composite covers sticking together with the drainage mat (Fig. 35).

Fig. 35. Bonding of drainage mat and composite cover

This was caused by resin seepage through the holes in the covers when the composite was pressed in the vacuum bag. The photo (Fig. 36) shows holes in the covers through which the resin seeped, leading to bonding with the drainage mat.

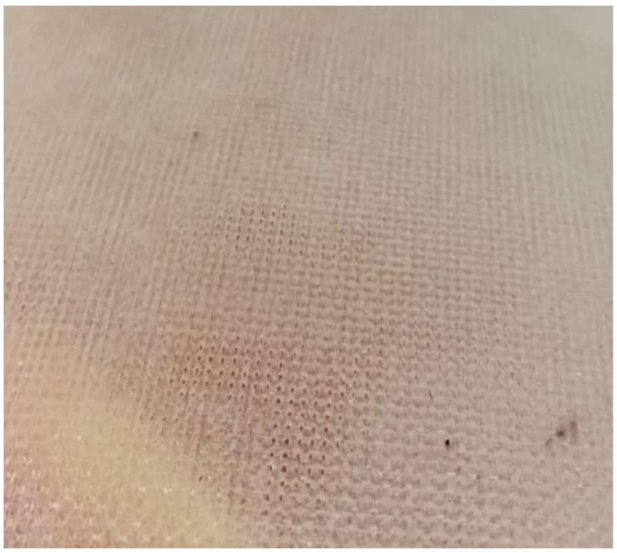

Fig. 36. Holes visible in the composite cover

4.2. The second method to run phase III of the composite manufacture

Learning from the erroneous assumptions in the first attempt to produce a three-phase composite, in the second method it was decided to use PET film and delamination. Their use does not pose the risk of the covers sticking to any of the materials. It also ensures good resin seepage and drainage of excess resin when pressing in the vacuum bag (Fig. 37).

Fig. 37. Layers used in phase III of the composite

Unfortunately, this method also proved unsuitable for the manufacture of the composite. When pressing the composite layers together in the vacuum bag, the holes in the covers led to the absorption of most resin by the delamination. This was assumed to be the case when manufacturing the composite using this method, however unexpectedly a lot of resin was absorbed by the delamination, which was only designed to drain the excess resin (Fig. 39-39).

Fig. 38. View of the composite surface

Unfortunately, due to limited possibilities, as the three-phase composite manufacture method appears to be the longest and most time-consuming technique, it was not possible to prepare more composites using this method and expose them to strength testing. Also, testing both three-phase composites was considered unreliable due to the significant imperfections of these materials.

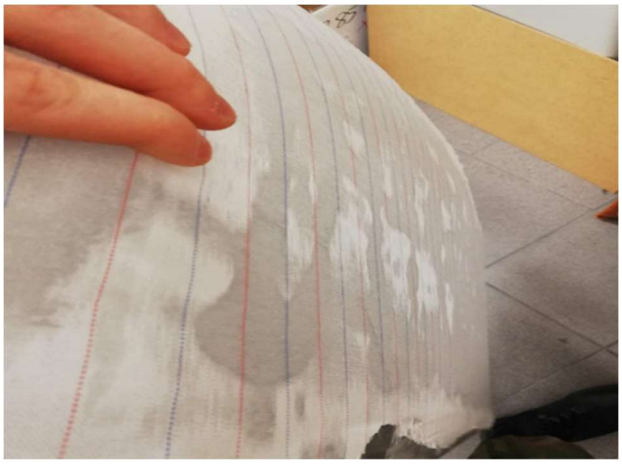

Fig. 39. Resin mostly absorbed by delamination

5. Comparison of properties of the manufactured composites

5.1. Comparison of the composite manufacturing process

Each method of preparing sandwich composite materials is characterised by a different manufacture time, amount of materials required and difficulty of the manufacture. The two-phase method is characterised by the need to consume materials in two phases. In order to prepare the first phase, the following are needed: a drainage mat, PET film, delamination. Once the materials had been used, they cannot be re-used in phase II, so again the following items are needed for phase II: a drainage mat and PET film. When comparing this method with the single-phase composite manufacturing technology, it is important to note significantly higher material consumption. The single-phase method only requires the use of a drainage mat, delamination and PET film in one phase of production rather than two. The three-phase method is the one that consumes the largest amounts of materials, since in the first, second and third phases all the above-mentioned materials are used and they can be used once only.

The manufacture time of the composites with these different methods also varied significantly. The three-phase method was the technique requiring the longest manufacture time, as it took approximately two hours to make each cover in phase I and phase II. Besides it is necessary to add a minimum curing time for each phase in the vacuum bag, equal to six hours. The preparation of phase III required one hour, thus the total composite manufacture time, using the three-phase method, was equal to 23 hours.

The use of the single-phase method was characterised by the preparation time of components equal

to 3 hours. When adding the curing time in the vacuum bag, which was six hours, it appeared that the total manufacture time was nine hours. Compared to the three-phase method, the techniques vary noticeably.

When producing the composite using the two--phase method, the preparation process for both the first and second phases took two hours each. It is also necessary to add six hours for the curing process of the composite in the vacuum bag for the first and the second phase. Therefore, the total manufacture time for the two-phase composite was 16 hours.

By contrasting the time and effort involved in preparing the composite with the successive methods, it can be concluded that the method which was the most challenging was the single-phase method, as it required at least two persons in the manufacture process. The process of preparing two covers at the same time and arranging the materials appropriately in the composite manufacture was the most demanding of all methods. The two-phase method also required two persons in the manufacture process, however, it required less work in the preparation of the individual composite components compared to the single-phase method. When producing the composite using the three-phase method, one person was sufficient in the production process, which is a significant advantage of this method.

5.2. Comparison of mechanical properties of single-phase and two-phase composites

As indicated by the results of the strength tests of the single- and two-phase composites, the two--phase composites had significantly higher mechanical strength in all tests. The average Young's modulus at bending for the two-phase composites was 1,160 MPa, while the average bending strength was 11.54 MPa. In the single-phase composites, the average Young's modulus was 25% lower at 876 MPa, while the average bending strength was 9.68 MPa, 16% lower, i.e. it was 16 % lower.

The mean longitudinal modulus of elasticity for the two-phase composites determined during the static tensile test was 812.25 MPa, while the modulus of elasticity for the single-phase composite was equal to 608.75 MPa. The difference in the modulus value between the two composites is 203.5 MPa. The average tensile strength of the two-phase composite was 18.175 MPa; for the single-phase composite it was 14.095 MPa, therefore it was 23% lower.

A test carried out on a pendulum hammer to estimate the ability of the composites to carry dynamic loads by determining their impact strength, made it possible to specify the average impact strength for two-phase composites plane loaded to equal 4.239 kJ/m^2, which was 26% higher than the impact strength specified when the single-phase composite was loaded onto its plane. For edge-loaded two-phase composite samples, the impact strength was 6,322 kJ/m^2 and was thus 30% higher than the impact strength determined with edge-loading of the single-phase composite. The single-phase composite had an impact strength of 3.157 kJ/m^2 for plane-impacted samples, while for the edge-impacted samples this value was equal to 4.457 kJ/m^2.

The final test of the composite was to examine adhesion between the cover and the core of the two-phase composite. The test was an attempt to determine the bonding strength between the covers and the core. The average value of the destructive forces for the two-phase composite was equal to 441.4 N, however, the value for the single-phase composites was 353.2 N, i.e. it was 20 % lower.

All the conducted strength tests indicate better mechanical properties of the two-phase composite. It featured higher bending strength, tensile strength, better impact strength and adhesion between the cover and the honeycomb core. The obtained results prove that the two-phase method achieves a mechanically stronger composite, while the single-phase composites are created at a lower cost and in a shorter time; however, they are worse than two-phase composites in terms of their strength. A factor that determines the inferior mechanical properties of the single-phase composite is the phenomenon of losing some of the resin under the influence of gravity by the freshly saturated layers of glass fabric located on top of the composite. The resin seeps into the second composite cover, which results in one of the covers not being sufficiently saturated with resin. Nevertheless, the amount of resin remaining in the cover allows the covers to cure properly and bond to the honeycomb core. This method can, therefore, be used when a large number of composites need to be produced, with the least amount of auxiliary materials and in a short manufacture time. The two-phase method, on the other hand, achieves a mechanically stronger composite using more material and a longer production time.

6. Conclusions

Based on the experiment, the following conclusions were drawn:

1. The composites made with the single-phase method are characterised by the shortest manufacture time as well as the lowest material consumption;
2. The results of the strength tests indicate that mechanical strength is a significant drawback in the manufacture of a single-phase composite;
3. The two-phase method requires a longer manufacture time and more material consumption, however,

it makes it possible to prepare a composite with higher strength compared with the single-phase method;
4. The three-phase method requires the longest composite manufacture time has the highest material consumption of all the methods;
5. The two-layer covers with fibreglass reinforcement, prepared using the vacuum bag method, do not have a uniform structure. This causes the resin to seep into the other layers of the composite during the bonding process of the covers to the core inside the vacuum bag, during the three-phase method.
6. In the process of curing the composite in a vacuum bag, the resin-soaked glass fibre should be on a PET film or some other uniform material without holes. The use of a material with holes causes the resin to seep into the lower layers of the components, resulting in improper bonding of the composite.

References

1. Boczkowska A., Krzesiński G. 2016. Composites and techniques of their production. Oficyna Wydawnicza Politechniki Warszawskiej. Warszawa.
2. Królikowski W. 2012. Polymer structural composites. Wydawnictwo Naukowe PWN, Warszawa.
3. Ochelski S. 2018. Experimental methods of mechanics of structural composites, WNT. Warszawa.
4. Castane B., Bouvet C., Ginot M., 2020 Review of composite sandwich structure in aeronautic applications, Composites Part C: Open Access, Vol 1, 2020, 100004, https://doi.org/10.1016/j.jcomc.2020.100004.
5. Thomsen O. 2009. Sandwich Materials for Wind Turbine Blades – Present and Future. Journal of Sandwich Structures & Materials 11. 7-26. 10.1177/1099636208099710.
6. Krishnasamy S., Muthukumar C., Thiagamanin S., Rangappa S, Siengchin S. 2022. Sandwich Composites: Fabrication and Characterization. CRC Press.
7. Komorek A., Przybyłek P., Szczepaniak R., Godzimirski J., Rośkowicz M., Imiłowski S. 2022. The Influence of Low-Energy Impact Loads on the Properties of the Sandwich Composite with a Foam Core. Polymers. 14. 1566. https://doi.org/10.3390/polym14081566.
8. Mouritz A.P. 2012. Introduction to Aerospace Materials. Woodhead Publishing.
9. Ostwal R.S., Dumre A., Takalkar A., Mb A., Krishnan R., Padmanabhan, 2014. Influence of Post Curing on the Flexural Properties of a Rigid Polyurethane or Polyisocynurate Foam-Glass/Epoxy Face Sheet Sandwich Composite. International Journal of ChemTech Research. 6(6):974-4290.
10. Reuterlöv S., 2002. Cost effective infusion of sandwich composites for marine applications, Reinforced Plastics, 46(12), 2002, 30-34, doi.org/10.1016/S0034-3617(02)80224-7.
11. Krzyżak A., Mazur M., Gajewski M., Drozd K., Komorek A., Przybyłek P. 2016. Sandwich Structured Composites for Aeronautics: Methods of Manufacturing Affecting Some Mechanical Properties, International Journal of Aerospace Engineering, vol. 2016, Article ID 7816912, 10 pages,. https://doi.org/10.1155/2016/7816912
12. Calabrese L., Di Bella G., Fiore V., 2016. Manufacture of marine composite sandwich structures, Editor(s): Graham-Jones J., Summerscales J. in Woodhead Publishing Series in Composites Science and Engineering, Marine Applications of Advanced Fibre-Reinforced Composites, Woodhead Publishing, pp. 57-78, doi.org/10.1016/B978--1-78242-250-1.00003-X.
13. Menta N.S., Chandrashekhara V.G., Berkel K., Sha T.R., Wu J., Pfitzinger P. 2012. Out-of-Autoclave Sandwich Structure: Processing Study. International SAMPE Technical Conference, 48.
14. Khan A. S. 1996. International Journal of Plasticity. University of Maryland Baltimore County. Baltimore.
15. 4125:2001/A1:2011 – Kompozyty tworzywowe wzmocnione włóknem – Oznaczanie właściwości przy zginaniu.

TiAM kwartalnik naukowo-techniczny
TECHNOLOGIA I AUTOMATYZACJA MONTAŻU
ZESPOŁÓW • MASZYN • URZĄDZEŃ

Władysław Zielecki[1], Ewelina Ozga[2]

DOI: 10.7862/tiam.2022.4.4

RELATIONSHIP BETWEEN SURFACE ROUGHNESS AND LOAD CAPACITY OF ADHESIVE JOINTS MADE OF ALUMINUM ALLOY 2024-T3 AFTER SHOT PEENING

ZALEŻNOŚĆ MIĘDZY CHROPOWATOŚCIĄ POWIERZCHNI I NOŚNOŚCIĄ POŁĄCZEŃ KLEJOWYCH STOPU ALUMINIUM 2024-T3 PO PNEUMOKULKOWANIU

Abstract

The aim of the work was to investigate the influence of selected shot peening parameters on the load capacity of adhesive joints and on the surface roughness of samples made of aluminum alloy 2024-T3. The research was also aimed at verifying whether it is possible to assess the load capacity of adhesive joints on the basis of the surface roughness parameters after shot peening. The treatment variants were developed according to the matrix of the Hartley's PS/DS-P:Ha3 plan. Shot peening time varied from 60 to 180 s, ball diameter from 0.5 to 1.5 mm and compressed air pressure from 0.3 to 0.5 MPa. As a result of the analysis of the correlation between the load capacity of connections and the surface roughness, it can be concluded that the greatest relationship exists between the load capacity and the Rku parameter. The regression analysis shows that the load capacity of the connections should increase along with the increase of the Rku parameter. The study also showed that the Rku parameter is also most strongly associated with the deflection of the Almen strips. The Almen strip deflection increases with the increase of the Rku parameter. The regression equation describing the influence of shot peening parameters on the value of the Rku parameter indicates that the value of the Rku parameter increases with the increase of the treatment time and the decrease of the ball diameter and the compressed air pressure.

Keywords: shot peening, single-lap adhesive joint, load capacity, surface roughness, Hartley's PS/DS-P: Ha3 plan, Almen test

Streszczenie

Celem pracy było zbadanie wpływu wybranych parametrów pneumokulkowania na nośność połączeń klejowych oraz chropowatość powierzchni próbek ze stopu aluminium 2024-T3. Badania miały również na celu sprawdzenie, czy możliwa jest ocena nośności połączeń klejowych na podstawie parametrów chropowatości powierzchni po pneumokulkowaniu. Warianty pneumokulkowania opracowano zgodnie z matrycą planu Hartleya PS/DS-P:Ha3. Czas obróbki zmieniał się w zakresie od 60 do 180 s, średnica kulek od 0,5 do 1,5 mm i ciśnienie sprężonego powietrza od 0,3 do 0,5 MPa. W wyniku analizy korelacji miedzy nośnością połączeń i chropowatością powierzchni można stwierdzić, ze największa zależność występuje pomiędzy nośnością a parametrem Rku. Analiza regresji wskazuje, ze wraz ze zwiększaniem wartości parametru Rku nośność połączeń również powinna wzrastać. W ramach pracy wykazano również, że parametr Rku jest parametrem chropowatości najsilniej związanym ze strzałką ugięcia płytek Almena. Strzałka ugięcia płytek Almena wzrasta wraz ze wzrostem parametru Rku. Równanie regresji opisujące wpływ parametrów pneumokulkowania na wartość parametru Rku wskazuje, że wartość parametru Rku wzrasta wraz ze zwiększaniem czasu kulkowania i zmniejszaniem średnicy kulek i ciśnienia sprężonego powietrza.

Słowa kluczowe: pneumokulkowanie, jednozakładkowe połączenie klejowe, nośność, plan Hartleya PS/DS-P: Ha3, próba Almena

1. Introduction

Adhesives have been known and used for thousands of years. However, the most intensive development of adhesive technology has occurred in the last century. One of the precursors of bonding is the aviation industry. In addition, this technology is widely used in the railway, automotive, construction and electronics industries. It is also increasingly used in medicine and biology [5].

Adhesive connections have many advantages. One of the greatest is the excellent weight-to-strength ratio compared to alternative mechanical connections. Moreover, adhesive bounds are characterized by better

[1] dr hab. inż. Władysław Zielecki, prof. PRz, Wydział Budowy Maszyn i Lotnictwa Politechniki Rzeszowskiej, Katedra Technologii Maszyn i Inżynierii Produkcji, al. Powstańców Warszawy 8, 35-959 Rzeszów, e-mail: wzktmiop@prz.edu.pl, ORCID: 0000-0002-7864-5525.
[2] mgr inż. Ewelina Ozga, Wydział Budowy Maszyn i Lotnictwa Politechniki Rzeszowskiej, Katedra Technologii Maszyn i Inżynierii Produkcji, al. Powstańców Warszawa 8, 35-959 Rzeszów, e-mail: e.guzla@prz.edu.pl, ORCID: 0000-0002-7359-6007.

stress distribution, good fatigue resistance, good corrosion resistance, possibility of connecting thin and fragile substrates, possibility of connecting different materials and aesthetic. Nevertheless, adhesive joints have drawbacks as well. The disadvantages of this technology are, above all, the toxicity and flammability of many adhesives, the need for an appropriate substrate surface preparation, duration of curing, limited strength in extreme or severe conditions (for example in elevated temperature) [4, 12].

The most commonly used type of adhesive connections is single lap joint. The shear stress distribution in the zone of the overlap is uneven. The maximum stresses are situated at the edges of the lap. By reducing these stresses, the strength of the connections can be increased [12, 15].

One of the methods that enable reducing such stress peaks is shot peening of the overlap zone. Shot peening is an example of dynamic stream burnishing. It is a cold working process which involves bombarding the treated surface by small spherical particles [21, 28]. If the tool is in the form of balls which are propelled by a stream of compressed air, then it is referred to pneumatic shot peening [16, 36]. The intensity of the pneumatic shot peening treatment can be controlled by changing the process parameters such as processing time, ball diameter, compressed air pressure, number of nozzles and the distance of nozzles from the workpiece [36]. The intensity of the shot peening process can be analyzed using the Almen test. The Almen test consists in one-sided shot peening of specially prepared, standardized strips (Almen control strips). There are three types of the strips: N, A and C. The types differ in thickness. The selection of the appropriate type of the Almen strip depends on the intensity of the process. N type strips are used for low, A for medium, C for high shot peening intensity. Shot peening processing causes the strips to bend. The measure of the shot peening intensity is the deflection value of the Almen control strips [38].

As already mentioned, pneumatic shot peening of the outer surfaces of the laps is one of the methods of strengthening the adhesive joints. Pneumatic shot peening leads to the constitution of compressive residual stresses in the outer layer of the treated surface. The edges of the overlap are deformed and pressed against the joined material. The introduced compressive stresses reduce the concentration of stresses resulting from the external load and effectively increase the strength of the joints [35, 36].

The effect of pneumatic shot peening treatment on adhesive joints strength has been analyzed in several studies. Zielecki [36] analyzed adhesive joints made of S235JR steel. One group of the connections was characterized by a rigid adhesive joint (Epidian 5 (CIECH Sarzyna S.A, Nowa Sarzyna, Poland) composition with Z1 hardener), and the other by a flexible adhesive joint (Epidian 5 composition with PAC hardener). The joints were shot peened for 60 s with 2 mm diameter balls and pressure ranging from 0.35 to 0.55 MPa. As a result of pneumatic shot peening, the strength of the samples with a flexible joint increased by 17-27%. Moreover, the increase in strength was proportional to the increase in compressed air pressure. In the case of samples with a rigid joint, the increase in strength was 93-112%.

Zielecki and Korzyńska [31] used pneumatic shot peening process to strengthen the adhesive bonds made of titanium alloy Ti6Al4V. The treatment was carried out for 10 to 30 seconds. The diameter of the balls was 4.5 mm and the pressure was 0.6 MPa. The strength of the connections increased by 42-63%. It was also found that increasing the treatment time led to an increase in the adhesive joint strength.

In another work Korzyńska et al. [16] managed to increase the strength of connections made of titanium alloy Ti6Al4V by 18-57%. Moreover, it has been shown that there is a relationship between the strength of the joints and the state of stress after shot peening.

The possibility of strengthening the adhesive joints made of aluminum alloy 2024 with the method of pneumatic shot peening was investigated in [30]. The treatment time was 60-180 s, balls diameter 2-2.5 mm and compressed air pressure 0.2-0.3 MPa. The maximum increase in load capacity was 20.3% (treatment time 120 s, ball diameter 2 mm, pressure 0.2 MPa).

Shot peening affects not only the adhesive joints strength, but also the geometric structure of the treated surface. As a result of the treatment, numerous indentations of spherical shape, small depth and radius many times greater than the depth are formed [36]. According to the research results presented in [14], as the treatment time is lengthened, the surface roughness initially increases and then begins to decrease.

Moreover, shot peening increases the hardness of the treated surface. The increase of microhardness results from grain refinement and work hardening [3]. The authors of the work [23] point out that the pressure of compressed air has a greater influence on the hardness and the number of defects than the processing time. With increasing pressure, the number of defects decreases and the hardness increases. However, when a certain pressure limit is exceeded, the treated surface deteriorates again. According to [24] surface hardening induced by shot peening improve the wear behavior of treated elements.

Another analyzes show that shot peening have a beneficial effect on fatigue strength. In the work [18] 51CrV4 steel was tested. It has been shown that the fatigue strength of the samples shot peened for 10

minutes with 2 mm diameter balls and at 0,6 MPa compressed air pressure increased by 1.5%. The positive effect of shot peening on fatigue strength was also observed in [2]. It has been shown that the shot penning treatment of X80 steel samples increases their resistance to crack initiation, which in turn leads to an increase in fatigue strength and an increase in resistance to hydrogen embrittlement. Moreover, shot peening also has a beneficial effect on the fatigue strength of elements with chrome coatings [7].

Laber [20] compared the influence of the surface layer condition after burnishing or grinding on the tribological properties of ductile iron. As a result of the conducted analyzes, it was shown that a more favorable condition of the surface layer is obtained in the burnishing. Such layer is characterized by a lower surface roughness according to the Ra parameter, greater strengthening and higher values of compressive residual stresses, which favorably influences the tribological properties.

In many cases, the functional properties are very closely related to certain properties of the surface layer – surface roughness, hardness or residual stresses. Grzesik [8, 9, 10, 11] in several works presented considerations on the influence of individual surface roughness parameters on the functional properties of machine parts. On the basis of the observations presented by him, it can be concluded that reducing the roughness causes an increase in fatigue strength. However, when the Ra (arithmetical mean height) takes values from 2.5 to 5 µm, then the material microstructure and the residual stress have a greater influence. If there is no residual stress, then the value of the parameter Ra less than 0.1 µm strongly affects the fatigue strength [8, 11]. Grzesik [9] also draws attention to the fact that the sensitivity of fatigue strength to surface roughness values increases with increasing material strength (e.g. for precipitation hardening aluminum alloys or for hardened steels). It also explains that the propagation and nucleation of fatigue cracks is largely dependent on the surface roughness.

In the works [8, 11] it was noted that high values of Sq (root mean square height) and Sds (summit density) are associated with high unevenness and high density of peaks per unit area, and thus with a high friction coefficient. Moreover, the static friction coefficient may largely depend on the effects of skewness (Rsk) and kurtosis (Rku). Positive skewness (Rsk>0) reduces the friction coefficient. If the skewness is negative (Rsk<0) then the friction is more intense than in the Gaussian distribution (Rku = 3, Rsk = 0).

According to the observations presented in [8], the real contact area of the element increases with the increase of surface roughness, and thus the corrosion resistance decreases. Therefore, height parameters (mainly Sz – maximum height) and the arithmetic mean summit curvature (Ssc) have the greatest influence on the corrosion properties. Surfaces dominated by deep valleys are more prone to corrosion than anisotropic surfaces.

The surface roughness has a significant influence on adhesion and bonding. For more developed surfaces, coating is more effective and adhesive joints are stronger. In the case of adhesive joints, the geometric structure of the surface should be adapted to the type of adhesive. In the work [37] the influence of roughness parameters of surface treated in the milling process on the strength of adhesive joints was investigated. It has been proved that in the case of joints connected with elastic adhesives, the parameters lr (profile length ratio), Δa (average absolute slope) and Δq (root mean square slope) have a large impact on the strength of the joints. In turn, according to the results presented in [32], the shear strength of joints connected with an elastic adhesive is proportional to the following parameters: Sq Spd (Spd – density of peaks), Spc (arithmetic mean peak curvature), Sdr (developed interfacial ratio), Sdq (root mean square gradient). The strongest correlation occurs between the strength of connections and the product of Sq Spd parameters. Similar studies were carried out in the work [34]. In this case, the surface roughness parameters in the 2D system were analyzed. According to the results of the analysis, the parameters most strongly correlated with the strength of adhesive joints are Rlr, Rda, Rdq. Rlr is the profile length factor equal to the ratio of the actual (developed) profile length to the length of the sampling or evaluation length, on which it was determined, Rda is the arithmetical mean slope and Rdq is the root mean square slope [33].

In summary, shot peening process can be used to strengthen adhesive joints and has a beneficial effect on many technological and functional properties of the workpieces. Additionally, it has numerous advantages, such as low energy consumption, low cost and simplicity [22]. Nevertheless, research on the impact of pneumatic shot peening on the strength of adhesive joints is uncommon, partial and concerns mainly joints made of steel and titanium alloys. Therefore, it is justified to conduct more profound analyzes of the effect of the pneumatic shot peening on the strength of adhesive joints made of other frequently used alloys. Moreover, the conducted analysis of the literature shows that surface roughness has a significant influence on many functional properties. Surface roughness measurements, especially in the 2D system, are characterized by simplicity and low costs. Accordingly, it is reasonable to investigate the relationship between the surface roughness parameters after shot peening

and the load capacity of adhesive joints after shot peening.

The aim of the work was to investigate the influence of the pneumatic shot peening treatment on the load capacity of adhesive joints and surface roughness of samples made of aluminum alloy 2024-T3. The research also included an analysis of the effect of pneumatic shot peening on the deflection of the Almen strips. The tests were carried out according to Hartley's PS/DS-P:Ha3 plan, described in [17]. As part of the work, the analyzes of regression and correlation between the load capacity and surface roughness parameters, between the Almen strip deflection and surface roughness parameters and between the load capacity and the Almen strip deflection were carried out. The performed research allowed for selection the roughness parameters that would enable the evaluation of the correctness of the strengthening treatment.

2. Experimental details

The adhesive connections were made of plates cut from a sheet of EN AW-2024-T3 aluminium alloy. This alloy is mainly used in the aerospace, engineering, defence and automotive industries. One of the biggest advantages of this alloy is high strength to weight ratio. Apart from that it distinguishes itself through high temperature resistance and good fatigue strength [6, 19]. The chemical composition of aluminium alloy 2024-T3 is summarized in Table 1.

Table 1. Chemical composition of EN AW-2024-T3 aluminium alloy [6]

Component, weight %											
Si	Fe	Cu	Mn	Mg	Cr	Ni	Zn	Ti	V	Others*	Al
max 0.50	max 0.50	3.8-4.9	0.30-0.90	1.2-1.8	max 0.10	-	max 0.25	max 0.15	-	max 0.05	remaining
*Others, total ≤ 0,15%											

The adherend surfaces were prepared for bonding. For this purpose the surfaces were subjected to abrasive blasting with 95A electrocorundate. The parameters of the treatment were: time 30 s, grain size 27 mm and air pressure 0.7 MPa. The average values of selected roughness parameters after abrasive blasting were respectively: Rz = 25.95 µm, Ra = 4.53 µm, Rv = 13.8 µm, Rq = 5.67 µm, Rku = 2.99, RSm = = 0.141 mm. The surfaces were also degreased using acetone.

The next step was bonding the samples with the use of two-component epoxy adhesive – Loctite EA3430. Information about the adhesive can be found in the product description [13]. The samples were cross linked in a mechanical press, which allowed the proper pressing of the adherent surfaces. The cross-linking time was 3 days and the temperature was 24°C. The dimensions of the aluminium alloy plates were 100x25x2 mm. The length of the joint lap was 12.5 mm.

Subsequently, the overlap zones of the joints were subjected to the pneumatic shot peening process with different treatment time t [s], ball diameter d [mm] and compressed air pressure p [MPa] (Fig. 3).

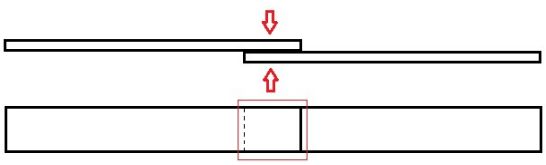

Fig. 1. Scheme of the adhesive joint with marked zones of shot peening

The treatment variants were developed according to the matrix of the Hartley's PS/DS-P:Ha3 plan. The main values of the parameters (input factors), change intervals and coded values are listed in Table 2 and the scheme of the adhesive joint with marked zones of shot peening is shown in Figure 1.

The strength of the adhesive joints after shot peening was measured in a static tensile test. The connections were loaded until they were broken. The breaking force was adopted as the load capacity Pt [N] of the adhesive joint. The static tensile test was carried out in accordance with PN EN 1465:2009 [25].

The tests also included measuring the surface roughness parameters of the plates cut from a sheet of EN AW-2024-T3 aluminum alloy and subjected to shot peening with the processing parameters listed in Table 2. The test was carried in a 2D system. 2D roughness measurements are more often used in industry than 3D measurements because they are easier and cheaper. The measurements were performed with a Taylor Hobson SURTRONIC 25 contact stylus profilometer and TalyProfile Lite software. The evaluation length was 12.5 mm. The measurements were performed in accordance with the PN-EN ISO 4287:1999 standard [26].

The final stage of the tests was to assess the intensity of shot peening using the Almen test according to SAE J443 standard [27]. Almen control strips of A2 type (hardness 44-50 HRC, thickness 1.32 mm, flatness ± 0.038 mm) were used for the research. Shot peening parameters are shown in Table 2. One side of the strips was processed. As a result of

pneumatic shot peening, compressive residual stresses were constituted in the surface layer of the samples. This stresses caused the strips to bend. The deflection of the Almen control strips was measured with a TSP-3B measuring device.

Table 2. Treatment variants, main values of the parameters, change intervals and coded values

Factor's name	Value at the top and bottom level		Central values of input factors	Variation units	Method of encoding factor
Processing time t [s]	+ –	180 60	$x_{10} = \frac{180+60}{2} = 120$	$\Delta x_1 = \frac{180-60}{2} = 60$	$x_1 = \frac{t-120}{60}$
Ball diameter d [mm]	+ –	1.5 0.5	$x_{10} = \frac{1.5+0.5}{2} = 1$	$\Delta x_2 = \frac{1.5-0.5}{2} = 0.5$	$x_2 = \frac{d-1}{0.5}$
Pressure p [MPa]	+ –	0.5 0.3	$x_{10} = \frac{0.5+0.3}{2} = 0.4$	$\Delta x_3 = \frac{0.5-0.3}{2} = 0.1$	$x_3 = \frac{p-0.4}{0.1}$

Treatment variants			
No.	x_1	x_2	x_3
1	–	–	+
2	+	–	–
3	–	+	–
4	+	+	+
5	–	0	0
6	+	0	0
7	0	–	0
8	0	+	0
9	0	0	–
10	0	0	+
11	0	0	0
12	Non-peened		

3. Discussion and results

Table 3 presents the average values of surface roughness parameters, the average values of the deflection of the Almen strips and the average values of load capacity of adhesive joints after pneumatic shot peening.

Based on the results of measurements presented in Table 3, it can be concluded that shot peening treatment can be used to strengthen adhesive joints made of aluminum alloy 2024-T3. The highest load capacity was obtained for the shot peening variant no. 10 (processing time 120 s, ball diameter 1 mm, pressure 0.5 MPa) and for variant no. 6 (processing time 180 s, ball diameter 1 mm, pressure 0.4 MPa). The load capacity of the joints in variant no. 10 is 33.4% greater than the load capacity of non-peened joints. On the other hand, the lowest load capacity was obtained for the variant no. 4, which is characterized by the highest shot peening parameters (processing time 180 s, ball diameter 1.5 mm, pressure 0.5 MPa).

Table 3. The average values of surface roughness parameters, the average values Almen strip deflection and the average values of load capacity of adhesive joints after pneumatic shot peening

No	Pt, N	f_A, mm	Rp, µm	Rv, µm	Rz, µm	Rc, µm	Rt, µm	Ra, µm	Rq, µm	Rsk	Rku	RSm, mm	Rdq, °	Rda, °
1	8166	0.071	5.67	5.49	11.16	6.06	18.88	1.90	2.37	0.0823	3.04	0.171	8.662	5.444
2	7168	0.051	3.47	3.61	7.08	3.40	12.00	1.13	1.43	-0.0371	3.07	0.129	7.228	4.454
3	8226	0.043	2.59	3.16	5.75	3.94	9.49	1.15	1.42	-0.3792	2.82	0.335	4.236	2.154
4	4819	0.242	5.92	4.91	10.82	7.36	19.46	2.22	2.72	0.1356	2.50	0.310	5.952	3.546
5	8781	0.049	5.10	5.84	10.94	6.49	18.74	1.96	2.45	-0.2156	3.03	0.234	7.350	4.466
6	9410	0.08	5.75	5.90	11.64	6.54	19.48	2.09	2.61	0.0043	2.95	0.206	8.086	5.140
7	7005	0.035	4.02	3.82	7.83	4.07	12.92	1.33	1.65	0.1009	2.90	0.144	7.152	4.480
8	7097	0.152	5.19	4.48	9.68	6.81	16.16	2.03	2.45	0.1688	2.50	0.311	5.432	3.260
9	8688	0.027	5.04	5.90	10.94	6.28	19.48	1.94	2.40	-0.1862	2.99	0.211	8.034	4.838
10	9443	0.054	6.45	6.55	12.98	7.29	26.20	2.27	2.87	0.0294	2.89	0.222	8.564	5.414
11	8633	0.067	5.67	6.50	12.16	7.16	21.02	2.11	2.65	-0.1134	3.11	0.215	8.628	5.306
12	7079	-	-	-	-	-	-	-	-	-	-	-	-	-

* Pt – load capacity, f_A – Almen strip deflection.

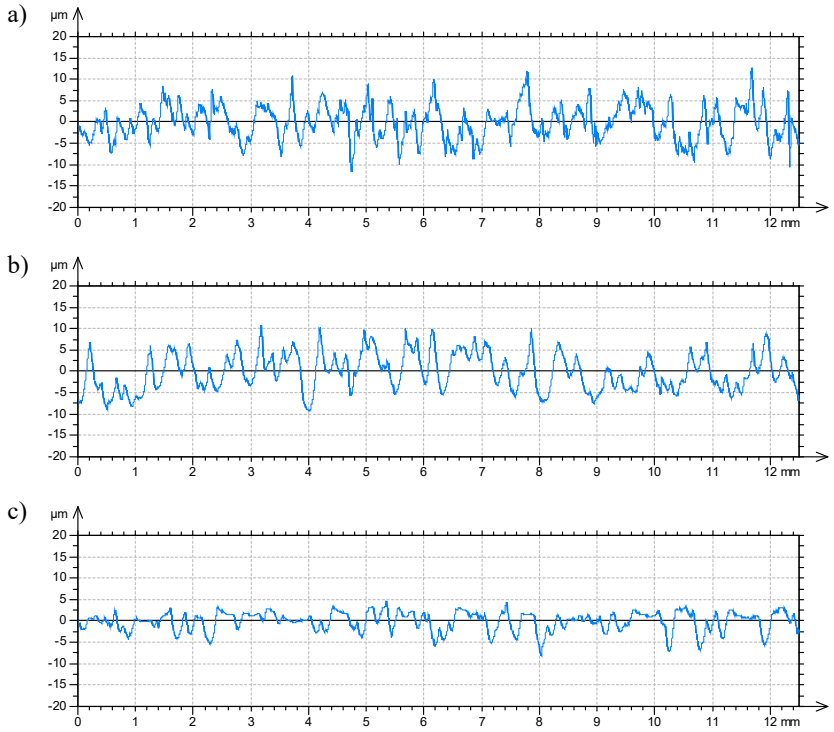

Fig. 2. Selected surface profiles: a) surface profile for treatment variant no. 10 (highest load capacity of adhesive joints), b) surface profile for variant no. 4 (lowest load capacity of adhesive joints), c) surface profile for variant no. 3

In the case of variant no. 4, the low load capacity of the adhesive joint could be caused by assuming too high values of the shot peening parameters. Too intensive treatment could damage the cohesive or adhesive bonds and weaken the joints. Figure 2 shows selected surface profiles after shot peening.

As a result of shot peening, numerous spherical-shaped indentations were formed on the treated surface. The Figure 2 shows that the geometrical structure of the surface may differ significantly depending on the values of the processing parameters. Compared to Fig. 2a and Fig 2b, Fig. 2c show a much smaller (incomplete) surface coverage with traces of shot peening.

The first step in the analysis of the test results was to determine the relationship between the surface roughness parameters and the load capacity of adhesive joints (after shot peening). Table 4 and Figure 3 show the results of the correlation analysis, the regression equations, and the results of assessing the significance of the coefficients.

Table 4. Regression equations, coefficients of linear correlation between the surface roughness parameters and the load capacity of adhesive joints (after pneumatic shot peening), results of assessing the significance of the coefficients

Parameter	Independent variable	Pv1	Regression equation	Pv2	Linear correlation coefficient R	Pv3
Pt	Rp	0.179	$y_{Pt}=7070+176x_{Rp}$	0.656	0.152	0.656
Pt	Rv	0.274	$y_{Pt}=4852+606x_{Rv}$	0.091	0.533	0.091
Pt	Rz	**0.036**	$y_{Pt}=5804+213x_{Rz}$	0.281	0.357	0.281
Pt	Rc	0.240	$y_{Pt}=7243+119x_{Rc}$	0.710	0.127	0.710
Pt	Rt	0.274	$y_{Pt}=6148+102x_{Rt}$	0.284	0.355	0.284
Pt	Ra	0.394	$y_{Pt}=7046+494x_{Ra}$	0.652	0.154	0.652
Pt	Rq	0.594	$y_{Pt}=6810+501x_{Rq}$	0.568	0.194	0.568
Pt	Rsk	0.566	$y_{Pt}=7811-3694x_{Rsk}$	0.150	-0.465	0.150
Pt	Rku	0.485	$y_{Pt}=-4016+4139x_{Rku}$	**0.031**	**0.647**	0.031
Pt	RSm	**0.036**	$y_{Pt}=8983-4574x_{RSm}$	0.496	-0.230	0.496
Pt	Rdq	0.306	$y_{Pt}=4523+475x_{Rdq}$	0.109	0.510	0.109
Pt	Rda	0.306	$y_{Pt}=5194+625x_{Rda}$	0.135	0.480	0.135

Pt – load capacity, Pv1 – probability level in the one-way analysis of variance (ANOVA), Pv2 – probability level for independent variable in the regression analysis, Pv3 – probability level in the analysis of the linear correlation coefficient

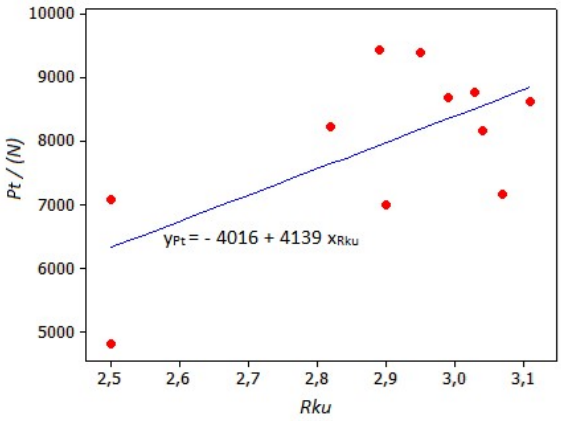

Fig. 3. The load capacity of joints Pt versus surface roughness parameter Rku

According to the results of the one-way analysis of variance ANOVA (Table 4), in the adopted range of variability of the input parameters, only the independent variable Rz and RSm influences the Pt parameter in a statistically significant way. This is confirmed by the Pv1 values, which only in these two cases are lower than 5%.

Based on the regression equations (Table 4), it can be concluded that increasing the values of the roughness parameters contributes to increasing the load capacity of the adhesive joints (the exceptions are the parameters Rsk and RSm). The assessment of the significance of the regression equation coefficients shows that only in the case of the parameter Rku, the influence of the independent variable on the equation result is statistically significant (Pv2<0,05). However, the coefficient of determination shows that in the case of the parameter Rku, only 41.9% of the results of the load capacity of adhesive joints can be described by the obtained regression equation.

It was assumed in the research that a strong correlation between the variables occurs when the absolute values of the linear correlation coefficients are greater than 0.7. According to the results of the correlation analysis (Table 4), in the adopted range of variability of the input parameters, the strongest relationship occurs between the load capacity of the adhesive joints and the roughness parameter Rku. The linear correlation coefficient in this case is 0.647. Therefore, it is not a strong correlation. Slightly lower values of the correlation coefficient were obtained for the parameters Rv and Rdq (for Rv R=0.53, for Rdq R=0.51). The weakest correlation occurs for the parameters Ra, Rp and Rc (R=0.15÷0.13).

In the next step, it was checked which roughness parameter is most strongly correlated with the deflection of the Almen strips. Table 5 and Figure 4 show the results of the correlation analysis, the regression equations, and the results of assessing the significance of the coefficients.

Table 5. Regression equations, coefficients of linear correlation between the surface roughness parameters and the deflection of the Almen strips, results of assessing the significance of the coefficients

Parameter	Independent variable	Pv1	Regression equation	Pv2	Linear correlation coefficient R	Pv3
f_A	Rp	0.112	y_{fA}=-0.0247+0.0208x_{Rp}	0.246	0.382	0.246
f_A	Rv	0.417	y_{fA}=0.0892-0.0020x_{Rv}	0.915	-0.037	0.915
f_A	Rz	0.179	y_{fA}=0.0290+0.00497x_{Rz}	0.602	0.177	0.602
f_A	Rc	0.251	y_{fA}=-0.0457+0.0210x_{Rc}	0.138	0.477	0.138
f_A	Rt	0.417	y_{fA}=0.0427+0.00207x_{Rt}	0.653	0.153	0.653
f_A	Ra	0.066	y_{fA}=-0.0450+0.0679x_{Ra}	0.166	0.449	0.166
f_A	Rq	0.727	y_{fA}=-0.0340+0.0498x_{Rq}	0.212	0.409	0.212
f_A	Rsk	0.824	y_{fA}=0.0871+0.211x_{Rsk}	0.071	0.564	0.071
f_A	Rku	0.362	y_{fA}=0.781-0.243x_{Rku}	**0.003**	**-0.807**	0.003
f_A	RSm	0.179	y_{fA}=-0.0359+0.509x_{RSm}	0.083	0.544	0.083
f_A	Rdq	0.106	y_{fA}=0.194-0.0159x_{Rdq}	0.272	-0.363	0.272
f_A	Rda	0.033	y_{fA}=0.167-0.0200x_{Rda}	0.327	-0.327	0.327

f_A – Almen strip deflection, Pv1 – probability level in the one-way analysis of variance (ANOVA), Pv2 – probability level for independent variable in the regression analysis, Pv3 – probability level in the analysis of the linear correlation coefficient

The results of the one-way analysis of variance ANOVA (Table 5) indicate that, in the adopted range of variability of the input parameters, almost all of the independent variables do not significantly affect the dependent variable (Almen strip deflection). Only the independent variable Rda influences the f_A parameter in a statistically significant way (Pv1<0,05).

According to the regression equations (Table 5), it can be concluded that with the increase of the roughness parameters Rv, Rku, Rdq and Rda, the deflection of the Almen strips decreases. In other cases, increasing the roughness parameters leads to an increase in the deflection of the Almen strips. The evaluation of the significance of the regression equation coefficients

indicates that only the independent variable Rku significantly influences the result of the regression equation (Pv2<0.05). The Pv2 probability values for the remaining variables are greater than 0.05.

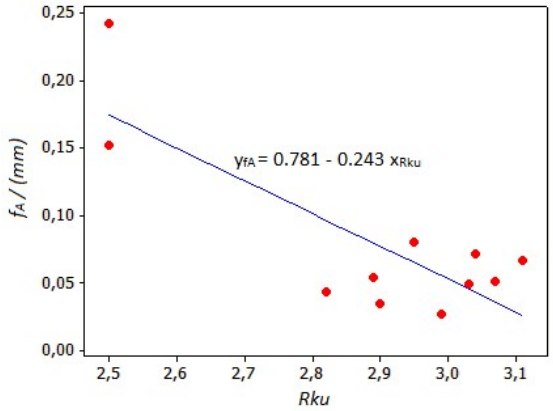

Fig. 4. The Almen strip deflection f_A versus surface roughness parameter Rku

In addition, there is a strong correlation between the independent variable Rku and the deflection of the Almen strips. The value of the linear correlation coefficient in this case is -0.806. The weakest correlation was observed between the Almen strip deflection and the roughness parameter Rv.

As part of the research, the relationship between the load capacity of adhesive joints and the deflection of the Almen strips was also analyzed. It was shown that the linear correlation coefficient is -0.733. Therefore, there is a strong correlation between the load capacity and the Almen strip deflection. According to the regression equation (Figure 5), the load capacity of the connections decreases as the Almen strip deflection increases.

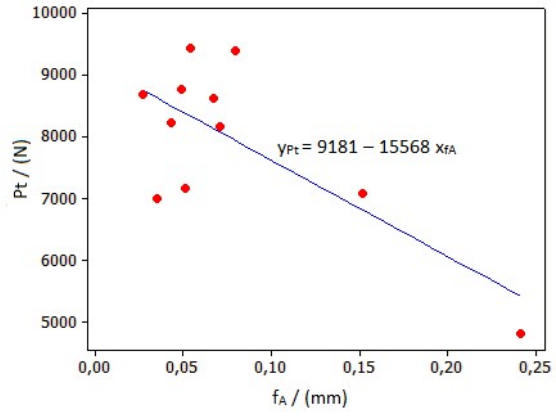

Fig. 5. The load capacity of joints Pt versus the Almen strip deflection f_A

The conducted analyzes show that the roughness parameter most strongly correlated with both the load capacity of the joints and the Almen strip deflection is the parameter Rku. Therefore, the Rku parameter can be used to evaluate the deflection of the Almen strips and the load capacity of adhesive joints after shot peening.

The value of the Rku (kurtosis) parameter is calculated from the formula (1):

$$Rku = \frac{1}{Rq^4}\left[\frac{1}{lr}\int_0^{lr}\left|Z^4(x)\right|dx\right] \tag{1}$$

where: Rq – root mean square height, lr – evaluation length, $Z(x)$ – roughness profile equation, Z_i – height distribution of the 1- point of the surface roughness, n – number of points on the x-axis for which the Z_i value is determined.

In the Rku formula, the value of the root mean square is in the fourth power. Therefore, the values of the Rku parameter largely depend on the depth of the indentations and the height of the peaks of the profile. In the case of a profile with very slender peaks, the value of the Rku parameter may exceed 20. If the height distribution is normal, then the Rku=3. The values of the Rku parameter can be used to infer about surface defects [1, 29].

Due to the fact that the Rku parameter can be used to assess the load capacity of adhesive joints after shot peening, the next stage of was to develop a regression equation describing the influence of shot peening on the value of the Rku parameter. The equation was developed according to the methodology of Hartley's plan PS/DS-P:Ha3 described in [17]. The equations determined according to the methodology of the Hartley's plan PS/DS-P:Ha3 take the shape of a second-order polynomial (2):

$$\begin{aligned} y = {} & b_0 + b_1x_1 + b_2x_2 + b_3x_3 + \\ & + b_{11}x_1^2 + b_{22}x_2^2 + b_{33}x_3^2 + \\ & + b_{12}x_1x_2 + b_{13}x_1x_3 + b_{23}x_2x_3 \end{aligned} \tag{2}$$

where: x_1 – coded value for the treatment time t [s], x_2 – coded value for the ball diameter d [mm], x_3 – coded value for the pressure p [MPa] and $b_0,\ldots,b_{23}$ – regression equation coefficients.

Table 6 and Figure 6 show the detailed results of Rku roughness measurements together with the results of mathematical model.

Table 6. Results of tests and calculations for the roughness parameter Rku

Variant				Results of the test of Rku parameter					Results of the calculations			
No.	x_1	x_2	x_3	y_1	y_2	y_3	y_4	y_5	$\overline{y}_i$	$S^2(y)_i$	$\hat{y}_i$	$(\overline{y}-\hat{y}_i)^2$
1	-	-	+	3.06	2.88	3.24	3.31	2.70	3.04	0.06	3.14	0.01
2	+	-	-	3.32	3.06	3.05	2.95	2.97	3.07	0.02	3.14	0.00
3	-	+	-	2.50	3.55	2.70	2.83	2.50	2.82	0.19	2.34	0.22
4	+	+	+	2.50	2.41	2.68	2.45	2.47	2.50	0.01	2.34	0.02
5	-	0	0	3.26	2.63	3.03	2.92	3.32	3.03	0.08	2.96	0.01
6	+	0	0	2.66	2.88	2.69	2.97	3.57	2.95	0.14	2.96	0.00
7	0	-	0	2.85	3.18	2.83	2.86	2.77	2.90	0.03	2.94	0.00
8	0	+	0	2.25	2.40	2.68	2.54	2.62	2.50	0.03	2.54	0.00
9	0	0	-	3.15	3.11	3.09	2.57	3.04	2.99	0.06	2.96	0.00
10	0	0	+	2.97	2.70	2.99	3.19	2.59	2.89	0.06	2.96	0.00
11	0	0	0	2.63	2.88	2.90	3.28	3.86	3.11	0.23	2.96	0.02
Σ	-	-	-	-	-	-	-	-	31.80	0.90	-	0.30

* $\overline{y}_i$ – average value of Rku parameter, $S^2(y)_i$ – variance of experimental results, $\hat{y}_i$ – value of Rku parameter determined using regression equation (3), $(\overline{y}-\hat{y}_i)^2$ – variance determined using regression equation (3).

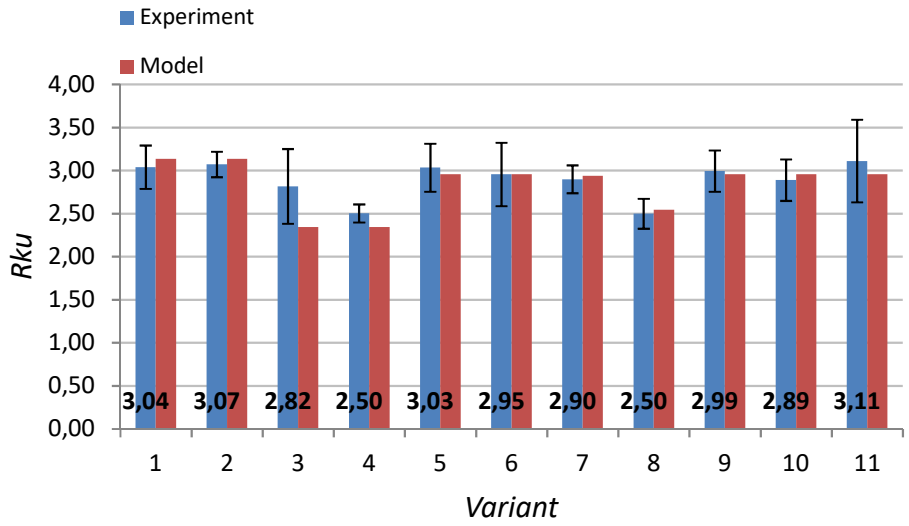

Fig. 6. Results of the tests (with values and standard deviation) and the calculations for the roughness parameter Rku

The obtained results of the surface roughness parameter Rku were evaluated for repeatability with the use of the Cochran criterion. The calculated G value is 0.26 and is less than the critical value ($G_{0,05;11;4} = 0.3096$). Therefore, the repeatability of the experimental conditions can be considered as satisfactory.

In the next steps, the values of the coefficients of the regression equation were determined and then their significance was assessed. The results of the calculations and the results of the significance assessment are presented in Table 7.

After elimination of the irrelevant coefficients, decoding the equation using appropriate values from Table 2 and re-arranging, the following regression equation was obtained (3):

$$y_{Rku} = 0{,}9042 + 0{,}01316\,x_t + 1{,}345\,x_d + \\ + 3{,}948\,x_p - 0{,}8708\,x_d^2 - 0{,}0329\,x_t x_p \quad (3)$$

where y_{Rku} is the surface roughness parameter Rku, x_t is the processing time variable, x_d is the ball diameter variable and is the x_p compressed air pressure variable. The regression equation (3) describes the effects of peening time, ball diameter and compressed air pressure on the surface roughness parameter Rku. The obtained model is nonlinear. The values of the parameter Rku calculated from the model (3) are presented in the penultimate column in Table 6. The model and experimental values are similar. The linear correlation coefficient is 0.83. Figure 7 shows graphs developed from the regression equation (3).

Table 7. Critical values, calculated values and significance assessment

Coefficient	Critical value	Calculated value	Significance of coefficient	
b_0	0.1422	2.9576	$\|b_0\| > b_{0kr}$	Relevant
b_1	0.1052	-0.0600	$\|b_1\| < b_{kkr}$	Irrelevant
b_2	0.1052	-0.1983	$\|b_2\| > b_{kkr}$	Relevant
b_3	0.1052	-0.0750	$\|b_3\| < b_{kkr}$	Irrelevant
b_{11}	0.1657	0.0773	$\|b_{11}\| < b_{kkkr}$	Irrelevant
b_{22}	0.1657	-0.2177	$\|b_{22}\| > b_{kkkr}$	Relevant
b_{33}	0.1657	0.0243	$\|b_{33}\| < b_{kkkr}$	Irrelevant
b_{12}	0.1289	-0.0865	$\|b_{12}\| < b_{kjkr}$	Irrelevant
b_{13}	0.1289	-0.1975	$\|b_{13}\| > b_{kjkr}$	Relevant
b_{23}	0.1289	-0.0705	$\|b_{23}\| < b_{kjkr}$	Irrelevant

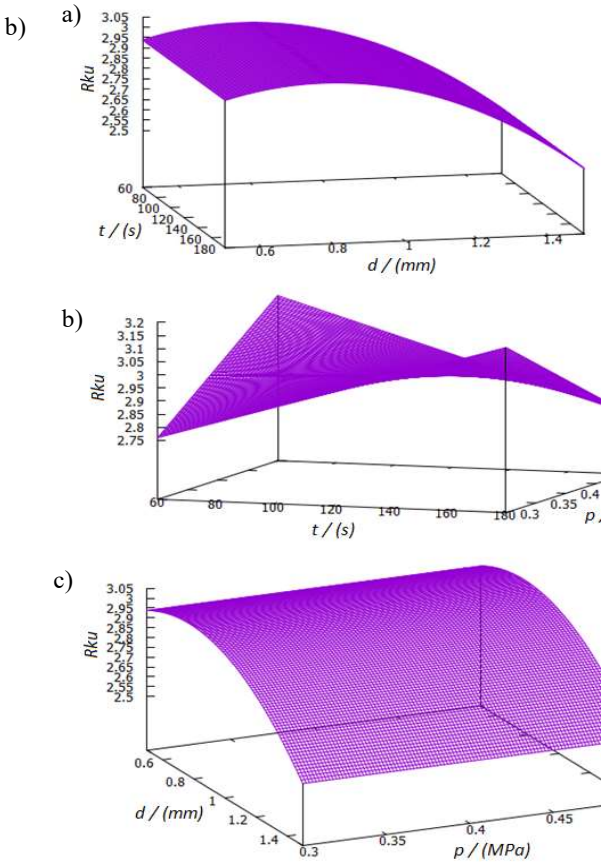

Fig. 7. Graphs showing: a) the effect of the time and ball diameter on Rku (p=0.4 [MPa]), b) the effect of the time and the pressure on Rku (dk =1 [mm]), c) the effect of the ball diameter and the pressure on Rku (t=60 [s]).

Based on the regression equation (3) and the obtained graphs (Fig. 7), it can be concluded that for the assumed area of variability of the input factors, increasing the shot peening time contributes to increasing the value of the Rku parameter. On the other hand, increasing the diameter of the balls and the pressure of compressed air decreases the value of the Rku parameter.

4. Conclusion

On the basis of the conducted analyzes, it was shown that in the adopted range of variability of the input factors:

- the roughness parameter, which is most strongly correlated with both the deflection of the Almen strips and the load capacity of adhesive joints after shot peening is the Rku parameter (the values of the linear correlation coefficient are respectively 0.647 and -0.807),
- there is a strong correlation between the load capacity of the adhesive joints and the deflection of the Almen strips (the value of the linear correlation coefficient is -0.733),
- the load capacity of the adhesive joints after shot peening increases with decreasing the value of the Rku parameter and the Almen strip deflection,
- the value of the Almen strip deflection increases with the increase of the Rku parameter,
- the value of the Rku parameter increases with the increase of the treatment time and the decrease of the ball diameter and the compressed air pressure.

Summarizing, the Rku roughness parameter can be used to predict the load capacity of adhesive joints after shot peening. The Almen test can be applied at the start of a batch of parts to check and document the shot peening process. Then, the correctness of the shot peening process can be assessed on the basis of the

surface roughness. The Almen test is quite expensive. Moreover, mounting of the Almen strips to the workpiece means that such a part often has to be additionally reinforced locally in the place where the control strip was fixed. Therefore, the assessment of the load capacity of the adhesive joints after shot peening on the basis of the surface roughness allows for a significant reduction in costs and simplification of the process. As a result, it can be successfully used by enterprises that use shot peening for strengthen adhesive joints.

References

1. Adamczak S. 2008. *Pomiary geometryczne powierzchni: zarysu kształtów, falistość i chropowatość*. Warszawa: Wydawnictwo Naukowo-Techniczne.
2. An T., Li S., Qu J., Shi J.,Zhang S., Chen L., Zhenga S., Yanga F. 2019. "Effects of shot peening on tensile properties and fatigue behavior of X80 pipeline steel in hydrogen environment". *International Journal of Fatigue* 129 : 105235.
3. Chaib M., Megueni A., Ziadi A., Guagliano M., Belzunce F., J., V. 2016. "Experimental study of the shot peening treatment effect on austenitic stainless steel". *International Journal of Materials and Product Technology* 53 : 298--314.
4. Custódio J. 2015. Structural Adhesives. W: *Materials for Construction and Civil Engineering*. *Science, processind and design* , 717-772. Springer.
5. da Silva Lucas F. M. , Öchsner Andreas , Adams Robert D. 2018. Introduction to Adhesive Bonding Technology. W: *Handbook of Adhesion Technology*, 1-8. Springer--Verlag Berlin Heidelberg.
6. Dobrzański L. 2010. *Leksykon Materiałoznawstwa. Praktyczne zestawienie norm polskich, zagranicznych i międzynarodowych. Cz. 4, rozdział 1: Metale nieżelazne i ich stopy.* Warszawa: Wydawnictwo Verlag Dashofer.
7. Dzierwa A. 2008. Kulowanie jako metoda poprawy wybranych właściwości warstwy wierzchniej elementów z powłokami chromowymi. W: *Współczesne problemy w technologii obróbki przez nagniatanie. Tom 2*, 241-248. Gdańsk: Katedra Technologii Maszyn i Automatyzacji Produkcji. Wydział Mechaniczny Politechniki Gdańskiej.
8. Grzesik W. 2015. "Effect of the machine parts surface topography features on the machine service". *Mechanik* 8-9 : 587-593.
9. Grzesik W. 2019. "Influence of surface roughness on fatigue life of machine elements – developments in experimental investigations and simulation". *Mechanik* 5-6 : 307-313.
10. Grzesik W. 2016. "Influence of surface textures produced by finishing operations on their functional properties". *Journal of Machine Engineering* 16 : 15-23.
11. Grzesik W. 2016. "Prediction of the Functional Performance of Machined Components Based on Surface Topography: State of Art". *Journal of Materials Engineering and Performance* 25 :4460-4468.
12. Her S.C., Chan C. F. 2019. "Interfacial Stress Analysis of Adhesively Bonded Lap Joint". *Materials* 12 : 2403.
13. https://tds.henkel.com/tds5/Studio/ShowPDF/?pid=EA%203430&format=MTR&subformat=HYS&language=PL&plant=WERCS&authorization=2 [Loctite EA 3430 technical data, access September 2022].
14. Iswanto P.T., Yaqin R.I., Akhyar, Sadida H.M. 2020. "Influence of shot peening on surface properties and corrosion resistance of implant material AISI 316L". *Metalurgija* 59 : 309-312.
15. Kavdir E.Ç., Aydin M.D. 2020. "The experimental and numerical study on the mechanical behaviors of adhesively bonded joints". *Composites Part B* 184 : 107725.
16. Korzyńska K., Zielecki W., Korzyński M. 2018. "Relationship between residual stress and strength of single lap joints made of Ti6Al4V alloy, adhesively bonded and treated using pneumatic ball peening". *Journal of Adhesion Science and Technology*, 1849-1860.
17. Korzyński M. 2013. *Metodyka eksperymentu. Planowanie, realizacji i statystyczne opracowanie wyników eksperymentów technologicznych*. Warszawa: Wydawnictwo WNT.
18. Kubit A., Bucior M., Zielecki W., Stachowicz F. 2016. "The impact of heat treatment and shot peening on the fatigue strength of 51CrV4 steel". *Procedia Structural Integrity* 2 : 3330-3336.
19. Kuczmaszewski J., Pieśko P., Zawada-Michałowska M. 2016. "Surface roughness of thin-walled components made of aluminium alloy EN AW-2024 following different milling strategies". *Advances in Science and Technology Research Journal* 10 : 150-158.
20. Laber S. 2010. "The influence of the condition of the surface layer on tribological properties spheroidal ferretic cast iron after pressing". *Tribologia* 1 : 51-60.
21. Lin Q., Liu, H., Zhu C., Chen D., Zhou S. 2020. "Effects of different shot peening parameters on residual stress, surface roughness and cell size". *Surface & Coatings Technology* 398 : 126054.
22. Liu J., Yue Z, Geng X., Wen S., Yan W. 2018. *Long-Life Design and Test Technology of Typical Aircraft Structures.* National Defense Industry Press and Springer Nature Singapore Pte Ltd.
23. Omari M. A., Mousa H. M., AL-Oqla F. M., Aljarrah M. 2019. "Enhancing the surface hardness and roughness of engine blades using the shot peening process". *International Journal of Minerals, Metallurgy and Materials* 6 : 999-1004.
24. Palacios M., Bagherifard S., Guagliano M., Fernández Pariente I. 2014. "Influence of severe shot peening on wear behaviour of an aluminium alloy". *Fatigue & Fracture & Engngineering Materials & Structures* 37 : 821–829.
25. PN EN 1465:2009 Adhesives – Determination of tensile lap-shear strength of bonded assemblies. Warsaw: Polish Committee for Standardization.
26. PN-EN ISO 4287:1999. Specifications of product geometry – Geometric structure of the surface: profile method – Terms, definitions and parameters of the geometric structure of the surface. Warsaw: Polish Committee for Standardization.
27. SAE J443 Procedures for Using Standard Shot Peening Test Strip.
28. Sherafatnia K., Farrahi G.H., Mahmoudi A.H., Ghasemi A. 2016. "Experimental measurement and analytical

determination of shot peening residual stresses considering friction and real unloading behavior". *Materials Science & Engineering* 657 : 309–321.
29. Zaleski K., Matuszak J., Zaleski R. 2018. *Metrologia warstwy wierzchniej*. Lublin: Wydawnictwo Politechniki Lubelskiej.
30. Zielecki W., Bąk Ł., Guźla E., Bucior M. 2019. "Statistical analysis of the influence shot peening arameters on the capacity of single lap adhesive joints from aluminim alloy 2024". *Technologia i Automatyzacja Montażu* 1 : 30-34.
31. Zielecki W., Korzyńska K. 2016. „Umacnianie zakładkowych połączeń klejowych stopu tytanu Ti6Al4V metodą pneumokulowania". *Technologia i Automatyzacja Montażu* 1 : 44-47.
32. Zielecki W., Pawlus P., Perłowski R., Dzierwa A.2013. "Surface topography effect on strength of lap adhesive joints after mechanical pre-treatment". *Archieve of Civil and Mechanical Engineering* 13 : 175-185.
33. Zielecki W., Pawlus P., Perłowski R., Dzierwa A. 2011. „Analiza wpływu struktury geometrycznej powierzchni w układzie 3D na wytrzymałość połączeń klejowych". *Technologia i Automatyzacja Montażu* 1 : 33-37.
34. Zielecki W., Perłowski R., Pawlus P. 2009. The analysis of the effect of surface topography on strength of lap glued joints. W: *Procedings of 12th International Conference on Metrology and Properties on Engineering Surfaces*. Reszów: Publications Rzeszów University of Technology.
35. Zielecki W., Perłowski R., Trzepieciński T. 2007. „Analiza stanu naprężeń w spoinie zakładkowego połączenia klejowego umocnionego metodą pneumokulowania". *Technologia i Automatyzacja Montażu* 1 : 31-33.
36. Zielecki W. 2008. *Determinanty určujúce pevnostné vlastnosti lepených spojov.* Habilitačná práca. Koszyce.
37. Zielecki W. 2007. „Wpływ rozwinięcia struktury powierzchni na wytrzymałość zakładkowych połączeń klejowych". *Technologia i Automatyzacja Montażu* 2, 3 : 108-111.
38. Zyzak P. 2015. "Evaluation of shot stream parameters using indicators of the test with control plates". *Mechanik* 8-9 : 374-381.

TiAM kwartalnik naukowo-techniczny
TECHNOLOGIA I AUTOMATYZACJA MONTAŻU
ZESPOŁÓW • MASZYN • URZĄDZEŃ

Paweł Przybyłek[1], Andrzej Komorek[2], Simone Taddeo Kaczor Di Paola[3], Łukasz Komorek[4]

DOI: 10.7862/tiam.2022.4.5

INFLUENCE OF THE SHAPE OF THE IMPACTOR ON RESIDUAL STRENGTH, SIZE AND NATURE OF DAMAGE TO CFRP

WPŁYW KSZTAŁTU BIJAKA NA WYTRZYMAŁOŚĆ SZCZĄTKOWĄ, WIELKOŚĆ I CHARAKTER USZKODZEŃ CFRP

Abstract

The experimental tests presented in this work concern the impact resistance test and residual strength properties after an impact performed by a drop tower INSTRON CEAST 9340. The authors prepared samples of a composite material with a polymeric matrix L285 and H285 hardener, reinforced with eight ply fabric of carbon fibre. Two shapes of the impactor (spherical and V-shape) were used to perform the testing. The samples were impacted by three values of energy (10, 15, 20 [J]). Three-point bending tests were performed to the residual strength of the samples subjected to impact tests and compared to samples which had not been damaged earlier. The study showed differences in the influence of the shapes of the impactor on the nature of the composite damage. After the test, conclusions were drawn about the influence of the shape of the impactor on the area of composite damage and its character. Also, its influence on residual strength was described. Despite the clear differences in the area of damage to composites impacted by different impactors, this does not have a significant influence on the residual strength.

Keywords: laminates, puncture resistance, impact strength, residual strength, bending strength

Streszczenie

Przedstawione w pracy badania eksperymentalne dotyczą badania udarności oraz właściwości wytrzymałości szczątkowej po uderzeniu wieżą zrzutową INSTRON CEAST 9340. Autorzy przygotowali próbki materiału kompozytowego z osnową polimerową L285 i utwardzaczem H285, wzmocnionego tkaniną ośmiowarstwową z włókna węglowego. Do badań wykorzystano dwa kształty impaktora (kulisty i V). Próbki były poddawane działaniu trzech wartości energii (10, 15, 20 [J]). Próby zginania trzypunktowego przeprowadzono do wytrzymałości szczątkowej próbek poddanych próbom udarności i porównano z próbkami, które wcześniej nie uległy uszkodzeniu. Badania wykazały różnice we wpływie kształtów impaktora na charakter uszkodzenia kompozytu. Po przeprowadzeniu badań wyciągnięto wnioski dotyczące wpływu kształtu impaktora na obszar uszkodzenia kompozytu i jego charakter. Opisano również jego wpływ na wytrzymałość resztkową. Pomimo wyraźnych różnic w obszarze uszkodzeń kompozytów pod wpływem różnych impaktorów, nie ma to istotnego wpływu na wytrzymałość szczątkową.

Słowa kluczowe: laminaty, odporność na przebicie, wytrzymałość na uderzenie, wytrzymałość resztkowa, wytrzymałość na zginanie

1. Introduction

Composite materials are now widely used in aviation structures due to their good strength-to-weight ratio and stiffness, which significantly reduces the weight of the structure compared to the materials used so far, e.g. aluminum alloys [1-4]. The most commonly used composites in the construction of airplanes and helicopters are laminates, i.e. layered composites [5-7]. In addition, in recent years, the dynamically developing field of aviation related to UAVs began to use more and more structural materials with a small thickness [8-11]. Many composite components can be exposed to low-energy impact loads perpendicular to the component surface [12, 13].

[1] PhD. Eng. Paweł Przybyłek (corresponding author), Polish Air Force University, ul. Dywizjonu 303, 35, 08-530 Dęblin, Poland, e-mail: p.przybylek@law.mil.pl, ORCID: 0000-0002-7544-3813.
[2] DSc. Eng. Andrzej Komorek, Polish Air Force University, ul. Dywizjonu 303 No. 35, 08-530 Dęblin, Poland, e-mail: a.komorek@law.mil.pl, ORCID: 0000-0002-2293-714X.
[3] Eng. Simone Taddeo Kaczor Di Paola, Polish Air Force University, ul. Dywizjonu 303 No. 35, 08-530 Dęblin, Poland, e-mail: s.kaczordipaola4754@wsosp.edu.pl
[4] Eng. Łukasz Komorek (corresponding author), Polish Air Force University, ul. Dywizjonu 303 No. 35, 08-530 Dęblin, Poland, e-mail: l.komorek5374@wsosp.edu.pl

This type of load is especially common in the maintenance process of aircraft [14-16] and despite the low energy value, they often result in deterioration of the strength properties of the composite element [17--21]. There are numerous conditions for this impact: hailstones and bird strikes being the most significant ones, owing to their high chance of occurrence [22--25]. On the other hand, a tyre piece can strike the wing structures and the ice coming from the propeller blade edge could also impact the nacelle of the aircraft engine[26]. Therefore, the study of impact behaviors and residual strength of CFRP laminates is necessary to improve the impact resistance and damage tolerance of the composite . The damage evaluation criteria (including dent depth, DDPA (delamination damage projection area), energy dissipation, RBS (residual bending strength), etc.) are vital for the assessment of the damage status of laminates [17-21]. Due to the damage caused by the action of transverse impact loads, the following can be distinguished:

- BVID – barely visible impact demage,
- VID – visible impact demage.

BVID defined by two aircraft manufacturers, Airbus and Boeing, is damage caused by an impact and it is determined only by the depth and area of the damage, which cannot be detected during inspection, visual inspection under typical lighting conditions from a distance of 1.5 m [28]. There are many studies in the literature that determine the influence of various factors on puncture resistance, damage tolerance or other strength parameters [22]. They are analyzed and checked experimentally in order to find the best solutions. The basic factors are the architecture of the fabric and the properties of the matrix, which have the most significant influence on the puncture resistance of composites reinforced with fiber. The secondary factors include: fiber hybridization, matrix hybridization, hygrothermic factors, the sequence of layering, impactor geometry (mass, size, shape), impact repeatability [29]. The constituent and geometrical parameters are broadly investigated parameters in the study of impact mechanics of composites. Relatively little interest has been given in the literature to the impactor shape, size, velocity, mass, and angle and this effect is still not entirely formulated. [30-34]. The influence of the impactor in specific, the combined effects of impactor nose shape, the angle of obliquity, mass, size and boundary condition on the impact resistance of composite materials are not clearly addressed [22]. Due to the very wide use of such materials for the construction of aircraft covers, tests were carried out on the resistance of composites to low-energy impact loads to which composite structures of aircraft are exposed during everyday operation. This is a very important feature due to the fact that at low energy values (1… 3 J) no signs of material destruction are visible from the side of load application. This is evidenced by the amount of research conducted in the last two decades, eg. in [35] the authors presented historical developments in the study of composite structures under high velocity impact events by analyzing 27 works on this subject in various terms. Moreover, as previously mentioned, despite the many studies carried out on the influence of the shape, mass and size of the "impactor" on the impact resistance, this effect is still not clearly formulated. For many reasons (including economic), visual inspection remains the most popular method of locating impact damage of aircraft structure and it has been included in relevant normative documents for many years [36,37]. Visual inspection is relatively fast as a primary method and has a large field of view for the in-service inspection of composite structures. Therefore, visual inspection is also one of the important basis for defining Barely Visible Impact Damage (BVID). Therefore, it is necessary to determine the correlation between the size of the damage and the decrease in strength properties in order to unequivocally carry out the damage assessment, which will allow to make a decision on the efficiency of the aircraft. This article presents the results of tests of the puncture resistance of CFRP subjected to a three-energy (10, 15, 20 [J]) impact and two-shape impactors. As a comparative parameter, the damage surface areas of the laminate from the impact side and the opposite side were adopted, and the peak values of force, energy and displacement were taken into account (Peak force [N], Peak Energy [J], Peak displacement [mm]) and relative properties: Peak force on thicknes [kN/m], Peak energy on thicknes [J/m]. Moreover, in order to analyze and evaluate the influence of the shape of the "impactor" and the impact energy on the strength properties of the tested composite, the bending strength and bending modulus of the previously impacted specimens were determined.

2. Experimental investigation

2.1. Preparation of samples for testing

A symmetric cross-ply laminate was made using the hand lamination method. It was then placed in a Mecamaq hydraulic press for 24 hours under a pressure of 1 [MPa].

The composite matrix is a certified aerospace epoxy resin, L285, cross-linked with H285 hardener (Table 1).

The reinforcement was a carbon-fibre fabric designated GG-416 T and produced by G. ANGELONI with a twill weave (diagonal) and the parameters shown in Table 2.

Table 1. Parameters of resin L285 and hardener H285

List of mechanical parameters for LG285 resin		
Parameter	Unit	Value
Bending strength	MPa	110 – 120
Modulus of elasticity in bending	MPa	2,700 – 3,300
Tensile strength Rm	MPa	75 – 85
Compressive strength	MPa	130 – 150
Elongation	%	5 – 6.5
Fatigue strength	KJ/m-2	38 – 48
Shore hardness	-	85

Table 2. Parameters of reinforcement fabric

Symbol	Weight (g/m^2)	Weave
GG 416 T	416	Dual 2 2/ 2
	Fibre/Bundle	
	Matrix	Matrix
	carbon 800 tex	carbon 800 tex
	Thickness (mm)	
	0.41	

Thirty-four 60x80mm rectangular samples were prepared from the composite. They were grouped into seven batches.

2.2. Impact resistance tests

The impact resistance tests were conducted on an INSTRON CEAST 9340 drop tower. The samples were subjected to transverse impact loads of 10, 15, and 20 J energies. Two "impactors" were used, the first one with a spherical shape, 20 mm in diameter, and the second one wedge-shaped (V-shaped) with an opening angle of 30° and a striking edge radius of 3 mm (Fig. 1). A series of at least 3 samples was made for each energy and each impactor. The samples were placed on the stage without fixing.

Fig. 1. Shapes of 'impactors' used in the tests

The examination parameters for specific energies have been presented in Table 3.

A number of parameters were obtained as a result of the research. The parameters were later used to analyse the impact resistance in the aspect of the 'impactor' shape. Damage to the composites was caused as a result of the impact on the test material, which was assessed. The damage areas of the laminate on the impacted side and the opposite side were used as a comparative parameter. The selected and representative images along with marked areas of damage, after an impact, with different energies and impactors are presented in Figure 2 and Figure 3.

Table 3. parameters of impact resistance test

Impact energy [J]	Weight [kg]	Height of the impactor [mm]	Impact speed [m/s]
10	2.65	385.0	2.72
15		577.0	3.33
20		770.0	3.85

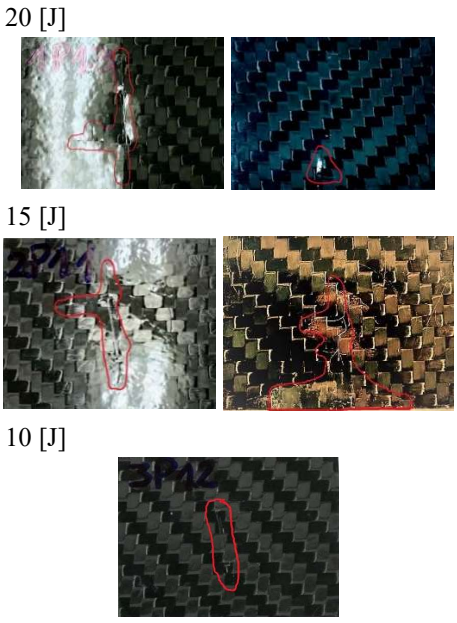

Fig. 2. Damage area of a sample impacted by a wedge-shaped impactor from the impacted side and opposite side

In the case of samples struck with a wedge 'impactor' on the impacted side, the composite was damaged with a shape reflecting that of the impactor (Fig. 2). Depending on the energy of the impact, there was cracking of the reinforcement along the fibres of the fabric with a different depth and area. For an impact energy of 10 [J], the damage on the impacted side is tiny, with an average area of approximately 150 mm^2. Furthermore, no damage to the laminate was observed on the side opposite to the impacted side.

The surface of the samples impacted by the spherical impactor caused damage in the form of an indentation, which initiated cracks in the horizontal and vertical cross-shaped reinforcement fabric (Fig. 3). Similarly to the previous 'impactor', the area of damage depends on the energy of the impact. Damage was observed on the surface opposite to the impacted area for each energy. For the highest energy value (20 [J]) there is also a clear perforation of the laminate.

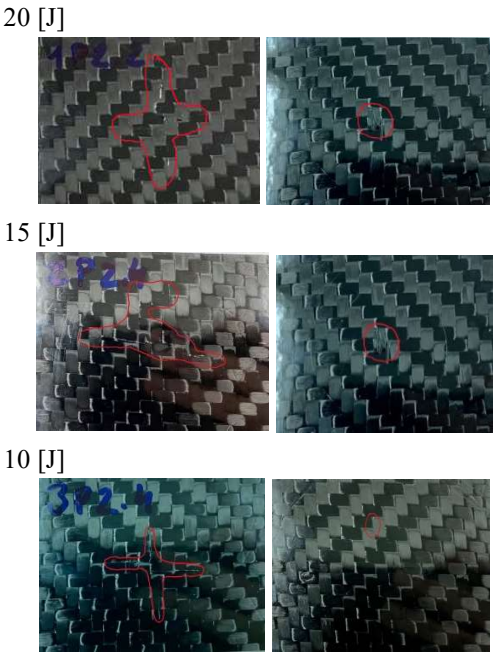

Fig. 3. Damage area of a sample struck by a spherical shaped impactor from the impacted side and opposite side.

When comparing the damage areas on the impacted side (Fig. 4) and on the opposite surface (Fig. 5), some regularities can be noticed in the aspect of the shape of the "impactor."

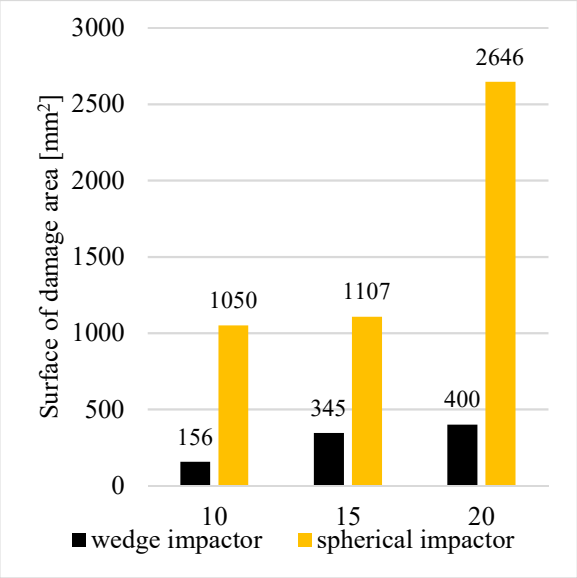

Fig. 4. Damage area on the impacted side

The damage area of the tested composite is always larger for a spherical 'impactor'. The damage to the samples is approximately 6.5 times greater with a spherical 'impactor' on the struck surface (Fig. 4). However, on the surface opposite to the impacted surface (Fig. 5), the damage is comparable and only approximately 10 % larger for the spherical impactor. On both the impacted and counter-impacted surfaces, the difference in damage size for both impactors depends on the impact energy. The largest damage area was recognized after impact with 20 [J] energy, but especialy in the counter-impacted surface difrence for wedge impactor is about 30% and about 80% for spherical impactor.

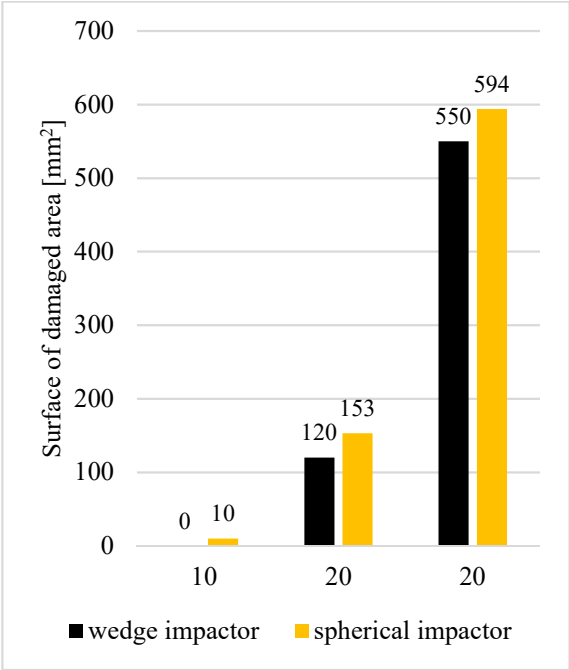

Fig. 5. Surface area of damage on the opposite side from the impacted side

Other recorded parameters were also taken into account for a more detailed analysis of puncture resistance. Peak force, energy and deformation (peak force [N], peak energy [J], peak displacement [mm]) and relative properties were considered to assess puncture resistance: peak force on thickness [kN/m], peak energy on thickness [J/m]. The dropping hammer is equipped with a force sensor; based on its value, the energy (1), (2), and deformation (3) are calculated according formulas presented below.

$$E_i = \int_i F(\varepsilon) \tag{1}$$

$$E_i = \sum_{i=0}^{i-1} E_i + t_{sampling} \frac{F_i v_i + F_{i-1} v_{i-1}}{2} \tag{2}$$

$$\varepsilon_i = \sum_{i=0}^{i-1} \varepsilon_i + t_{sampling} \frac{v_i + v_{i-1}}{2} \tag{3}$$

where: $t_{sampling}$ – sampling time,
ν – rate of change of strain,
F – measured force.

The results, which were used to analyse the puncture resistance of the tested material in terms of the 'impactor' shape are presented in Table 4.

Table 4. Results of the examination: impact resistance

Impact energy [J]	Peak Force [N]	Peak Energy [J]	Peak Displacement [mm]	Peak force on thickness [kN/m]	Peak energy on thickness [J/m]
"Wedge impactor"					
10	7,234.93	9.68	2.31	3,448.28	6,649.17
15	8,556.96	14.22	3.16	2,966.24	4,985.07
20	9,956.87	19.19	3.57	2,527.13	3,439.11
"Spherical impactor"					
10	6,723.84	9.59	2.83	2,241.28	3,197.02
15	8,379.74	14.58	3.78	2,912.90	5,073.39
20	9,006.27	17.08	4.07	3,175.00	6,20.11

Based on the obtained parameters, it can be concluded that the force transmitted by the test material mainly depends on the value of the impact energy and is highest for the highest impact energies. It only slightly depends on the shape of the "impactor". The differences in peak force values (Peak Force) are only about 10 % and increase with the impact energy. In order to analyse the puncture resistance in detail, a comparison was also made of the force variation (Fig. 6, Fig. 7) over time and the force variation with respect to deformation (Fig. 8, Fig. 9).

By comparing the characteristics of force variation over time, it is possible to see significant differences in the behaviour of the examined material when impacted with different 'hammers'. In the case of a 'spherical impactor', the change in impact energy does not affect the way the composite responds to the impact; also the shape of the curve indicates its elastic nature.

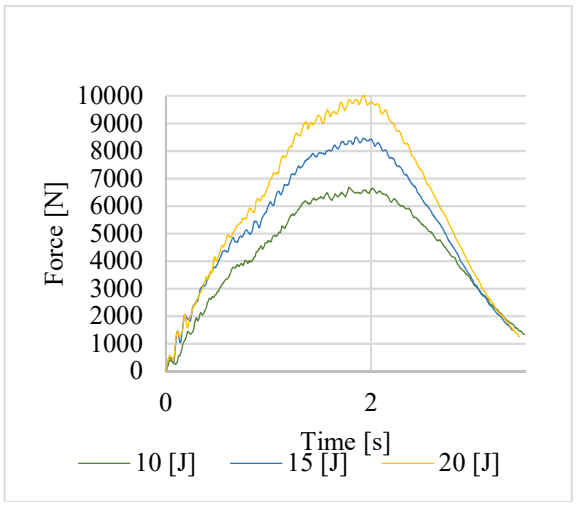

Fig. 6. Force variation during in impact with a spherical "impactor"

In addition, the response (contact) time of the composite is identical for all impact energies. In the case of a 'wedge hammer', the nature of the curve (Force-Time) (Fig.7) indicates permanent deformation under impact loading and damage within the composite.

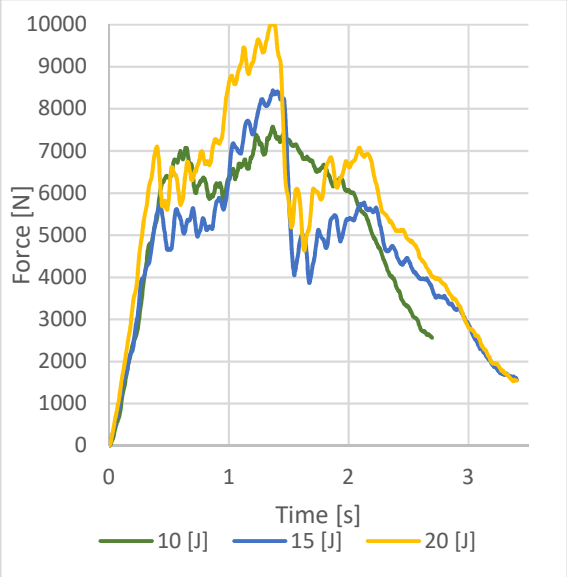

Fig. 7. Force variation curves during an impact with a wedge-shaped impactor

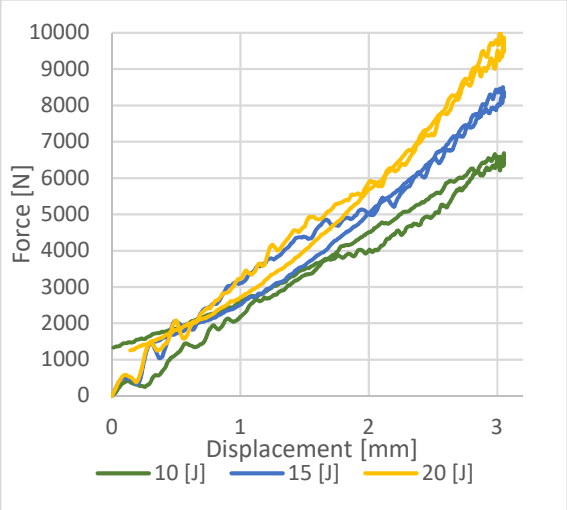

Fig. 8. Force-deformation curves for the impact of a spherical "impactor"

Furthermore, the nature of the composite response for an impact energy of 10 [J] is different for all impact energies, the force at which the destruction process of the F_{ini} composite is initiated. It is similar and it can be assumed that this is the value of the load at which the impact layer of the composite perforates and thus breaks the fibres of the reinforcement. An oscillation of force values can then be observed, which are indicative of specific 'stress waves' in the material and damage to the matrix 'layer' occurring in-between the reinforcement layers. The force then builds up until it reaches its maximum value of F_{max} (Peak Force). The

rapid decrease in its value, after F_{max} has been reached, indicates deceleration of the damage process and the true puncture resistance of the test material. For the impact energies of 15 and 20 [J], a repeat increase in force can be observed until another specific extreme is reached, which indicates the response of the next reinforcement layer to the load. On the basis of these changes, it can be estimated that the "wedge hammer" caused internal damage to the laminate and that its depth along the thickness of the test material depends on the impact energy.

The characteristics of the change in force versus deformation (Fig. 8, Fig. 9) allow the energy absorbed by the laminate to be estimated (area inside the curve--area under the force-deflection curve).

The slope of the curve provides an estimate of the stiffness of the composite and the shape of the curve indicates the nature of the damage to the composite. In the case of tests carried out with two different shape impactors, there was no complete perforation of the composite, as evidenced by the closed loop of the curve and the return of the force with respect to deformation at the initial value. However, there is clearly a change in the nature of the composite's response to an impact depending on the shape of the 'impactor'. Also, the value of the absorbed energy depends on the type of used 'impactor'.

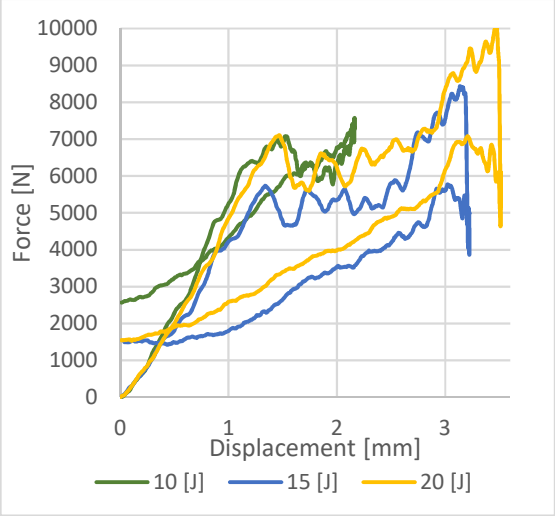

Fig. 9. Force vs. deformation curves for a wedge-shaped impactor

Furthermore, in the case of the 'wedge impactor', the amount of absorbed energy depends on the value of the impact energy, as indicated by the changes in the shape of the force-deformation characteristics (Fig. 9).

2.3. Bending flexular strength test

In the next stage of experimental testing, the samples previously subjected to transverse impact loads (impact) were tested to determine the residual strength, i.e. the bending strength.

The test was conducted in a three-point bending scheme on a ZWICK/ROELL Z5 testing machine in accordance with PN EN ISO 178, at the support span of L=46 mm (Fig. 10).

As a result of the study, the following were determined:

σ_{fM} – bending strength [MPa],

E_f – modulus of elasticity in bending [GPa].

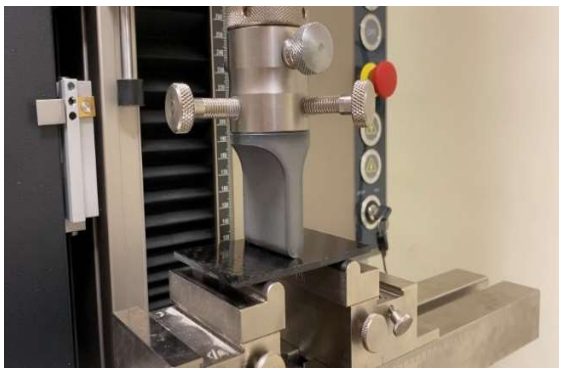

Fig. 10. Bending flexural strength test

The obtained results were related to the control (non-impacted) samples and the results are presented in Figures 11, 12, 13.

The changes in the bending strength values are mainly dependent on the impact energy and, compared to the control samples (not subjected to an impact), there was a decrease of approximately 40% for an impact energy of 10 [J], 50% for an impact energy of 15 [J] and 60% for an impact energy of 20 [J].

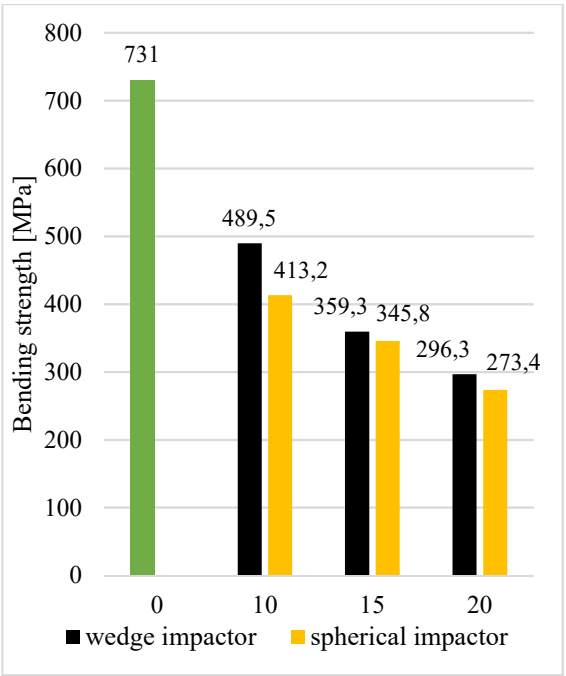

Fig. 11. Bending strength σ_{fM} [MPa]

In all the cases, the "wedge impactor" resulted in a greater decrease in bending values strength. However, depending on the shape of the "impactor", the differences are negligible: approximately 10% for an energy of 10 [J], approximately 3% for an impact energy of 15 [J] and 20 [J]. In the case of changes in the modulus of elasticity in bending, the 'spherical impactor' caused its even larger decline: 35% for an impact energy of 10 [J], 50% for an impact energy of 15 [J] and 60% for an impact energy of 20 [J].

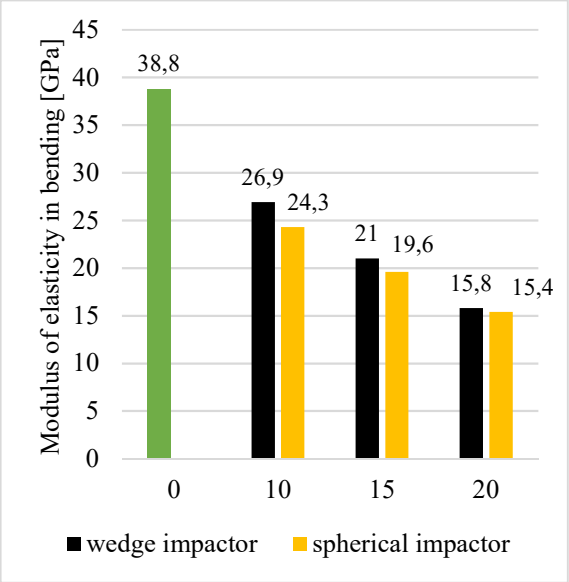

Fig. 12. Modulus of elasticity in bending E_f [GPa]

The differences with regard to the 'impactor' shape are minimal and decrease along with an increase in an impact energy: approximately 5% for an impact energy of 10 [J], approximately 3% for an impact energy of 15 [J] and 1% for an impact energy of 20 [J].

3. Conclusions

The conducted puncture resistance tests made it possible to estimate the effect of impacts with two 'impactor' shapes and three energies (10, 15, 20 [J]) on both the extent and nature of damage to the layered composite with a carbon fibre reinforcement and on the degradation of the strength properties: bending strength σ_{fM} and the modulus of elasticity in bending E_f. It also made it possible to formulate conclusions.

The shape of the impactor influences the magnitude of the analysed parameters, such as damage area or strength parameters, declining along with an increasing impact energy;

The damage area of the tested composite is always larger for the spherical 'impactor'. However, on the surface opposite to the impacted surface damage, the damage is comparable and is only approximately 10% larger for the spherical impactor.

The "wedge impactor" resulted in a greater decrease in bending strength. However, the variation in its value mainly depends on the impact energy; the differences in the aspect of the 'impactor' shape decrease with an increasing impact energy, amounting to approximately 10% for the impact energy 10 [J], approximately 3% for the impact energy 15 and 20 [J].

Detailed comparisons of the force variation curves (Fig. 6, Fig. 7) over time and of the force variation with respect to deformation makes it possible to conclude that the "wedge impactor" caused internal damage to the laminate and that its "depth along the thickness of the examined material depends on the impact energy.

References

1. Soutis Constantine. 2005. Fibre reinforced composites in aircraft construction. Progress in Aerospace Sciences. Volume 41, Issue 2, 143-151, doi.org/10.1016/j.paerosci.2005.02.004.
2. A.J. Beck, A. Hodzic, C. Soutis, C.W. Wilson, 2009. IOP Conf. Ser.: Mater. Sci. Eng.
3. Y.X. Zhang, Zhi Zhu, Richardson Joseph, Isfakul Jamal Shihan. 2020. Damage to aircraft composite structures caused by directed energy system: a literaturę review. Defence technology. https:// doi.org/10.1016/j.dt.2020.08.008.
4. Fengyang Jiang, Zhidong Guan, Zengshan Li, Xiaodong Wang. 2021. A method of predicting visual detectability of low-velocity impact damage in composite structures based on logistic regression model. Chinese Journal of Aeronautics. 34(1): 296–308.
5. Królikowski Wacław 2012, Polimerowe kompozyty konstrukcyjne. Warszawa, Wydawnictwo Naukowe PWN.
6. Bruno Castanie, Christophe Bouvet, Malo Ginot. 2020. Review of composite sandwich structure in aeronautic applications , Composites Part C: Open Access 1.
7. Xianfeng Yang, Jingxuan Ma, Dongsheng Wen, Jialing Yang. 2020. Crashworthy design and energy absorption mechanisms for helicopter structures: A systematic literature review, Progress in Aerospace Sciences 114.
8. Qi Liu, Zhangzhi Ge, Wei Song. 2016. Research Based on Patent Analysis about the Present Status and Development Trends of Unmanned Aerial Vehicle in China, Open Journal of Social Sciences, Vol. 4, No. 7.
9. Daeil Jo, Yongjin Kwon. 2017. Development of Rescue Material Transport UAV (Unmanned Aerial Vehicle), World Journal of Engineering and Technology, Vol. 5, No. 4.
10. Jiawen Yu. 2018. Design and Optimization of Wing Structure for a Fixed-Wing Unmanned Aerial Vehicle (UAV), Modern Mechanical Engineering, Vol. 8, No. 4.
11. Mohamed M. ElFaham, Ayman M. Mostafa, G.M. Nasr. 2020. Unmanned aerial vehicle (UAV) manufacturing materials: Synthesis,spectroscopic characterization and dynamic mechanical analysis(DMA, Journal of Molecular Structure 1201. https://doi.org/10.1016/j.molstruc.2019.127211.
12. R.C. Batra, G. Gopinath, J.Q. Zheng. 2012. Damage and failure in low energy impact of fiber-reinforced polymeric

composite laminates, Composite Structures, Volume 94, Issue 2. 540-547.https://doi.org/10.1016/j.compstruct.2011.08.015.
13. G. Perillo, J.K. Jørgensen. 2016. Numerical/Experimental Study of the Impact and Compression after Impact on GFRP Composite for Wind/Marine Applications, Procedia Engineering, Volume 167. 129-137, https://doi.org/10.1016/j.proeng.2016.11.679.
14. Ravi B. Gondaliya. 2016. Improving Damage Tolerance of Composite Sandwich Structures Subjected to Low Velocity Impact Loading: Experimental and Numerical Analysis, Dissertations and Theses, Embry-Riddle Aeronautical University Daytona Beach.
15. Ercan Sevkat, Benjamin Liaw, Feridun Delale, Basavaraju B. Raju. 2009. Drop-weight impact of plain-woven hybrid glass–graphite/toughened epoxy composites, Composites: Part A 40. 1090–1110.
16. U.S. Department of Transportation, Federal Aviation Administration, 'Composite aircraft structure', Advisory Circular AC No: 20-107B, Change 1, 24 August 2010.
17. Qihui Lyu, Ben Wang, Zhenqiang Zhao, Zaoyang Guo. 2022. Damage and failure analysis of hybrid laminates with different ply-stacking sequences under low-velocity impact and post-impact compression, Thin-Walled Structures 180.
18. Mubarak Ali, S.C. Joshi, and Mohamed Thariq Hameed Sultan, 2017. Palliatives for Low Velocity Impact Damage in Composite Laminates, Advances in Materials Science and Engineering, 16 pages.https://doi.org/10.1155/2017/8761479.
19. Ramesh Talrejaa, Nam Phanb. 2019. Assessment of damage tolerance approaches for composite aircraft with focus on barely visible impact damage, Composite Structures 219. 1–7.
20. Botelho E.C., Silva R.A., Pardini L.C., Rezende M.C. 2006. A review on the development and properties of continuous fiber/epoxy/aluminum hybrid composites for aircraft structures. Materials Research. 9(3): 247–256. doi: 10.1590/S1516-14392006000300002.
21. Komorek A., Przybyłek P. 2012. Examination of the influence of cross-impact load on bend strength properties of composite materials, used in aviation. Eksploatacja i Niezawodność. 14, 265-269.
22. J. Jefferson Andrew, Sivakumar M. Srinivasan, A. Arockiarajan, Hom Nath Dhakal, 2019. Parameters influencing the impact response of fiber-reinforced polimer matrix composite materials: A critical review, Composite Structures 224.
23. Airoldi A., Cacchione B. 2006. Modelling of impact forces and pressures in Lagrangian bird strike analyses. Int J Impact Eng 32:1651–77.
24. Anghileri M., Castelletti L.M.L., Invernizzi F., Mascheroni M. 2005. A survey of numerical models for hail impact analysis using explicit finite element codes. Int J Impact Eng 31:929–44.
25. Stanislav Dubinskii, Vitaliy Senik, Yuri Feygenbaum, 2019. The Significance of In-Service Factors for the Visual Detectability of Impact Damage in Composite Airframe, Journal of Nondestructive Evaluation. 38:91 https://doi.org/10.1007/s10921-019-0632-3.
26. M. Droździel, P. Jakubczak, J. Bieniaś. 2021. Low-velocity impact resistance of thin-ply in comparison with conventional aluminium-carbon laminates, Composite Structures, Volume 256.
27. Jianwu Zhoua, Binbin Liaob, Yaoyao Shia, Yangjie Zuoc, Hongliang Tuod, Liyong Jiae, 2019. Low-velocity impact behavior and bending tensile strength of CFRP Laminates, Composites Part B 161. 300–313.
28. S.N.A. Safri, M.T.H. Sultan, N. Yidris, F. Mustapha, 2014. Low Velocity and High Velocity Impact Test on Composite Materials – A review, The International Journal Of Engineering And Science, Volume 3, Issue 9, 50-60.
29. S. Shah, S. Karuppanan, P. Megat-Yusoff i Z. Sajid, 2019. Impact resistance and damage tolerance of fiber reinforced composites: A review. Composite Structures, tom 217. 100-121.
30. Mitrevski T., Marshall I.H., Thomson R., Jones R. 2006. The influence of impactor shape on the damage to the composite laminates. Compos Struct. 76:116–22.
31. Zhou G., Lloyd J.C., McGuirk J.J. 2001. Experimental evaluation of geometric factors affecting damage mechanisms in carbon/epoxy plates. Composites Part A. 32:71–84.
32. Dhakal H.N., Zhang Z.Y., Bennett N., Reis P.N.B. 2012. Low-velocity impact response of non-woven hemp fibre reinforced unsaturated polyester composites: Influence of impactor geometry and impact velocity. Compos Struct. 94:2756–63.
33. Zarei Hamed, Sadighi Mojtaba, Minak Giangiacomo. 2017. Ballistic analysis of fiber metal laminates impacted by flat and conical impactors. Compos Struct ;161:65–72. ISSN 0263-8223.
34. Artero-Guerrero J.A., Pernas-Sánchez J., López-Puente J., Varas D. 2015. Experimental study of the impactor mass effect on the low velocity impact of carbon/epoxy woven laminates. Compos Struct. 133:774–81. ISSN 0263-8223.
35. N. Razali, M.T.H. Sultan, F. Mustapha, N. Yidris, M.R. Ishak. 2014. Impact Damage on Composite Structures – A Review, The International Journal Of Engineering And Science (IJES). Volume 3. Issue 7. 08-20.
36. FAA. Advisory circular composite aircraft structure. Washington D.C.: Federal Aviation Administration; 2009. Report No.: 20–107 (B); . SAE International. CMH-17 Composite Materials Handbook volume 3. polymer matrix composites materials usage, design, and analysis. Warrendale: SAE. International 2012.
37. Spencer F.W. 1996. Visual inspection research project report on benchmark inspections. Washington D.C.: Federal Aviation Administration. Report No: DOT/FAA/AR-96/6.

TiAM kwartalnik naukowo-techniczny
TECHNOLOGIA I AUTOMATYZACJA MONTAŻU
ZESPOŁÓW • MASZYN • URZĄDZEŃ

Monika Lubas[1]

DOI: 10.7862/tiam.2022.4.6

THE VISUAL RESEARCH OF CHANGES IN THE GEOMETRY OF A RIVET JOINT FOR MATERIAL MODEL EFFECT FOR SIMULATION RIVETED JOINTS MADE OF EN AW 5251

BADANIA WIZUALNE ZMIAN GEOMETRII POŁĄCZENIA NITOWEGO NA POTRZEBY OCENY DOBORU MODELU MATERIAŁOWEGO W PRZYPADKU POŁĄCZENIA WYKONANEGO Z EN AW 5251

Abstract

The paper presents the results of a numerical analysis of a single-lap joint with a blind rivet and its geometrical verification by inside views from the experiment. The research aimed to determine how the results of numerical analyses (FEM) were influenced by the method of modeling the material model and how it relates to the experimental results. As part of the analyses, a discrete riveted model and material model: linear and nonlinear were constructed. The analyses took into account various load cases (500, 800, and 900 N) to better illustrate the relationship between the numerical and experimental results. A new methodology of visualizing changes in a riveted joint's geometry was used to validate the results. The technology of making riveted joint cross-sections was developed during a static tensile test. Samples of a single lap joint with blind rivets made of aluminum sheets were subjected to a shear load. Deformations were "frozen" during the test, and sections were prepared. The microscope photos allowed for the development of a method for visualizing the deformation of the hole and rivet. The numerical results (for various loads and various material configurations) were compared with the experimental results of geometric parameters (i.e. angles between sheets or other dimensions) on the riveted joint cross-sections. The obtained results help to understand the mechanism of failure of the blind rivet under load and the complex state of loads in various stages of deformation.

Keywords: blind rivet, numerical analysis, nonlinearity, deformation

Streszczenie

W pracy przedstawiono wyniki analizy numerycznej połączenia zakładkowego z nitem zrywalnym oraz weryfikację geometrii przekrojów połączeń z eksperymentu. Badania miały na celu określenie, jaki wpływ na wyniki analiz numerycznych (MES) ma sposób modelowania modelu materiałowego i jaki ma on związek z wynikami eksperymentalnymi. W ramach analiz skonstruowano model dyskretny połączenia nitowego oraz model materiałowy: liniowy i nieliniowy. W analizach uwzględniono różne przypadki obciążeń (500, 800 i 900 N), aby lepiej zilustrować związek między wynikami numerycznymi a wynikami eksperymentalnymi. Do walidacji wyników zastosowano nową metodologię wizualizacji zmian w geometrii połączenia nitowego. Technologia wykonywania przekrojów połączeń nitowych została opracowana podczas statycznej próby rozciągania. Próbki pojedynczego połączenia zakładkowego z nitami zrywalnymi i arkuszami aluminiowymi poddano testom ścinającym. Odkształcenia zostały „zamrożone" podczas eksperymentu, następnie przygotowano przekroje połączeń. Zdjęcia mikroskopowe pozwoliły na opracowanie metody wizualizacji deformacji otworu i nitu. Wyniki numeryczne (dla różnych obciążeń i różnych konfiguracji materiałów) porównano z wynikami eksperymentalnymi parametrów geometrycznych (tj. kąta między blachami, kąta obrotu nita itd.) na przekrojach połączeń nitowych. Uzyskane wyniki pozwalają zrozumieć mechanizm niszczenia nitu zrywalnego pod obciążeniem oraz złożony stan obciążeń w różnych stadiach odkształcenia.

Słowa kluczowe: nit zrywalny, analiza numeryczna, model nieliniowy, odkształcenia

1. Introduction

Riveted joints are indispensable elements in the design and construction of thin-walled structures and are widely used in many industries [27, 34], including aviation [36]. The most frequently used types of rivets are solid rivets, blind rivets, rivet nuts, and the newly used SPR self-piercing rivets [29]. Most often, solid rivets are used in lap rivet joints, but usually, access from two sides is required when is formed the head. Thin-walled pro-files are connected with blind rivets. The advantages of blind rivets include connection with

[1] MSc. Eng. Monika Lubas, Department of Aerospace Engineering, Faculty of Mechanical Engineering and Aeronautics, Rzeszow University of Technology, al. Powstańców Warszawy 8, 35-959 Rzeszow, Poland, e-mail: m.lubas@prz.edu.pl, ORCID: 0000-0003-1031-7055.

one-sided access, low cost, uncomplicated riveting process, and the possibility of disassembly and reassembly of the joined elements [26, 29]. The geometric parameters, working conditions, and the type of material influence the choice of technology of connection and the type of rivet.

Research on riveted joints was discussed both in experimental and numerical research. The widest group of works are experimental studies of riveted joints. Skorupa [36], carried out an analysis of secondary bending in the lap and overlay riveted joints during the fatigue test. The work [28] described the results of shear tests of joints made with different joining systems. Furthermore, Qasim [33] presented experiments on blind rivets, which concerned the influence of the hole diameter, rivet length, and joint thickness on the shear stresses, mechanical behavior, and in particular the strength. Many authors were focused on the study of static and fatigue tests. In publication [28], the authors presented the results of the experimental analysis of the strength of a single-lap joint in a shear test at 23, 400, 600, and 800°C. They proved that the load capacity of a riveted joint drops drastically with increasing temperature during the static test.

Another author [20] presented the influence of the distance from the rivet to the edge of the sheet on the quality and strength of the joint, and in the article [12] the influence of the configuration of the multilayer joint was examined. The technology of SPR between different combinations of materials has also been investigated experimentally by Jiang et al. [18, 19, 22]. Additionally, in [22], the authors conducted microtopographic observations and hardness measurements and compared the results with P-SPR riveted joints.

The comparison of the experiment with numerical research can be found in many works [3, 16, 25]. The test results indicate that residual stresses and plastic deformation can change the location of the crack initiation and the crack propagation plane.

A separate group of articles [10, 37] was publicized on the research on riveted joints made with the new mechanical method, self-piercing riveting (SPR). Moraes [25] simulated the riveting process using a nonlinear finite element model and the joint deformation process. The authors presented the impact of these processes on the residual stresses and the model of joint failure. Other authors [1, 34] presented results about the fatigue and static strength of cross-shaped SPR joints with aluminum alloy plates at various loading angles.

In many publications, the authors compared the types of connections such as hybrid, adhesive, and riveted joints. Authors [9, 11] presented the experimental results of the geometrical parameters and their influence on the strength. In addition, the results were verified with numerical investigations and shear damage models were also used to model the initiation of the damage in the joints. Furthermore, Pitta [30] presented an experimental and numerical analysis of repairs on carbon fiber-reinforced epoxy (CFRE) substrates, with CFRE and aluminum alloy doublers typical of aircraft structures. In the work [2], the authors described a numerical analysis of a single-lap hybrid (bonded/bolted) composite joint in tension with different load values and different bolt configurations.

The last group of publications of research on riveted joints is works that describe in detail the plastic deformation and changes in the geometry of the joint. In the work [15], the mechanical behavior of a riveted joint with an aluminum rivet under quasi-static load conditions was experimentally investigated and compared with the corresponding tests with the use of a steel rivet. The results of the experiments of the riveting process were then analyzed for the force-displacement curves and the cross-section geometry of the riveted joints. In the next article [14], the cross-sections of riveted joints were used to present the results of tension and shear for different loads. Then the influence of the depth of the die on the energy required before the joint failure and the influence of the rivet hardness on the joint strength were analyzed. Han in his work [13] carried out a microscopic inspection which showed that the quality of the joint was satisfactory despite the increasing level of deformation of the sheet. On the other hand, the article [21] examined two areas of fatigue of riveted aluminum lap joints and T-breaks: mechanisms of crack initiation and development, and the impact of fatigue on joint stiffness. There are many studies on fatigue tests of aircraft components [4-7]. Their approach to determining fatigue data would also be appropriate for aluminum materials used to build riveted joints.

All authors presented excellent work and insight into riveted joint strength investigations and numerical FEM modeling. However, the influence of the material model on the distribution of stresses and deformations was not given. Moreover, the experimental research presented only the results of static and fatigue in the form of graphs.

In this work, a numerical analysis of single-lap blind riveted joints was performed. The aim of the work, the assumption of numerical simulation, was the selection of the material model and modeling of joints and the influence of this model on plastic deformation. The results of the numerical tests were compared with a method of graphical visualization deformation of the rivet and the hole. The new technology allowed making cross-sections of riveted joints during a static

tensile test on a testing machine with different condition loads.

2. Numerical analysis

A numerical experiment was performed on a single-lap riveted joint with a blind rivet configuration using a 3D finite element model created and analyzed in commercial finite element code ANSYS 21R2.

The geometric model used in the analysis was the same as in the case of further experimental research (Figure 1). The riveted joint model was created corresponding to the procedure for tensile shear testing of a single joint (ISO 12996). Moreover, the assumptions were made to reflect the state of axial load in the experimental works.

The mechanical boundary conditions used during the numerical work were as follows:

- Fixed support (all degrees of freedom were fixed) for the left end of the sheet and the left additional surface.
- Allowed displacement (x = free, y = 0, z = 0) at the end of the sheet and right addition-al surface.
- The external load (force F) acts in the x-direction at the right end (Figure 1).

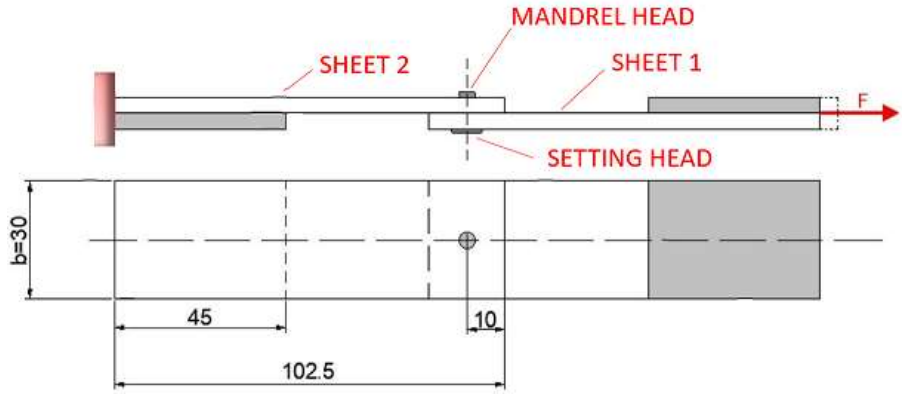

Fig. 1. The geometry of the specimen

The discrete model consists of three solids: a blind rivet and two sheets. The FE mesh contains more than 900 000 elements (tetrahedral elements with 10 nodes) with a quadratic square function – SOLID 187 (Figure 2). The size of the elements and their density was selected through a series of earlier numerical analyzes [23]. In the area of the rivet mandrel, the compaction of the elements was assumed on the contact surface (for more accurate results).

The presented numerical model of the riveted joint was created with the following contact conditions:

- Frictionless contact – sheet-to-sheet,
- Rough contact – sheet(hole)-to-rivet.

The selected contact models were defined based on an earlier series of simulations showing the actual separation of the cooperating elements [23].

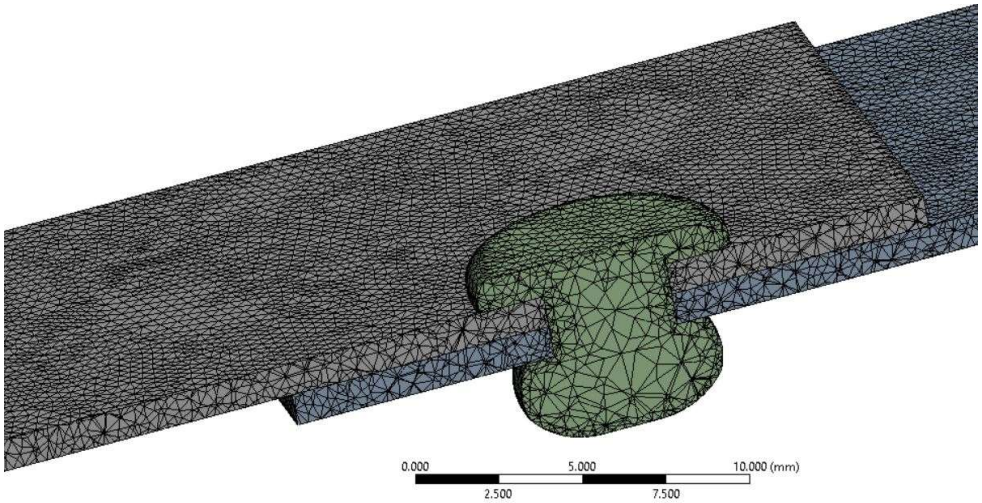

Fig. 2. Mesh riveted joint (cross-section)

The numerical analysis of the riveted joint was tested for two configurations of the material model [23]:

- Only linear elastic material model.
- Both nonlinear (elastic-plastic) models.

The stress-strain curves of the bilinear material model for a sheet and a blind rivet were created and shown in Figure 3. The material properties used to define the material models were presented in Table 1.

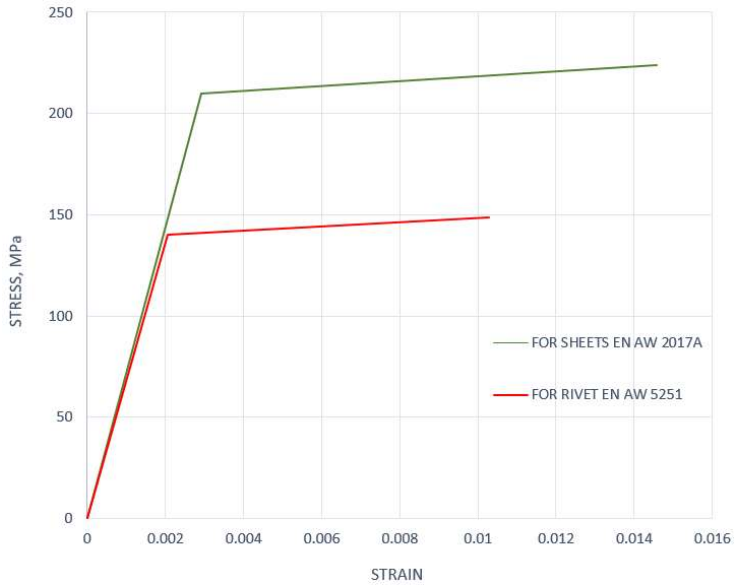

Fig. 3. Stress-strain curve of the bilinear material model for sheets and rivets

Table 1. Mechanical properties of the bilinear material model [31, 32]

Material data	Aluminum alloy EN AW 2017A (sheet)	Aluminum alloy EN AW 5251 (rivet)
Density, kg/mm^3	2700	2700
Young's Modulus, GPa	179	70
Poisson's ratio	0.3	0.3
Yield strength, MPa	288	140
Ultimate tensile strength, MPa	440	240
Tangent modulus, MPa	1200	1000

3. Experimental analysis

3.1. The geometry of joints and materials

For the experimental tests, we used 1 mm thick sheets of aluminum alloy EN AW 2017A. The basic mechanical properties of the sheets and rivets are shown in Table 1.

The prepared samples of sheet metal with dimensions as shown in Figure 1 were connected to EN AW 5251 aluminum alloy blind rivet [32] (diameter of hole 4 mm, length of shank 6 mm, a diameter of shank 4 mm, a diameter of setting head 8 mm) and correspond to the geometry of numerical analysis.

The rivet holes in the sheets were drilled and reamed. 12 samples of a single-lap riveted joint with a blind rivet were made, 4 samples for each load. All riveted joints were made with a pneumatic blind rivet gun with care and the same conditions for making the joint.

3.2. Experimental stand and methodology of measurements

Static tests of riveted joints were performed on a Zwick-Roell Z050 testing machine using Xforce P measuring head with a nominal force Fnom = 20 kN. The increase in the loading force was defined by the constant speed of displacement of the traverse of the machine L = 4 mm/min. Static tests were performed according to ISO 12996 [17].

The shear test was stopped at specific loads:

- F = 500 N,
- F = 800 N,
- F = 900 N.

These values were selected based on the maximum load capacity of 955 N for the riveted joint [24]. The

forces are 50, 80, and 95% of the total strength of the joint. The purpose of stopping the test with different applied loads was to stop further deformation of the joint and "freeze" the deformation state of the rivet. The special equipment was designed to allow the joint area to be flooded with a liquid mixture of polyurethane resin (F19 by Axson) (Figure 4).

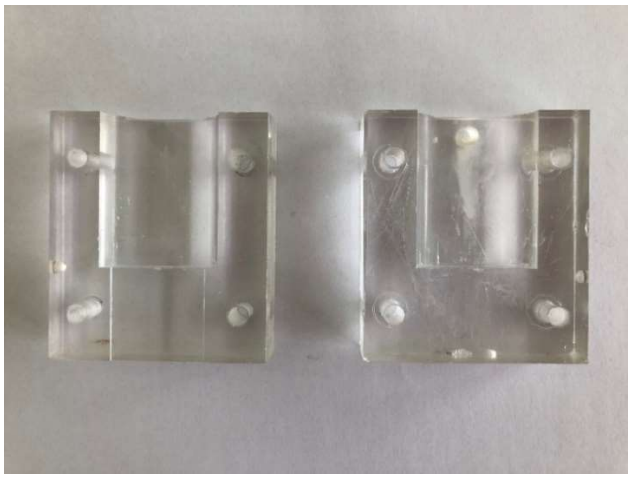

Fig. 4. The geometry of the special device

This device was a bipartite cuboidal form. After the installation of the sample, the was created a closed vessel for the binding mixture, covered the zone of the tested joint (Figure 5). The mold was made of polycarbonate (PC) to enable visual control of the correctness of the pouring process with the binder mixture. The working volume of the vessel was approx. 30 cm^3. After installation on the sample, the mold halves were screwed together with four M6 screws to form a tight seal on the sample. An opening was made in the upper part of the device to allow the liquid mixture to fill it. The adhesive was a polyurethane, two-component (polyol + isocyanate) casting resin F19 by Axson. The basic mechanical properties of the mixture are given in Table 2.

Fig. 5. Installation of the device on the sample

Table 2. Mechanical properties of the mixture [8]

Parameter	Standard	Value
Hardness, Shore D1	ISO 868-85	72
Young's Modulus, MPa	ISO 178-93	1200
Bending durability, MPa	ISO 178-93	50
Compression strength, MPa	ISO 604-93	48
Impact strength Charpy, kJ/m^2	ISO 179/1eU-93	16

Before the test, the working part and the joint area with the rivet were thoroughly cleaned and degreased to obtain the best possible adhesion between the binding mixture and the sample. Next, an anti-adhesive coating was applied to the internal walls of the special tool (form), preventing the device from sticking together permanently and destroying it.

During the static test, a binding mixture amount of 20 cm^3 (life approx. 6-8 minutes at a temperature of 25°C) was prepared. The mixture consisted of polyol and isocyanate in the proportion of 1:1. When the given force is reached, the tensile test was stopped. The mold was placed on the sample (Figure 5) and after obtaining tightness, was filled with the binding mixture using a syringe (Figure 6a). When the mixture was hardened, the deformations of the riveted joint were "frozen" (Figure 6b).

a) b)

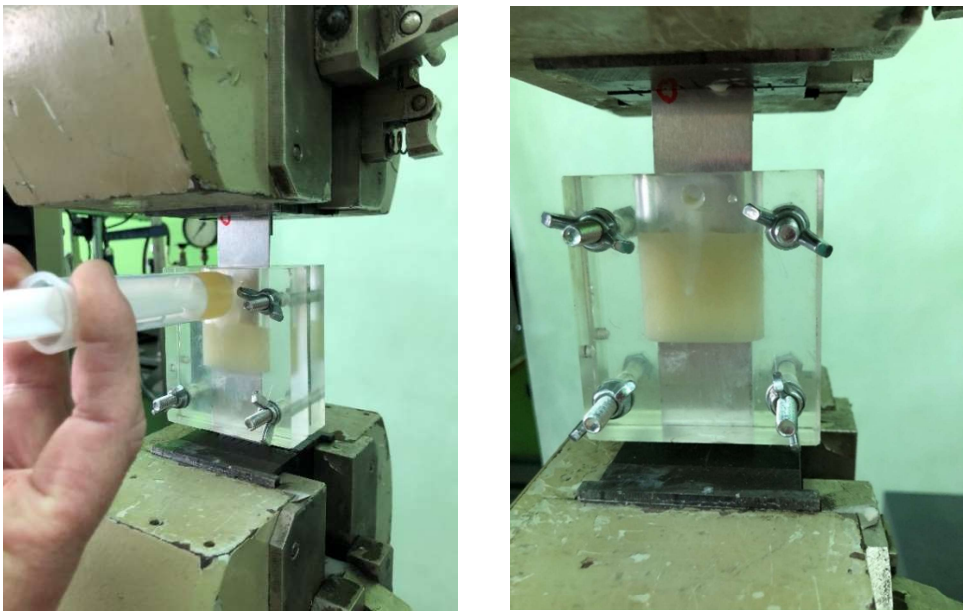

Fig. 6. Filling the device with the binding mixture (a); The sample fixed on the machine during curing (b)

The sample remains fixed on the tensile machine with a stopped load until the mixture reaches the hardening level (for approx. 2 hours). Then the mold was disassembled and the release of the sample was from the handles (Figure 7a). The sample was set aside for min. 24 h to obtain complete hardening of the binder mixture enabling further processing (Figure 7b).

a) b)

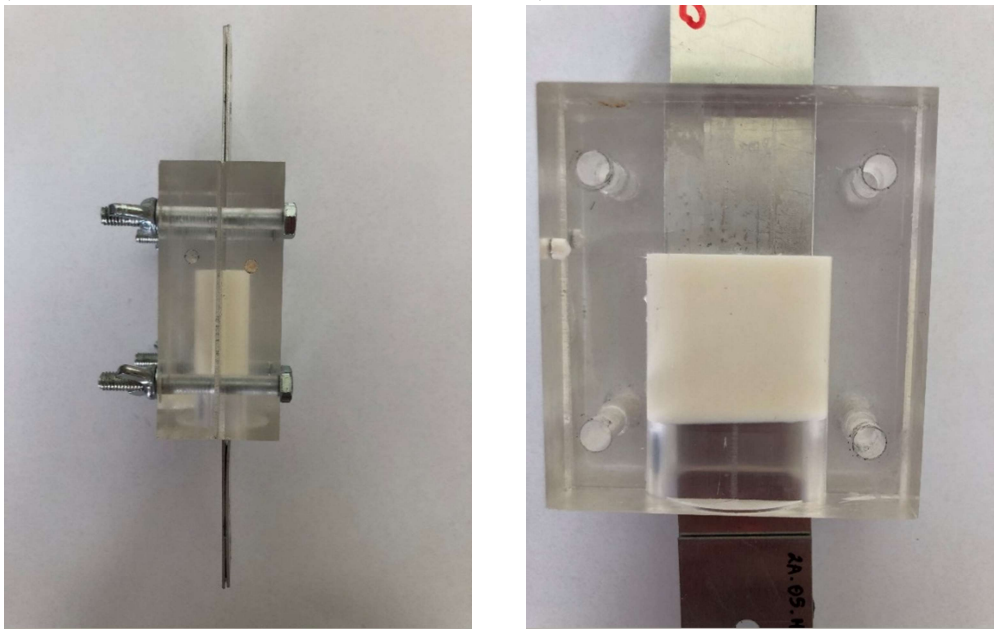

Fig. 7. Disassembling the device from the jaws of the machine (a); "Frozen" deformation of the joint (b)

The next step was to prepare the cross-section of the riveted joint. The sheets outside of the experimental zone were cut off and the sample in it was machined: was milled to 0.2 mm from the longitudinal symmetry plane of the joint, then was ground (<0.2 Ra) within the cross-sectional area.

The sample preparation process carried out in this way enables the optical analysis of the geometric deformation of the riveted joint, in a state close to the real at the moment of the application of the load. The obtained cross-section is then subjected to macro and microscopic analysis using an optical microscope, and

the photos taken allow us to compare and describe the observed changes in the geometry of individual connection elements, i.e. changes in the rivet and hole diameters.

4. Results and analysis

The prepared cross-sections from the numerical analysis and photos from the microscope allowed for the visualization of the deformation state of the riveted joint during the simulation and experiment for the measurement of specific geometrical parameters of the joint.

For the analysis, the following geometrical parameters were defined for the cross-section (Figure 8):

- Rivet deviation angle from the sheet α_1,
- Rivet rotation angle α_2,
- Tangle of sheets separated α_3,
- Diameter of the hole α_4.

The samples of riveted joints were examined for the same forces as were mentioned earlier in Chapter 3.

The definitions of the measured dimensions were presented in Figure 8.

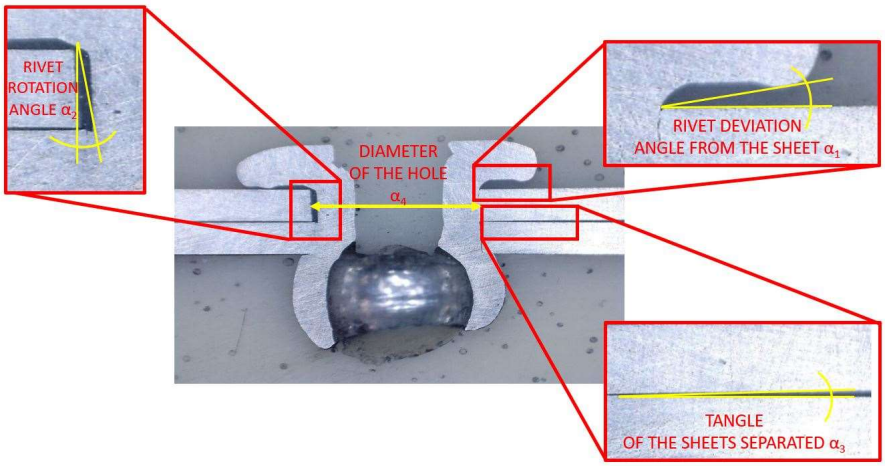

Fig. 8. Defined geometrical parameters of a riveted joint cross-section

The cross-sections made in the experiment were photographed using a microscope and processed for measurement, and some of them are presented in Figures 9-11.

Figure 9 shows the axial cross-section of the joint with a load of 800 N: "a" from numerical analysis and "b" from experimental work. The smallest deformation in the diameter of the hole was observed at $\alpha_4 = 4.03$ mm and a small tangle of sheets separated at $\alpha_3 = 1.42°$. The biggest displacements can be observed for the rivet rotation angle $\alpha_3 = 2.74°$. In the experiment, it was observed that the rivet head formed by the mandrel is visible. At the initial stage of the load (in the linear range of deformation), a slight displacement of the sheets was observed – the angle of the sheets separated $\alpha_3 = 2.27°$ and a small rotation of the rivet, the angle of which was $\alpha_2 = 8.11°$. On the other hand, a greater deviation angle of the rivet from the sheet metal, $\alpha_1 = 11.48°$, and a slight deformation of the hole $\alpha_4 = 4.06$ mm, can be observed.

a)

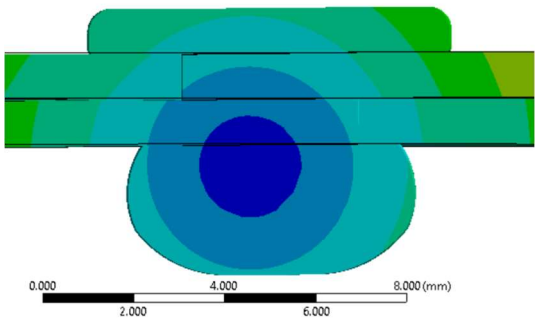

b)

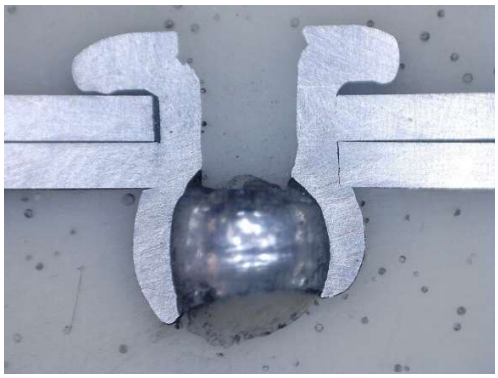

Fig. 9. Cross-section of the joint with load F = 800 N for a linear material model (a); Cross-section of the joint with load F = 800 N (b)

A further increase in the load (up to F = 900 N) causes an increase in deformation, as presented in Figure 10. With the force close to the value of the maximum capacity of the riveted joint, the deformation of the rivet is visible, mainly caused by the shear process. The rivet rotation angle was α_2 = = 23.44°, as the inner cylindrical surface of the rivet (initially smooth) was deformed (displaced and rotated) due to the local high shear stress. Moreover, in the advanced stage of loading, the gap between the joined materials was observed, with the sheet separation angle α_3 = 1.7°. The rivet deviation angle from the sheet was α_1 = 4.76° and was smaller compared to the load in the linear range. The displacement and rotation of the rivet resulted in much greater deformation of the hole and an increase in its diameter with the value of α_4 = 4.19 mm.

Figure 11 shows the axial cross-section of the joint with a load of 900 N: "a" shows the linear material model and "b" is for a nonlinear. The more significant deformation of the joint for the linear material model was observed. The tangle of the sheets separated was α_3 = 1.42° for the nonlinear model, and α_3 = 1.01° for the nonlinear. The rivet rotation angle compared to the nonlinear model was approximately twice as large. On the other hand, the values of the diameters of the hole were similar and comparable to the experiment.

Fig. 10. Cross-section of the joint with load F = 900 N

a)

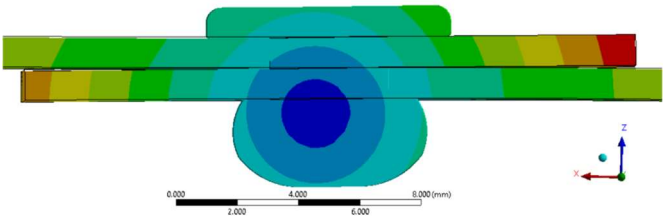

b)

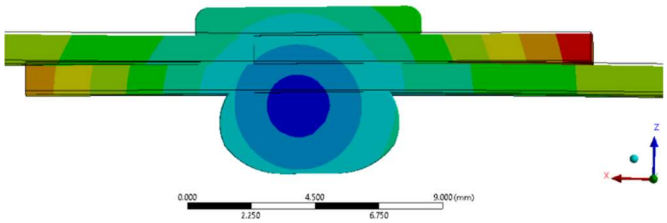

Fig. 11. Cross-section of the joint with load F = 900 N for a linear material model (a); Cross-section of the joint with load F = 900 N for a nonlinear material model (b)

The measured geometrical parameters from the numerical analysis and compared with the experiment work are presented in Table 3.

In the numerical analysis for both material models, the rivet deviation angle from the sheet α_1 having similar values was observed but was a big difference from the experiment. The greatest difference between the numerical analysis and the experiment was in the rivet rotation angle α_2 for a load of 900 N, and with a lower load, the differences were smaller. The smallest differences in numerical analyzes are for the tangle of sheets separated by α_3, up to 800 N, α_3 has higher values for the linear material model and over 900 N for the bilinear. Similar results for each material model were for the diameter of the hole, with slight differences with the experiment.

Table 3. Comparison of geometrical parameters of the riveted joint cross-section

Geometrical parameters	F = 500 N			F = 800 N			F = 900 N		
	Experiment	MES		Experiment	MES		Experiment	MES	
		Linear	Nonlinear		Linear	Nonlinear		Linear	Nonlinear
α_1	2.33°	0.56°	0.28°	11.48°	1.69°	1.43°	4.76°	1.16°	0.94°
α_2	3.55°	2.77°	2.13°	8.11°	2.74°	1.56°	23.44°	2.44°	1.52°
α_3	1.08°	0.87°	0.48°	2.27°	1.42°	1.01°	1.7°	0.82°	1.14°
α_4	4.05 mm	4.01 mm	4.01 mm	4.06 mm	4.03 mm	4.04 mm	4.19 mm	4.05 mm	4.03 mm

The geometrical parameters from the numerical analysis and experiment work were compared in Table 4. For low values of force (500 N) compared to the experimental data, for linear analysis, the greatest difference for the rivet deviation angle from the sheet by 76%, and nonlinear models by 88% were observed. The smallest percentage difference was observed for the diameter of the hole (about 1%). As the load increased, the percentage difference was increased, for the tangle of sheets separated by α_3 in the linear analysis was 20% compared to 500 N. Moreover, significantly changed the rivet rotation angle α_2, the value of which was decreased by more than 40% for both material models.

The opposite situation is for the results for the force of 900 N, compared to the experiment, the most significant difference is for the rivet rotation angle, i.e. a decrease by 89% (linear) and by 94% (non-linear), and the same is accurate for the angle α_1. However, for the tangle of the sheets separated for the linear analysis, the change was 52%, and for the nonlinear analysis by 33%. The smallest changes recorded for the diameter of the hole were 3% and 4%.

The greatest discrepancies in the measured parameters occur for the force of 900 N, and the smallest for 500 N (for α_2 and α_3). For all geometrical parameters of the riveted joint, for all numerical analyses, and only for the diameter of the hole, the differences do not exceed 4%.

Table 4. Percentage comparison of geometrical parameters of the riveted joint cross-section

Geometrical parameters	F = 500 N			F = 800 N			F = 900 N		
	Experiment %	MES		Experiment %	MES		Experiment %	MES	
		Linear %	Nonlinear %		Linear %	Nonlinear %		Linear %	Nonlinear %
α_1	100	24	12	100	15	12	100	24	20
α_2	100	78	60	100	34	19	100	10	6
α_3	100	81	44	100	63	44	100	48	67
α_4	100	99	99	100	99	99	100	97	96

5. Conclusion

In this work, numerical results of blind rivet joints for linear and nonlinear numerical material models were presented. The numerical results were compared with the experiment, with the new methodology of visualizing changes in the geometry of a riveted joint with a blind rivet. Detailed numerical and experimental displacement analysis and plastic deformation analysis were performed on the joint connection.

The results obtained from these investigations lead to the following conclusions:

1. For the lowest examined value of the force (500 N), little differences in deformations are observed in the numerical results, compared to the experimental ones.
2. The method of material modeling did not have a large impact on the value of the geometrical parameters of the joints obtained, estimated by numerical methods. The results closest to the experiment work are obtained from the linear analysis, i.e. the linear material model.
3. Large differences in results are caused by simplifications of the material model (bilinear instead of multilinear), so the plasticization process is not similar to that in the experimental tests.
4. Cross-section analysis with an increase in the destructive force showed a complex state of stress in the rivets, i.e. a combination of shear and bending at an advanced stage of deformation.
5. In the described experiment, the new technology of cross-sections allows the creation of a method of visualizing changes in the geometry of a riveted joint and performing these axial cross-sections under any load of the tensile machine, during various stages of static tests of riveted joints.

The performed numerical analysis and their reference to the experimental data may be the basis for research focusing on the possibility of using simple strength models (bilinear model instead of the multilinear model) in strength analyzes. The analysis could also focus on the linear range of forces and a greater load on riveted joints. The technology and method of visualizing changes in geometry can be used when designing riveted joints with blind rivets. Also, the results obtained help explain the failure of blind rivets. In the future, the prepared cross-sections can be used to calculate the grain size of the alloys for a given load during the static tensile test of the riveted joint.

References

1. Armentani E., Greco A., De Luca A., Sepe R. 2020. „Probabilistic Analysis of Fatigue Behavior of Single Lap Riveted Joints". *Appl. Sci.* 10, 3379.
2. Armentani E., Laiso M., Caputo F., Sepe R. 2018. „Numerical FEM Evaluation for the Structural Behaviour of

a Hybrid (bonded/bolted) Single-lap Composite Joint". *Procedia Struct. Integr.* 8: 137–153.
3. Atzeni E., Ippolito R., Settineri L. 2009. „Experimental and numerical appraisal of self-piercing riveting". *CIRP Annals – Manufacturing Technology* 58: 17–20.
4. Bednarz A. 2020. „Evaluation of Material Data to the Numerical Strain-Life Analysis of the Compressor Blade Subjected to Resonance Vibrations". *Advances in Science and Technology Research Journal* 14, 1.
5. Bednarz A. 2020. „Influence of the Amplitude of Resonance Vibrations on Fatigue Life of a Compressor Blade with Simulated FOD Damage". *Advances in Science and Technology Research Journal* 14,3.
6. Bednarz A., Misiolek W. 2020. „Assessment of the Impact of Shot-Peening on the Fatigue Life of a Compressor Blade Subjected to Resonance Vibrations". *Materials* 12, 5726.
7. Bednarz A., Misiolek W. 2021. „Numerical and Experimental Assessment of the Effect of Residual Stresses on the Fatigue Strength of an Aircraft Blade". *Materials* 14, 5279.
8. BN-89, 6376-02; "Tworzywa Sztuczne; Żywice epoksydowe ; Epidian 1, 2, 3, 4, 5, 6".
9. Bula K., Sterzyński T., Piasecka M., Różański L. 2020. „Deformation Mechanism in Mechanically Coupled Polymer–Metal Hy-brid Joints". *Materials* 13, 2512.
10. Choi D.-H., Han D.-W., Kim H.-K. 2017. „Fatigue life estimation of self-piercing riveted aluminum joints under mixed-mode loading". *Int. J. Fatigue* 97: 20–28.
11. Elzaroug M., Kadioglu F., Demiral M., Saad D. 2018. „Experimental and numerical investigation into strength of bolted, bonded and hybrid single lap joints: Effects of adherend material type and thickness". *Int. J. Adhes. Adhes.* 87: 130–141.
12. Han L., Chrysanthou A., Young K. 2007. „Mechanical behaviour of self-piercing riveted multi-layer joints under different specimen configurations". *Materials and Design* 28: 2024–2033.
13. Han L., Young K.W., Chrysanthou A., Sullivan J.M. 2006. „The effect of pre-straining on the mechanical behaviour of self-piercing riveted aluminium alloy sheets". *Materials and Design* 27: 1108–1113.
14. Haque R., Durandet Y. 2016. „Strength prediction of self-pierce riveted joint in cross-tension and lap-shear". *Materials and Design* 108: 666–678.
15. Hoang N., Porcaro R., Langseth M., Hanssen A. 2010. „Self-piercing riveting connections using aluminium rivets". *International Journal of Solids and Structures* 47: 427–439.
16. Huang L., Guo H., Shi Y., Huang S., Su X. 2017. „Fatigue behavior and modeling of self-piercing riveted joints in aluminum alloy 6111". *International Journal of Fatigue* 100: 274–284.
17. International Organization for Standardization. 2013. „ISO 12996:2013–Mechanical Joining–Destructive Testing of Joints–Specimen Dimensions and Test Procedure for Tensile Shear Testing of Single Joints". *International Organization for Standardization:* Geneva, Switzerland.
18. Jiang H., Luo T., Li G., Zhang X., Cui J. 2017. „Fatigue life assessment of electromagnetic riveted carbon fiber reinforce plastic/aluminum alloy lap joints using Weibull distribution". *International Journal of Fatigue* 105: 180–189.
19. Jiang H.' Sun L., Liang J., Li G., Cui J. 2019. „Shear failure behavior of CFRP/Al and steel/Al electromagnetic self-piercing riveted joints subject to high-speed loading". *Composite Structures* 230, 111500.
20. Li D., Han L., Thornton M., Shergold M. 2012. „Influence of edge distance on quality and static behaviour of self-piercing riveted aluminium joints". *Materials and Design* 43: 22–31.
21. Li D., Han L., Thornton M., Shergold M., Williams G. 2014. „The influence of fatigue on the stiffness and remaining static strength of self-piercing riveted aluminium joints". *Materials and Design* 54: 301–314.
22. Liang J., Jiang H., Zhang J., Wu X., Zhang X., Li G., Cui J. 2019. „Investigations on mechanical properties and microtopography of electromagnetic self-piercing riveted joints with carbon fiber reinforced plastics/aluminum alloy 5052". *Archives of civil and mechanical engineering* 19: 240–250.
23. Lubas M., Bednarz A. 2021. „Material Model Effect for Simulating a Single-Lap Joint with a Blind Rivet". *Materials* 14, 7236.
24. Lubas M., Witek L. 2021. „Influence of Hole Chamfer Size on Strength of Blind Riveted Joints". *Adv. Sci. Technol. Res. J.* 15(2):49–56.
25. Moraes J., Jordon J., Su X., Barkey M., Jiang C., Ilieva E. 2018. „Effect of process deformation history on mechanical performance of AM60B to AA6082 self-pierce riveted joints". *Eng. Fract. Mech.* 209: 92–104.
26. Mucha J. 2017. „Blind Rivet and Plastically Formed Joints Strength Analysis". *Acta Mechanica Slovaca* 21 (1): 62-69.
27. Mucha J., Witkowski W. 2011. „Nośność wybranych rozwiązań połączeń nitowych podczas próby ścinania i rozciągania". *Zeszyty Naukowe Politechniki Rzeszowskiej* 279, 83 (4/11).
28. Mucha J., Witkowski W. 2017. „Analiza wpływu obciążenia termomechanicznego na wytrzymałość połączenia z nitem zrywalnym". *Mechanik* 2, 35.
29. Mucha J., Witkowski W. 2017. „The experimental analysis of the double joint type change effect on the joint destruction process in uniaxial shearing test". *Thin-Walled Structures* 66: 39–49.
30. Pitta S., Roure F., Crespo D., Rojas J.I. 2019. „An Experimental and Numerical Study of Repairs on Composite Substrates with Composite and Aluminum Doublers Using Riveted, Bonded, and Hybrid Joints". *Materials* 12, 2978.
31. Polish Committee for Standardization. PN-EN 485-2+A1:2018-12. 2018. „Aluminium and Aluminium Alloys–Sheet, Strip and Plate–Part 2: Mechanical Properties". *Polish Committee for Standardization:* Warsaw, Poland.
32. Polish Committee for Standardization. PN-EN 573-3:2019-12. 2019. „Aluminium and Aluminium Alloys–Chemical Composition and Form of Wrought Products–Part 3: Chemical Composition and Form of Products". *Polish Committee for Standardization:* Warsaw, Poland.
33. Qasim B., Khidir T. 2021. „Study Strength of Blind Riveted Lap Joint Structure under Tensile Shear Force".

International Journal of Mechanical Engineering and Robotics Research 10, 7.
34. Rao H.M., Kang J., Huff G., Avery K. 2019. „Structural Stress Method to Evaluate Fatigue Properties of Similar and Dissimilar Self-Piercing Riveted Joints". *Metals* 9, 359.
35. Rudawska A., Warda T., Miłosz P. 2015. „Wytrzymałość połączeń klejowych i nitowych". *Technologia i Automatyzacja Montażu* 2: 56-59.
36. Skorupa M., Korbel A., Machniewicz T. 2009. „Analiza wtórnego zginania w mimośrodowych połączeniach nitowych". *Biuletyn WAT* 8, 2.
37. Sun X., Stephens E., Khaleel M. 2007. „Fatigue behaviors of self-piercing rivets joining similar and dissimilar sheet metals". *International Journal of Fatigue* 29: 370–386.